DOI: 10.1515/sspjce-2020-0013

Analyses of selected thermal-technical parameters of an innovative construction board with built-in infrared heating

Dominik Dubecký, Mária Kozlovská

Technical University of Košice, Slovakia
Civil Engineering Faculty, Institute of Technology, Economics and Management
e-mail: dominik.dubecky@tuke.sk, maria.kozlovska@tuke.sk

Abstract

The purpose of innovations is to increase the efficiency of work procedures, accommodating sustainability and efficiency trends. One of the preconditions of technological innovations is development of construction products. A prefabricated board with built-in infrared heating is an innovative product which reduces labour intensity at the construction site by featuring a heating system that is built directly into the construction board, which begins to perform its function immediately after it is built in. This article presents certain partial results of the research and development of an innovative board with built-in infrared heating, which is currently protected by a valid utility model. Nine material variants of the innovative board were analysed as part of the experimental research. The research focused on the pattern of changes in surface temperature over time. The results of the experiment, despite deviations from the anticipated behaviour of the individual boards, showed a link between thermal resistance and increase in surface temperature.

Key words: innovative board, infrared heating, surface temperature

1 Introduction

The construction industry is characterised by a high proportion of manual labour and a high number of construction processes. For instance, a family house involves approximately 290 partial construction processes [1]. The processes are interconnected and affect each other. The human factor significantly affects the efficiency of construction work, so it is necessary to develop and innovate construction products so as to minimise manual labour. One of the construction processes in the construction of buildings is the installation of a heating system. According to technology, heating systems can be divided into systems built into “wet” layers (e.g. hot water floor heating system) and systems built into “dry” layers (e.g. electric low-heat infrared heating system).

The heating system based on infrared foil is still quite rare in Slovakia compared to traditional heating systems. It is an electric heating system whose source of heat is infrared heating foil.

The basic principle of its functioning is based on a discovery by William Herschel from 1800, who described the existence of infrared radiation. Infrared radiation is emitted from all surfaces with a temperature higher than -273.15 °C, also known as the absolute zero (0 K) on the Kelvin scale [2]. The primary function of an infrared heater is the transfer of heat by emitting infrared radiation [3]. Infrared heating foil emits infrared radiation with a wavelength of 8-14 μm [4].

The use of infrared heating in buildings is beneficial not just from the structural point of view, but also in terms of efficiency, thanks to the exchange of radiating heat between the source and the radiated area. In addition, the infrared heating system is comfortable for the user, improving the quality of the internal environment, which is a necessity at the present time. The heating system's thermal response is rapid, requiring a short period of time to warm up [6]. The fact that the source of the infrared heating system is electricity is no less important, as it can be supplied from renewable resources. This means that the system can be sustainable, and it is a system that requires less electric energy consumption than electric heating using thermal cables. The basic element of the infrared heating system is IR heating foil (Fig. 1).

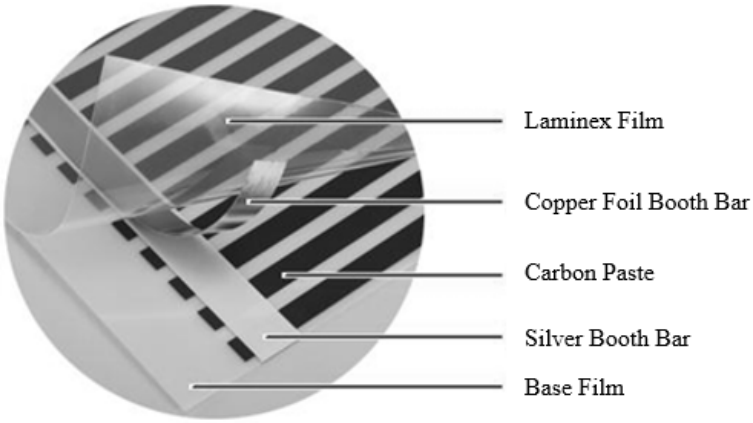

Figure 1: Infrared heating foil [7]

The core of infrared (IR) heating foil is carbon paste, acting as a thermal radiator. This paste can be applied in the form of stripes (Fig. 1) or as a homogeneous layer. Electricity transfer in IR foil is ensured by means of a conductive tape (Silver Both Bar), which connects the carbon paste. The protective film protects and connects all the layers to form single foil [7]. The installation of such a heating system is less complicated in terms of the number of work procedure steps involved. IR foil sheets only need to be unfolded and interconnected with a cable. The connecting cable is then connected to the power supply [8]. This heating system does not require the installation of a system of tubes or the difficult installation of a separator for regulating water temperature for the different parts of the system (like in the case of the hot water system), nor does it require the laborious job of inserting heating cables into the floor structure (like in the case of traditional electric heating).

In an effort to minimise the labour intensity of the construction of floor heating and of the development of so-called dry processes with the aim to make modern methods of construction more efficient, the authors of the article are developing an innovative construction board with infrared heating foil. The board is protected by a valid utility model, No. 7722 [9].

Its technical solution lies in enclosing heating foil between two boards, i.e. the supporting one and the covering one. The main advantage of the use of the innovative board is that the board and its heating are assembled in a single step. The individual boards are connected during assembly to create a functioning heating system.

The supporting board and the covering board are made from standard construction board, which can vary depending on material preferences, the purpose of the room where they will be installed, the thickness of the floor layers, etc. For this reason, it is necessary to examine and analyse the efficiency of the innovative board with built-in IR heating, especially in relation to the parameters influencing thermal comfort. This contribution presents certain partial results of the experimental research focused on analysing the impact of the thermal-technical characteristics of the nine selected types of construction boards on the increase in their surface temperature.

2 Materials and methods

The types of boards that are most commonly used in the construction industry were selected for the experimental measurements. In terms of material basis, the sample consisted of plasterboards (PB), chipboards (OSB), gypsum fibreboards (GFB), and magnesium oxide boards (MgO). PB boards were the largest sample, ranging from the most commonly used standard boards (GKB 12.5 AK) to special boards with improved thermal-technical parameters (Thermoboard). The thickness of the selected boards ranged from 12 to 12.5 mm to ensure that one of the input parameters (thickness) was as identical as possible for all samples. The only exception was the Brio gypsum fibreboard, which had a thickness of 18 mm, as this type of board is not available in thickness of 12 mm (although these are boards commonly used in floors), and the Thermoboard plus plasterboard, as this board is manufactured only in thickness of 10 mm. Tab. 1 presents the selected construction boards and their input parameters declared by the manufacturer.

Table 1: Parameters of the selected boards used for the experimental measurements

Name of board	Material basis	Thickness [mm]	Thermal conductivity λ[W/m]	Thermal resistance R[W/m^{2}K]
OSB 3	chipboard	12	0.13	0.092
GKB 12.5 AK	plasterboard	12.5	0.22	0.057
F146	plasterboard	12.5	0.25	0.050
Habito	plasterboard	12.5	0.25	0.050
Rigips RF	plasterboard	12.5	0.25	0.050
Thermoboard +	plasterboard	10	0.45	0.022
Superdoska	MgO	12	0.22	0.056
Rigidur H	Gypsum fibreboard	12.5	0.20	0.063
Brio	Gypsum fibreboard	18	0.25	0.072

The IR foil used in the experiments was selected from the commonly used and available foil types, although it is a new generation one, whose effective heating area is larger, as it has wider heating lamella compared to the older types (Fig. 2). 92% of the foil's area is designed for heating. The manufacturer of the selected IR foil is CALEO®, and its declared power is 130 W/m2. The foil is supplied in rolls with widths of 300mm, 500mm and 800 mm. Foil with a width of 500 mm was selected for the experiments, which can be cut every 250 mm along its length.

Figure 2: Caleo® infrared heating foil [10]

In the experiment, the IR foil was always placed between two identical boards (so-called single-type material variant). The measured board with built-in IR foil was attached to thermal insulation (Styrodur 2800 C 30 mm extruded polystyrene with dimensions of 1250mm x 600mm x 60mm).

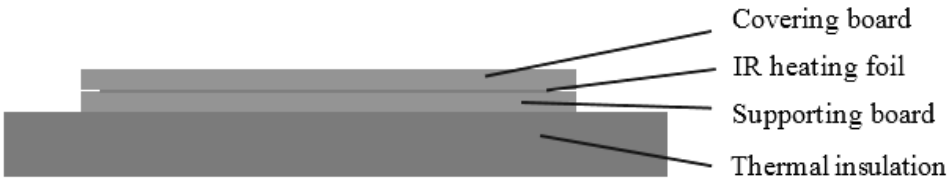

Figure 3: Schematic diagram of the experiment

The experimental measurements (Fig. 4) were performed in the experimental chamber of the Department of Civil Engineering of the Technical University of Košice, which ensured stable thermal conditions for all of the experimental measurements. The chamber is built in as a separate facility in the laboratories in the building's basement. The chamber is 3.7 m long, 2.8 m wide and 2.1 m high. The experimental chamber has no windows. Its walls are built from porous concrete blocks with plaster and paint on the surface. A water supply system for heating and cooling is built into the walls, allowing the temperature of each wall to be regulated separately. The floor of the experimental chamber is equipped with a water supply floor heating system, built into the "wet" concrete layer. The ceiling is from plasterboard boards, above which a capillary system for heating and cooling is built in. The experimental measurements did not require the different heating systems in the experimental chamber to operate, as it had turned out that the thermal conditions in the experimental chamber were stable (23°C +/- 0.5 °C in the summer period and 17.3°C +/- 0.5°C in the winter period) and there was no air flow in the experimental chamber when it was closed.

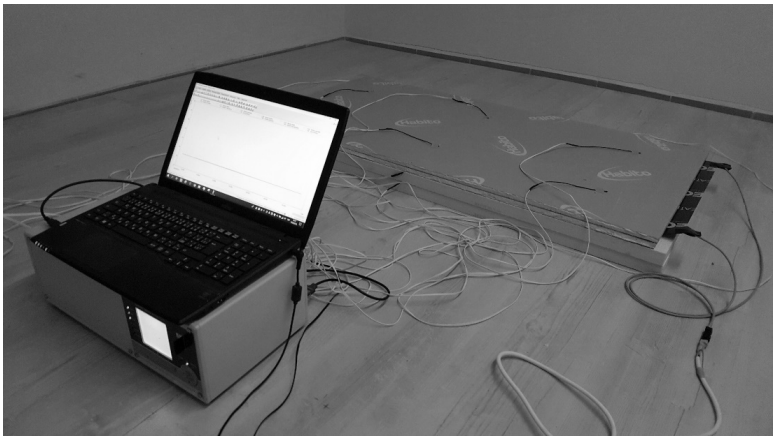

Figure 4: Experimental room with a measured sample and the measurement and recording equipment

AHLBORN NTC FN 0001 surface temperature sensors were used for the measurements (Fig. 5), with an operating range from -20 °C to + 100 °C. Data were recorded on the central measurement and recording station, i.e. the AHLBORN ALMEMO® 5690-2 datalogger.

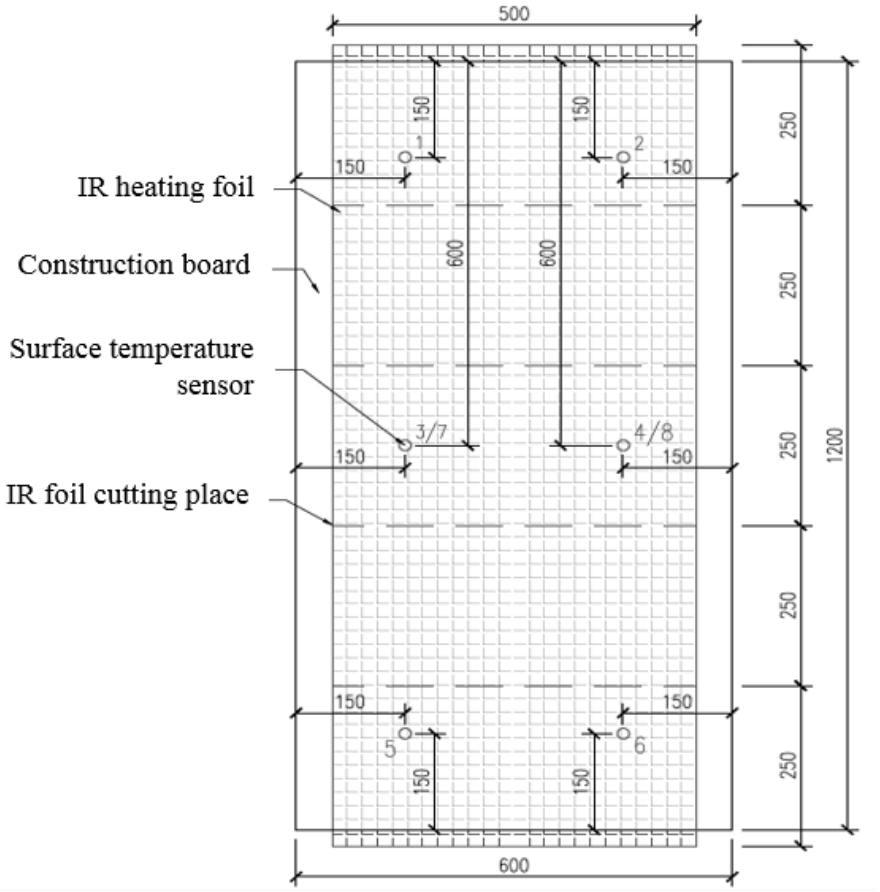

Figure 5: Diagram showing the locations of the sensors during the experiment

Note: Sensors 1 to 6 are placed on the board, and sensors 7 and 8 are placed under the board.

The sensors were connected and prepared on the board sample, always at least 24 hours before measurements to ensure that the temperature of the board was equalised with the temperature in the experimental chamber.

3 Results and discussion

The surface temperature increase period represents the period in which surface temperature increases by ΔT from the time heating is started. The recorded temperature changes for all measured variants, based on which the surface temperature increase period was analysed for the monitored temperature differences, is shown in Diagram 1.

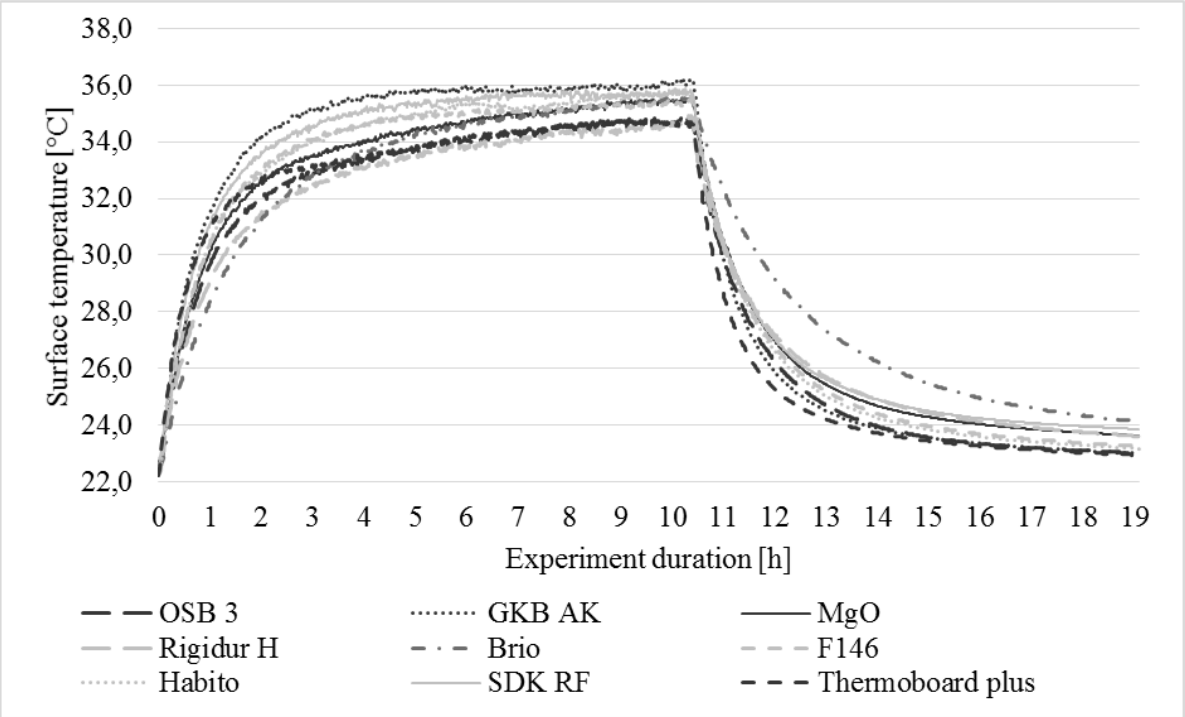

Diagram 1: Surface temperature changes for all nine measured variants of the prefabricated board with built-in IR heating

The analysed parameters are presented in Diagram 2: The temperature differences ΔT for which the temperature increase period was measured were 5°C and 10°C.

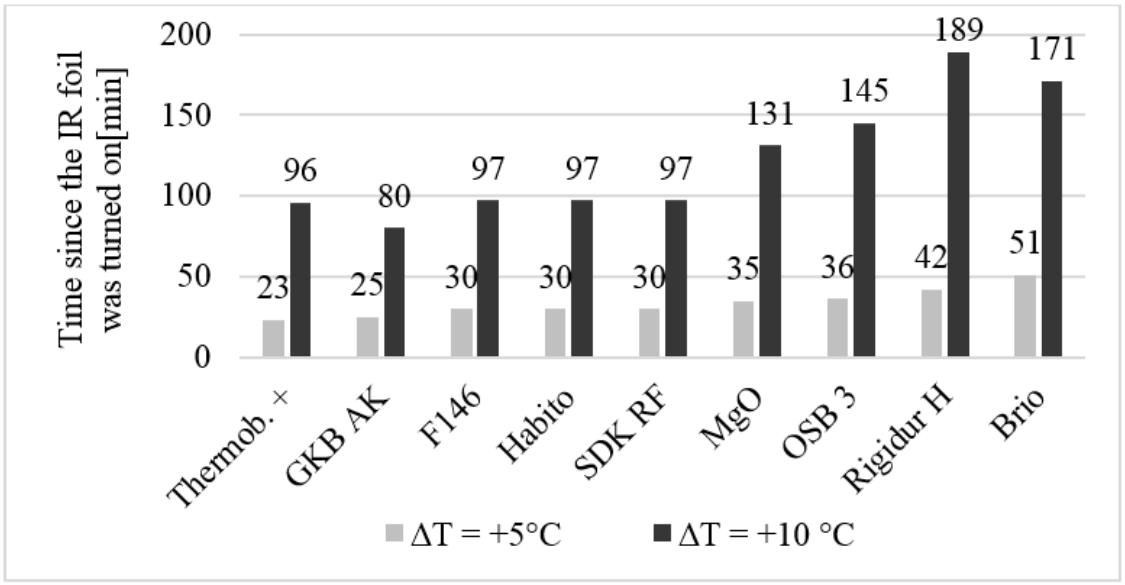

Diagram 2: Surface temperature increase period

The surface temperature change by ΔT=+5°C was the fastest for the Thermoboard plus PB board, and as it is a PB board that is particularly suitable for designs where faster spread of heat is required, this result had been anticipated. This was partly due to the fact that the material was 10 mm thick, which is 2.5 mm less compared to the other PB, and Thermoboard plus also has the lowest thermal resistance. The ordinary PB board of the GKB AK type reached ΔT=+5°C in 25 minutes. The other PB boards (F146, Habito and RF) reached the specified temperature difference in the same period of time, i.e. in 30 minutes. The MgO and the OSB boards reached the given difference in a similar period of time. The MgO board reached it in 35 minutes, and the OSB board reached it in 36 minutes. The Rigidur H gypsum fibreboard reached ΔT=+5°C in 42 minutes, and the Brio gypsum fibre floor board reached the specified difference in 51 minutes, as the Brio board is 18 mm thick and has the highest thermal resistance. The difference between the shortest and the longest period to reach the difference is almost twofold (28 minutes).

The ordinary PB board (GKB AK) was the fastest to reach the specified temperature difference ΔT=+10°C, i.e. in 80 minutes. Identical periods, i.e. 97 minutes, were recorded for the other PB boards, with the exception of Thermoboard plus, which reached the difference in 96 minutes. They were followed by the MgO board, which reached the difference in 131 minutes, and the OSB board, which reached the difference in 145 minutes. The gypsum fibreboards were the slowest to reach the difference ΔT=+10°C, with Brio, with a thickness of 18 mm, reaching it in 171 minutes and Rigidur H, with a thickness of 12.5 mm, taking as long as 189 minutes, which is the reverse of the results in the case of the ΔT=+5°C temperature increase. The difference between the shortest and the longest period to reach the difference is more than twofold (109 minutes).

As for the material basis, the PB boards required the shortest period of time to reach the specified temperature. They were followed by the MgO board and the OSB (chipboard) board. The gypsum fibreboard boards required the longest period of time to reach the specified temperature.

This experimental analysis also provides practical knowledge for the user regarding periods required to reach thermal comfort in a room. These data allow the user to judge how long in advance they need to turn on the heating in the given room for the floor to reach the desired temperature at the required time.
To be able to analyse the impact of thermal resistance on the speed of surface temperature increase, the individual samples in Tab. 4 are arranged in an ascending order according to thermal resistance.

Table 2: Surface temperature increase in relation to thermal resistance

	Thermo-board+	**F146**	**Habito**	**SDK RF**	**MgO**	**GKB AK**	**Rigidur H**	**Brio**	**OSB 3**
Material basis	PB	PB	PB	PB	MgO	PB	GFB	GFB	OSB
Thickness [mm]	10	12.5	12.5	12.5	12	12.5	12.5	18	12
R [W/m^{2}K]	0.022	0.050	0.050	0.050	0.056	0.057	0.063	0.072	0.092
λ [W/mK]	0.45	0.25	0.25	0.25	0.22	0.22	0.20	0.25	0.13
ΔT = +5°C [min]	23	30	30	30	35	25	42	51	36
ΔT = +10°C [min]	96	97	97	97	131	80	189	171	145
Difference [min] $\Delta T_5 - \Delta T_{10}$	73	67	67	67	96	55	147	120	109

Note: The variants are arranged in an ascending order according to thermal resistance

Despite the fact that the thermal resistance of Thermoboard plus is half that of the other PB boards, the surface temperature increase of ΔT=+5°C was only a little faster, and its ΔT=+10°C increase speed was even almost identical to that of the other PB boards, with the exception of the ordinary PB board (GKB AK), which reached the specified temperature difference 16 minutes faster. On the other hand, the OSB board reached the measured difference faster (145 minutes) than Rigidur H (189 minutes) and the Brio board (171 minutes), despite the fact that its thermal resistance is 20-30% higher.
Based on the values presented in this way, it is not immediately apparent whether there is a relation between the thermal resistance of the given covering board and its speed of surface temperature increase, or what relation it is. It had been supposed that an increase in thermal resistance would result in a proportionate increase in the temperature increase period. A trend analysis was used to confirm this supposition (Diagram 3).

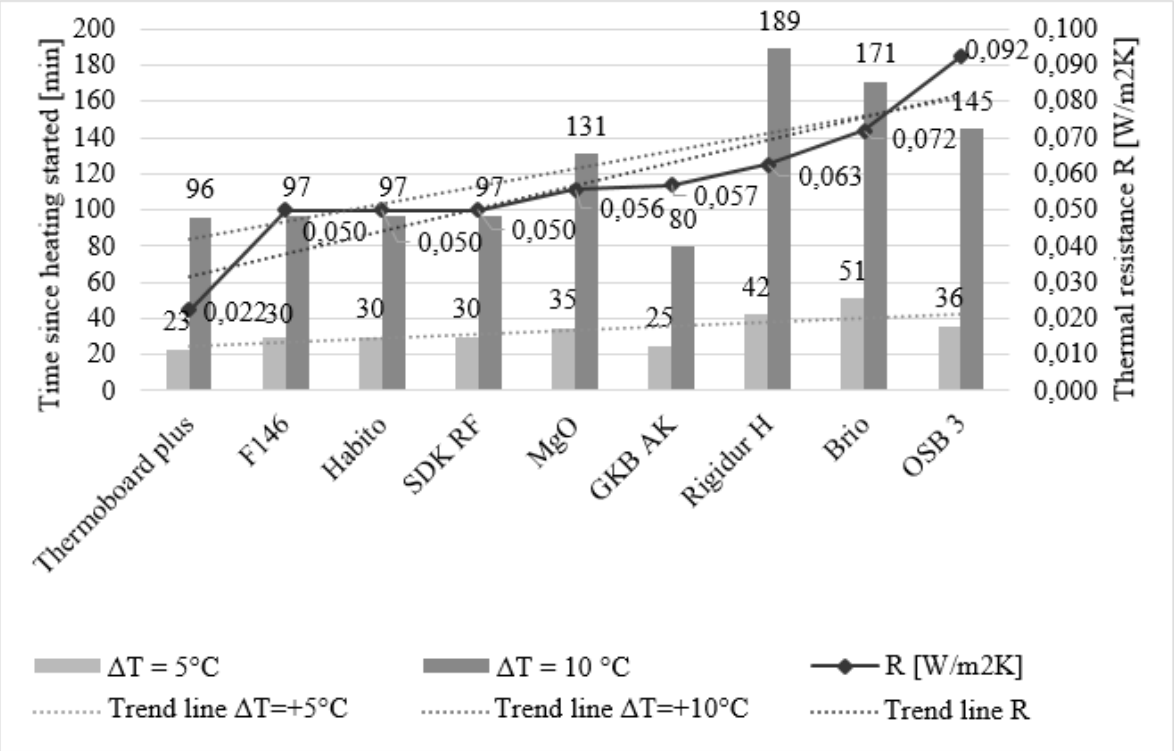

Diagram 3: Surface temperature increase in relation to thermal resistance

In Diagram 3, the samples are arranged in an ascending order according to thermal resistance. The trend connecting lines show linear relations, which confirms that, despite the deviations, there is a direct link between thermal resistance and surface temperature increase period. The deviations are also influenced by the internal material structure of the individual boards, which affects their internal thermodynamic processes.

4 Conclusion

Innovations are a necessary part of everyday life in the modern world. This trend also applies to the construction industry. This requires that attention be focused on introducing new and more efficient solutions. Product innovations are a natural consequence of the development of new materials and their potential to be used for the purpose of improving the existing technologies and work procedures. In order for a new product to reach the market, it must undergo research and development. Analyses of modern methods of construction have paved the way for the development of a new product, i.e. a prefabricated board with built-in infrared heating. This is an innovative construction board built by joining two structural boards, with IR heating foil enclosed between them. The individual boards are connected to allow conductivity between them, forming a continuous surface finish, which, in addition to performing its standard function of a base layer (floor), also performs another function, i.e. heating.

Nine construction boards, most commonly used for floors, were compared in the research, with four different materials bases – plasterboard, gypsum plasterboard, magnesium oxide board, and

chipboard. The article presented an analysis of the results of experimental measurements focused on the surface temperature increase period of the innovative board with built-in IR heating. It is this parameter that is an important user comfort factor influencing thermal comfort in interiors. The shortest surface temperature increase period was recorded for the PB board, and the longest period was recorded for the gypsum fibreboard boards. A relation between thermal resistance and surface temperature increase period was also established. The higher the thermal resistance, the shorter the surface temperature increase period. A deviation compared to the other samples was found particularly in the case of the Thermoboard + PB board and the GKB 12.5 AK PB board. The fact that the measurements showed deviations compared to the anticipated results calls for further analysis of materials in terms of thermodynamics and the impact of IR radiation on material structure.

Acknowledgements

The article presents a partial research result of the VEGA project - 1/0677/14 “Research of construction efficiency improvement through MMC technologies”.

References

[1] Dubecký, Kozlovská. (2018). Surface temperature analysis of the board with built-in infrared heating. Pollack Periodica. Volume 13, Issue 2, Pages 27-34. ISSN 1788-1994

[2] Wilson, McGranaghan. (2014). Infrared heating comes of age. Reinforced Plastics. Volume 58, Issue 2, Pages 43-47. ISSN 0034-3617

[3] Butturini, Ngo. (2008) Flux mapping of radiant electric heaters: repeatability considerations U.S. Consumer Product Safety Commission

[4] Naos Europe. (2012). Technical datasheet. 1.6.2020, http://naoseurope.eu/wp-content/uploads/2011/05/technical_datasheet_SK-v.08.12_2012.03.27.pdf

[5] Lipták-Váradi. (2017). Indoor air quality measurements in Hungarian residential buildings. Pollack Periodica. Vol. 12, No. 2, Pages 163–172. ISSN 1788-1994

[6] Brown, Farrelly, O’Shaughnessy, Robinson. (2016). Energy efficiency of electrical infrared heating elements. Applied Energy. Volume 162, Pages 581-588. ISSN 0306-2619

[7] Far Infra Co. Ltd. (2011). Hot film. 1.6.2020, http://www.korea-heating.eu/hot-film_eng.php

[8] Naos Europe. (2012). Installation guide. 1.6.2020, http://www.fulleko.sk/pics/naos/installation_guide_SK_-_v.01.26_2012.03.27.pdf

[9] Dubecký, Kozlovská. (2017) Prefabricated board with built-in infrared heating, valid utility model SK 7722 Y1. Pages 5. Banská Bystrica: ÚPV SR

[10] Infra Sunny. (2020) Elektrické podlahové kúrenie Caleo efficient. 1.6.2020, https://infra-kurenie.com/podlahove-infra-kurenie-pre-novostavby/

DOI: 10.1515/sspjce-2020-0014

Review on Alternatives of Aggregates with Alternative Materials in Eastern Africa

Cornelius Ngunjiri Ngandu

Egerton University
Faculty of Engineering, Department of Civil and Environmental Engineering
e-mail: ngunjiri55@yahoo.com

Abstract

Normal concrete, with bulky aggregate generally results to large amount of energy and natural resource requirement. Normal aggregates mining and river sand extraction, if done in unsustainably, potentially results in adverse environmental, health or hazardous impacts. There is therefore the need to research and utilize alternative more sustainable construction materials.
This main aim is to review properties of alternative aggregate or mixes with those aggregates within Eastern Africa. In this study, 23 reviews, at optimum aggregate replacement using volcanic materials, crushed rock sand and also fired bone generally indicated good strength performance. Majority of the alternative materials mixes presented indicated higher water absorption, lower slumps/workability and density, compared with the reference. Lower slump could affect compaction, strength or increase costs. Appropriate cost-effective admixtures or plasticizers are recommended while materials exhibiting lower strengths could be explored for non-structural use. Utilization of recycled waste for aggregate could help address resource scarcity and reduce construction environmental footprint.
There should be more research and development of proper procedures and techniques so as to ensure adequate bondage, optimal water/cement ratio and compaction and also use of cost-effective admixtures.

Key words: Aggregate, sustainable construction material, review, Eastern Africa

1 Introduction

Natural materials such as aggregates, because negative environmental effects that could escalate due to over exploitation and result in massive environmental footprints. Also, normal concrete's ingredients are bulky and the transportation, processing, mixing and placing of resultant material(s) could require a significant amount of energy and costs. According to [1] study on river Kivou, Kenya, sand mining caused river channel morphometric like depth and width, lowering of water table, hence drying up of shallow water, destruction of riparian vegetation and other negative social impacts such as conflict and drug abuse. Research by [2], at Ndarugu, Kenya indicated that quarry activities had some negative impacts such as loss of

biodiversity that affected the riparian region of River Ndarugu, dust and noise pollution and also some positive impacts such as creation of employment. Therefore, there is a need to research alternative construction materials that achieve the structural requirement as well as addressing the environmental sustainability issue. Under the sustainable development goals 9, target 9.4, part of that included upgrading infrastructure and making it sustainable, with increased resource-use efficiency [3]. According to [4], there is a need for continuous research and development to ensure building materials quality and durability. Engineers and researchers need to research on and the development of proper implementation criteria on alternative construction materials that meet the demand of construction in Eastern Africa region and also reduce the resource environmental footprint.
A major challenge of collection and disposal of waste in East Africa was identified as large amounts of generated waste [5]. Incidentally, some research has been conducted on use of recyclables in construction, with materials such as recycled plastics, glass, construction waste and this could potentially address the challenges of increased waste generation, uncollected waste and demand for construction materials.

2 Review on Alternative Aggregates

Tables 1 to 5 are clustered summary based on 23 sources, for alternatives from the Eastern Africa regions, namely:- Kenya, Ethiopia, Uganda, Tanzania & Rwanda. Abbreviations and terms in the *tables* include*:* [C]-Compression; [T]-Tensile/Split Tensile; [F]-Flexural; [SL]-Slump/workability; [D]-Density; [WA]:Water absorption material or mixture/water penetration; [E]:Modulus of Elasticity; [DF]:Deflection; [CF]:Compaction Factor; [CT]-Cost; [ML]:Mass loss; [AC]:Air Content; [V]:Void; [S]:Sorption; W:Weight; V:Volume; CA:Coarse Aggregate; FA:Fine Aggregate, the terms 'Lower'/'Higher' are comparisons to control/target/design mix and 'reducing'/'higher' are variation due to increase in alternative.
Scoria, from Ethiopia used by [6] indicated some main sample composition included:- SiO_2(52.53%), Al_2O_3(15.49%) and Fe_2O_3(11%) and also fineness modulus of 3.47, bulk density weight of 1165.7kg/m^3, water absorption capacity of 0.6%. According to [7], volcanic tuff had specific gravity and water absorption of 2.29 and 16% respectively and lapilli values for the same properties were 2.53 and 10.2% respectively. [13] study indicated bulk density, specific gravity and aggregate crushing value of 882kg/m^3, 1.754 and 47% and pumice of bulk density and specific gravity of 411kg/m^3 and 0.886, sand had bulk density and specific gravity of 1422kg/m^3 and 2.625. According to [19], pumice samples had average values of specific gravity, water absorption and dry density of 1.06, 32.98% and 574.6kg/m^3. According to [18], specific gravity of crushed rock sand was 2.55, sand ranged 2.55-2.63 and water absorption of crushed rock sand averaged 2.4% and of sand ranged 1.21% – 1.83%.

Fine aggregates chemical composition from various sources in Kenya, that included natural river sand, rock sand, quarry dust and material of quarry indicated SiO_2 +Al_2O_3+CaO range of 84.3% - 92.5%, the three components impact on the setting time, early and final strengths and physical properties indicated specific gravities range of 1.73 - 2.27, bulk densities between 1327kg/m^3 – 1684kg/m^3, water absorption of range 8.3% – 15.3% and fineness modulus range of 1.92 – 3.66 [27]. According to [21], crushed ceramic fine aggregates had 16.92% water absorption compared to 5% for river sand, hence recommended that crushed ceramic be used

when saturated surface dry condition to improve concrete workability.

Table 1: Properties of alternative (a) Natural Material:- Inorganics, Rock, Volcanics

Alternative Aggregate (Batch)	Strengths (MPa)		Other Properties Mix/Agg. & (Agg. Replaced)	Source
	Control/Mix strength/Design	At Optimal replacement		
Crushed rock sand-CRS (W)	[C]: 22.5; [T]: 1.28; [F]: 588.6; [E]: 22	@20%:- [C]:23.6; [T]:1.42; [F]: 686.7; [E]: 23	[WA]: Higher; [DF]:lower; *(FA)*	[18]
Volcanic pyroclastics/tuff-vt; or lapili-l (W)	[C]: 25.6	@25%:- [C]:vt:- 27.8; l:-27.2;	[SL]: Lower(vt); Higher(l) [WA]: Higher;*(FA)*	[7]
Pumice and scoria	[C]:17	[C]:24.9 (scoria); 15.6 (pumice)	[AC]:Higher; [SL]: Medium workability; [D]:lower; *(CA)*	[13]
Pumice	Normal Aggregate		[D]:Lower; [WA] higher; *(CA)*	[19]
Scoria (W)	[C]:33.28	[C]:35.3 (35%)	[SL]: Increasing; [D]: Lower; *(FA)*	[6]
Volcanic Rock	[C]: 25 -M25	[C]: 29.6		[20]

According to [9] study, the demolished hollow concrete blocks, fine aggregate replacement had fineness modulus, unit weight and absorption capacity of 2.9%, 1229.1kg/m^3 and 6.84% with river sand fineness modulus, unit weight and absorption capacity reported at 2.78%, 1505kg/m^3 and 1.73%. Crushed clay bricks had bulk specific gravity of 2.86 and absorption capacity of 14.95% [29]. According to [12], fine reclaimed asphalt pavement indicated: SiO_2 (58.85%), CaO (2%) and Al_2O_3 (15.6%). [28] indicated loose bulk density of 1152kg/m^3 and water absorption of 5.6% for recycled concrete aggregates. Table 2 shows research on alternative aggregates classified under (b) Building Construction Waste & Quarry Dust.

Palm kernel shell (PKS) is an organic aggregate, with high pore content hence high water absorption [25]. Research by [26] of PKS from Nsukka urban, Nigeria indicated chemical composition with:- C(46.75%), H(5.92%), O(37.97%), N(0.68%), S(<0.08%) and Cl(84ppm) and also composition of structural carbohydrates mainly composed of hemicellulose (26.16%) and lignin(53.85%) and the structural properties could support its application as low cost filler for building or roadworks material. [14] used PKS from Buggala Island-Ugandu, having specific gravity of 1.4, bulk density of 582.982kg/m^3 and Aggregate crushing value (ACV) of 2.15%, with Normal Weight Aggregate(NWA) and fine aggregates had specific gravities of 2.58 & 2.44 respectively, bulk densities of 1366.23kg/m^3 and 1665kg/m^3 respectively and ACV of 17.42% for NWA. [15] study indicated specific gravities of 1.09 and 1.01, bulk densities of 553.81kg/m^3 and 554.51kg/m^3, water absorptions of 35.64% and 30.41%, ACV values of 5.37% and 5.43%, and Aggregate Impact Value (AIV) values of 6.51% and 6.77% for untreated and treated PKS respectively. [16] reported the apparent specific gravity, water absorption (24 hours), loose bulk density, ACV and AIV of PKS at 1.44, 34.07%, 515.28kg/m^3, 2.3% and 4.74% respectively and coarse aggregate ACV and AIV values of

22.69% and 15.51% respectively. Table 3 are alternative aggregates under (c) Agricultural & Sludge.

Table 2: Properties of alternative (b) Building Construction Waste & Quarry Dust

Alternative Aggregate (Batch)	Strengths (MPa)		Other Properties Mix/Agg. & *(Agg. Replaced) *fresh*	Source
	Control/Mix strength/Design	At Optimal replacement		
Crushed ceramic waste (W)	[C]:24.534 [T]:1.9	[C]:21.517 [T]:1.7	[WA]: Higher; [SL]:Lower; *(FA)*	[21]
Ceramic tile waste	[C]:22; [T]:2.82;[F]:5.67	[C]:22.88MPa (5%); [T]:3.18; [F]:5.97	[CT]:Lower; *(FA)*	[22]
Ceramic concrete	[C]:19.03	[C]:17.83@50%	[SL]:Increase then Decrease *(FA & CA)*	[31]
Demolished hollow concrete block (W)	[C] :37.5	[C]: 32.1	[D]:Lower;[SL]:Reducing; *(FA)*	[9]
Crushed clay bricks(W)	[C]:17.92;[T]:≈1.48; [F]:≈2.9;	[C]:16.46(@20%); [T]:≈1.42(@20%); [F]:≈2.58;	[D]: Lower; *(CA)*	[8]
Recycled Concrete	[C]:≈29.5;	[C]:≈28;	[SL]:Reducing; *(CA)*	[30]
Reclaimed Asphalt pavement (W)	[C]: 26.72; [T]: 2.13;	[C]:20.87 (10%); [T]: 1.87(10%);	[SL], [CF], [D],[V],[S]: Lower; *(FA & CA)*	[12]
Quarry dust	[C]: 30 (Target)	[C]: 27.661		[27]

Table 3: Properties of alternative (c) Agricultural & Sewage Sludge

Alternative Aggregate (Batch)	Strengths (MPa)		Other Properties Mix/Agg. & *(Agg. replaced)*	Source
	Control/Mix strength/Design	At Optimal replacement		
Palm Kernel Shell (V)	[C]: 38.6; [T]:≈4.8	[C]: 25%:- 33.4; [T]:≈4	[SL], [D]:Lower; [WA]:Higher; *(CA)*	[14]
Palm Kernel Shell-Lime treated	[C]: 30.44; [T]: 3	[C]: 27.03; [T]: 2.51	[SL], [D]: Lower; [WA]: Higher; *(CA)*	[15]
Kernel shell	[C]:31.3; [T]:2.1; [F]:4.25	[C]:26.5 (25%); [T]:1.8 (25%);[F]:3.139	*(CA)*	[16]
Sewage sludge	[C](RT):38.04 ; [C](ET):7.08	[C](RT):39.29 (5%); [C](ET):8.51(5%);	5% ML (@ET, 8 hours): Lower *(FA)*	[23]

RT:Room Temperature; ET:Elevated Temperature;

Research by [28] had control concrete with volcanic scoria coarse aggregates, composed mainly of SiO_2(72.755%), Al_2O_3(13.482%), CaO(1.09%), Fe(6.082%), and also partial

replacement (5% to15% weight replacement) of the scoria, using pre-coated waste plastic, from plastic papers and/or bags, by hot process. The water absorption varied with pre-coated waste plastics, from 13.06% with 0% pre-coating to 5.97% with 15% pre-coating [28]. [31] used coarse and fine rubber tyre aggregate with dry rodden densities indicated at 706kg/m^3 and 674kg/m^3 respectively, and crushing value of coarse rubber tyre aggregate at 0.02%. Table 4 shows research on alternative aggregates classified under (d) Polymers and Rubber.

Table 4: Properties of alternative (d) Polymers and Rubber

Alternative Aggregate (Batch)	Strengths (MPa)		Other Properties Mix/Agg. & *(Agg. replaced)*	Source
	Control/Mix strength/Design	At Optimal replacement		
Waste rubber tires	[C]:40.91 (C25); [C]:49.26 (C30);	@10%:- [C]:35.6-C25; [C]:42.38-C30;	[SL]: Higher; [D]:Lower; *(CA)*	[11]
Waste rubber tyres	[C]: 19.03	[C]:4.15 (@50%)	[D], [SL]:Lower *(FA)*	[17]
	[C]: 19.03	[C]:4.1 (@50%)	[D], [SL]:Lower *(CA)*	
	[C]: 19.03; [F]:3.5 [T]:2.61	[C]:2.489 (25%);[F]:1.22; [T]:1.4	[D], [SL]:Lower *(FA & CA)*	
Plastic pre-coated to scoria(W)	[C]:32.505; [F]:3.21; [T]:2.74	@5% pre-coat, [C]:35.905; [F]:3.32; [T]:2.79	[SL], [D]:Deceasing; *(CA)*	[28]

Study by [24] indicated that bone aggregates had ACV of 29%, an indication of suitability of bones as aggregates in concrete, bulk density of crushed bones of 9.18 Kn/m^3 and 19.5% water absorption for fired bones, higher than of normal aggregates. Table 5 shows research on alternative aggregates classified under (e) others: sawdust and bones.

Table 5: Properties of alternative (e) other- sawdust and bones

Alternative Aggregate (Batch)	Strengths (MPa)		Other Properties Mix/Agg. & *(Agg. replaced)*	Source
	Control/Mix strength/Design	At Optimal replacement		
Sawdust, using OPC & PPC cements (V)	[C]:22.2 -OPC	[C]:21.4 (5%)	[SL]:Decreasing>5%; [D]:Decreasing; [WA]:Increasing; [CT]:Lower-PPC; *(FA)*	[10]
	[C]:23.2 -PPC	[C]:21.8 (5%)		
Fired bones	[C]: 21.25	[C]: 32.83 (@50%)	[D]: Lower *(FA & CA)*	[24]

2.1 Density/ Weight and Lightweight

Based on Tables 1 to 5, all the 13 sources where densities- fresh, aggregate or hardened- were tabulated, indicated that the densities were lower than those of control samples or natural aggregates. This applies to across the board, (a) to (e).
Reduced density -scoria as fine aggregate partial replacement in concrete- could help reduce

self-weight for designing hence reduces sections and attain savings [6]. Lower specific gravity of tuff/lapili replacement as fine aggregate are capability of light weight concrete [7]. Reduced density could mean reduced overall weight of building, hence savings on structural elements [8]. Density reduction, with increasing proportion of sawdust as fine aggregate was attributed to lesser density of sawdust [10]. Reducing weight as rubber percentage, increase, for Partial replacement of coarse aggregate in concrete study was attributed to lower specific gravity of rubber [11], also the same reason was possible the cause for reduced density with partial replacement of reclaimed asphalt pavement (RAP) coarse and fine aggregates [12].
Lower density, using of pumice or scoria as coarse aggregate was possible due to insufficient compaction or variation in empirical mix design formulae [13]. Lower weight of mixes with Palm Kernel Shell (PKS) partial replacement of coarse aggregate was possibly due to lower specific gravity of PKS [14, 15], lower compaction [14] and lead to porous concrete [14]. Based on [16] study, partial replacement of coarse aggregate with kernel shell and use of steel tyre, beam with 25% & 50% and optimal fiber content qualified as structural lightweight concrete.
Study by [17] on partial or full replacement of aggregate with waste tyre indicated that density decrease due to lighter weight rubber tyres.

2.2 Cost

Comparative costs of mixes with saw dust replacement for fine aggregate according to [10] were lower. Study of partial replacement of ceramic tile waste by [22] also indicated lower cost. Higher demand for cement, by use of pumice or scoria as coarse aggregate could be off-set by transportation cost of normal aggregate [13]. According to [22] use of ceramic waste as replacement for fine was cheaper than natural sand. Properties suitable for aggregate replacement, usage could save cost as an alternative construction material [6]. Partial replacement of sand with sawdust indicated lower cost with partial replacement [10].

2.3 Fresh Concrete

Overall, based on tabulation in *tables 1 – 5*, mainly indicated that slumps/workability were lower compared to the control/standard/design or reducing as alternative material content increased. Slump or workability indicators, based on extracted data tabulated in *tables 1,2,3 & 4* indicated that with increasing proportion of alternative aggregate: -In group (a.) [7] indicate lower/decreasing slump- fine alternative aggregate replacement using volcano tuff- and higher for lapili and [6] indicate higher/increasing slump (fine alternative aggregate replacement using scoria) and [13] indicated medium workability- coarse alternative aggregate replacement using scoria/pumice; -In group (b) 4 sources indicated lower/reducing slumps, 2 for alternative fine aggregates replacement, 1 for alternative coarse aggregates replacement and 1 for fine & coarse aggregate alternative. [31] indicated increasing then decreasing slump with ceramic concrete coarse and fine aggregate increase; -In group (c) 2 sources indicated lower slumps, 2 for alternative coarse aggregates replacement; -In group (d) 2 sources indicated lower/decreasing slumps and 1 higher;
According to [19] grading of aggregate has an effect on workability and suitability of concrete mix, and sieve analysis test on pumice coarse aggregate showed that they compared well with normal crushed aggregates. Decreasing workability, of tuff/lapili replacement as fine

aggregate was possibly due to insufficient water to lubricate the increased surface areas [7]. Slump and workability, for replacement of fine aggregate in concrete with crushed ceramic waste was affected by water absorption of aggregate [21]. Low values (≤25mm) slump was attributed to high absorption capacity of recycled fine aggregate, due to fine materials resulting from the old mortar, for the demolished hollow concrete block as (partial) replacement [9]. According to [12] study using reclaimed asphalt pavement (RAP) as coarse and fine aggregate partial replacement, decrease slump could be due to absorption of water by fine dust around the RAP and water could have been controlled by RAP particles, and possibly not able to move freely. Study on PKS as partial replacement of coarse aggregate, workability reduction, with increase in PKS amount was possibly due to absorptive value or use of finer PKS [14, 15] and reduced workability could have resulted to lower compaction and superplasticizers (SP's) usage to improve workability was recommended [14].
Slump loss increase, with increase in proportion of sawdust as fine aggregate indicated increasing sawdust retard hydration cement reaction, possibility due to lignin in sawdust [10].

2.4 Water Absorption/penetration, Sorption & Silt Content/Fineness

A majority of the sources as tabulated in *table 1,2,3 & 5* relating to absorption/sorption, showed higher or increasing results compared to the control/standard/design.
Higher water absorption of crushed rock sand (CRS) as fine aggregate replacement, could be due to high fineness of CRS [18]. [14] study on PKS partial replacement of coarse aggregate, high water absorption could have been due to convex surface micro-tiny pores. According to [10] study on partial replacement of sand by sawdust as fine aggregate, larger surface area need more water and increasing water permeability could have been due to porous nature of sawdust, with increasing sawdust amount. High sorption of reclaimed asphalt pavement (RAP) as coarse and fine aggregate partial replacement may have been be due to melted asphalt layer for RAP aggregate and also lower absorption by RAP aggregate [12].
[22] study on ceramic tile waste replacement of fine aggregate, recommended careful selection of w/c ratio, to avoid long curing period that would increase water absorption due to clay in ceramic tiles. [9] study on demolished hollow concrete block as (partial) replacement of fine aggregate indicated significantly higher silt content compared with the desired.

2.5 Strengths, Failure and Deformation Modes

Generally most studies for (a) Inorganics, Rock, and Volcanic Materials indicated higher optimum strengths, for maximum strengths, after replacement with alternative aggregate; however, most studies in Building Construction Waste & Quarry Dust, Agricultural & Sewage Sludge and Sawdust indicated lower strength after replacement of aggregates.
Comparison between highest/optimum strengths achieved by replacement material and control/design/standard as tabulated in *tables 1 to 5*, indicated:- In cluster (a) [13] indicated higher optimum/highest strength for scoria and lower for pumice, after replacement compared to the control/design and 4 sources in this group indicated higher optimum/highest strength after replacement, hence majority of the maximum strength after replacement indicated higher strength; In cluster (b) 7 sources indicated lower strengths, for optimum/maximum strength after replacement with alternative materials, with [22] indicated higher strength; In cluster (c) 3 sources indicated lower strengths, after (partial) replacement of coarse aggregate

and [23] indicated higher maximum strength after optimal partial replacement, of fine aggregate; In cluster (d) 2 sources indicated lower strength and [28] indicated source higher strength; in (e) [24], indicated higher strength, for the highest strength after replacement and [10] indicated lower strength.
Increased strength at -partial replacement of Scoria as fine aggregate- with increase scoria (at least to some %) was attributed to inherent physical properties (less silt and clay), almost similar water absorption, less silt could have aided in better hydration and better bondage, blending with scoria enabled well-graded size distribution, increase solid volume hence better strength and formation of paste/aggregate interaction decrease due to less filler or packing effect [6]. Some additive or admixtures could improve light weight concrete strength [13].
Tensile for concrete - though low assist in crack prevention [21]. [8] study on replacement of coarse aggregate with crushed clay bricks indicated that strengths were affected by:- lower specific gravity of bricks; Strength (compressive) reduction was attributed to mortar at bricks surface cracks in aggregate itself (could happen during crushing) other factors could be density, size interlocking and aggregate rigidity; Poor bonding between paste and brick could have possibly caused lower tensile strength. Lower workability with increasing PKS as coarse aggregate and lower compaction possibly cause strength reduction [14]. According to [15], reduced tensile strength with partial replacement of PKS as coarse aggregate may have been due to poor compaction and increased surface area of lime treated PKS.
Reducing strength with increase rubber proportion may have been due to reduced solid carrying material quantity and insufficient adhesion at the rubber aggregate surface [11] - modified. Study by [17] on partial or full replacement of aggregate with waste tyre indicated:- at failure generally specimen remain intact; increased cohesiveness with increased rubber tyres, hence could sustain deformation with less compression.
According to [24], study on bone as replacement (partial or full) for fine or/and coarse aggregate, specimen with higher bone content did not disintegrate compared to those with those that had less or no bone content. A possible reason for lower strength for sand replaced samples, with sawdust is the low compression strength of sawdust, since to some extend, the aggregate strength contribute to that strength of concrete [10].

2.6 Economic, Environmental, Energy, Information & Other Considerations

Aggregate extraction process is not environmentally friendly [22]. Tuff/lapili material as (partial) replacement of aggregate in concrete could be used to replace sand & reduce environmental degradation [7]. Diversification of aggregate material could reduce environmental degradation [21]. Solution on the dual challenge-of increasing waste and natural aggregate scarcity and cost- maybe eased by environmental protection [22]. According to [8] usage of waste clay in aggregate-coarse- can address issue of environmental threat of due to waste clay and conservation of natural materials.
Scoria is widely available in Ethiopia, usage could save energy as an alternative construction material [6]. [19] recommended that pumice could be used as light weight aggregate for domestic houses, with light loading and high strength not required and the aggregate availability in Kenya could potentially be produced commercially for low lightweight concrete. [9] study on recycling demolished hollow concrete block as (partial) replacement of fine aggregate could aid in reduction of environmental pollution, and promote construction sustainability and conservation of non-recyclable natural resources. [10] on partial

replacement of sand with sawdust, could aid in addressing the non-availability of sand in Tepi, Ethiopia.
Based on [8] study, 18.72% replacement of coarse aggregate with crushed clay bricks as coarse aggregate was recommended for use in non-load bearing members e.g. walls, facades or architectural units. Study by [17] on partial or full replacement of aggregate with waste tyre indicated that it could produce material that can sustain deformation with less compression hence suitable for footpath and/or architectural finishes, if they have light unit weight. [14], recommended the use of PKS as partial replacement of coarse aggregate, for structural low-cost (cost-effective) application, potentially reducing normal weight aggregate demand hence mining and reduce environmental pollution.
Figure 1 shows the comparison for strengths, slumps/workability and water absorption based on reviews in *tables 1 to 5*, groups (a) showing studies with highest optimum strengths.

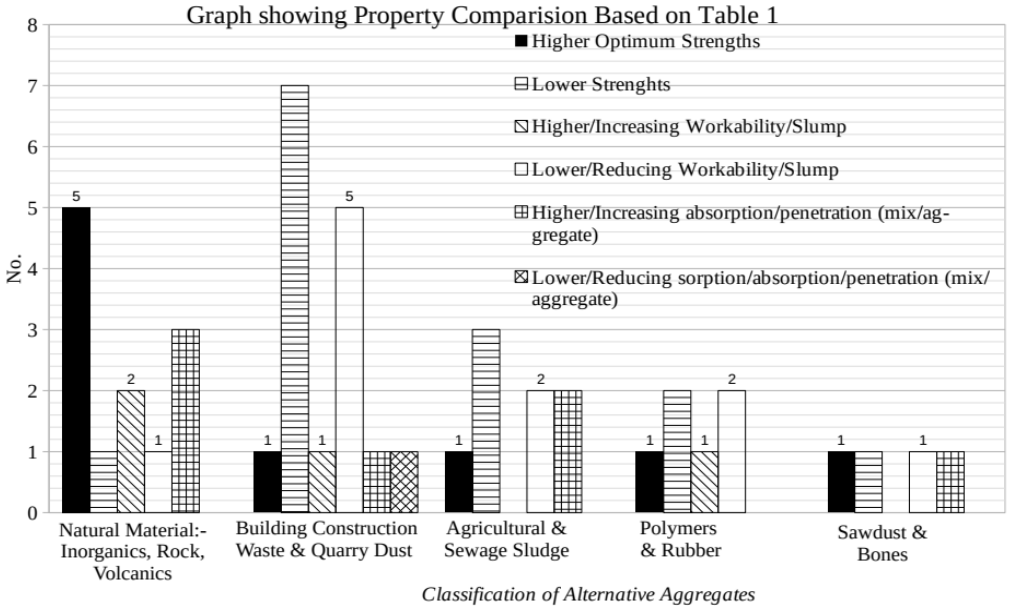

Figure 1: Property comparisons based on various clusters of aggregate types

3 Conclusion and Recommendation

Based on this review, strength performance for partial or full replacement, at optimum replacement, by use of Natural Material:- Inorganics, Rock such as scoria or rock volcano materials, had higher strengths (at optimum/maximum strength after replacement), also the same for [24] study for partial replacement of aggregate using fire bones. Hence, materials such as volcanic materials, crushed rock sand and also fired bone should be considered for aggregate replacement for structural sections concrete, at optimum replacement. However, the water absorption and density were generally lower or decreasing compared with the reference. Based on this, materials, such as rock and scoria at optimum replacement could be feasible for structural use, but adequate mix designs and standards should be developed to address issues such as water/binder ratio requirement and workability.
For (b) building construction waste & quarry dust, (c) agricultural & sewage sludge, (d) polymers and rubber and also sawdust in (e), mainly indicated generally lower or reducing

slumps with increase in alternative aggregate compared to reference value. Lower slumps/ workability could eventually affect compaction and strength. To address this, appropriate admixtures or plasticizers should be applied. Most strengths in clusters (b) to (d) were lower compared to the reference. Sustainable and large scale recycling of this materials, for structural or non-structural concrete or mortar could not only address resource scarcity but also may result to environmental benefit.

The two cost evaluation indicated that use of alternative materials for fine aggregates could result to lower cost for significantly large application. The use of alternative aggregates replacement could result to cost savings. However, with majority of studies indicating higher or increasing water absorption material, mixture, alternative aggregates or mixture/water penetration, compared to the control/standard/design, this could mean additional cost such as water, need for admixtures or need for more compaction effort or equipment.

There should be more research and development of proper procedures and techniques to ensure that particle bondage are strong, optimal water/cement ratio are achieve and compaction optimized. Further studies are required for modulus of elasticity of concrete having fired bones and the effect of fire [24] and the same for concrete or blocks where there is partial replacement of aggregates with alternative materials, having adequate strengths. There should be research and development towards a cost-effective, ready available admixture, additives and plasticizers that could be applied to improve alternative coarse and fine aggregates materials application in concrete or block making.

Acknowledgment

I acknowledge authors and publishers that have made it possible for accessibility of research used.

References

[1] Gathogo, & Amino (2017). Social-Environmental Effects of River Sand Mining: Case of Ephemeral River Kivou in Kitui County, Kenya. *IOSR Journal of Humanities and Social Science.22* (11), 31-37. DOI: 10.9790/0837-2211103137

[2] Waweru, S.W., Njoroge, J.B. & Adimo, A.O. (2018). Management Status and Perception of Post-Quarried Site in Ndarugu Kiambu, Kenya. *Africa Journal of Environmental Science and Technology*. *12* (8), 268-282. DOI: 10.5897/AJEST2018.2474

[3] United Nation Department of Economic and Social Affairs: Sustainable Development. *Building Resilient Infrastructure Promote Inclusive and Sustainable Industrialization and Foster Innovation*. Retrieved: 2020 https://sdgs.un.org/goals/goal9.

[4] Kitio (2017). Innovative Building Materials for Sustainable Construction in Africa. Topical Session Innovative Building Materials Global science & Technology Innovation Conferences. 2017: 23rd - 26th October, 2017.

[5] Aryampa, S. Maheshwari, B. Sabiili, E. Bateaanya, N.L. & Bukenya B. (2019). Status of Waste Management in East African Cities: Understand the Drivers of waste Generation, Collection and Disposal and Their Impacts on Kampala City's Sustainability. *Sustainability*. 11, 5523: DOI:10.3390/su11195523

[6] Getachew, K.W., Muge, M.D., Fekadu, F.F. & Tewodros, G. (2019). Suitability of Scoria as Fine Aggregate and its Effect in Properties of Concrete .*Suitability*, 11, 4647. DOI: 10-3390/5411174647

[7] Okwadha, G.D.O. & Ngengi, K.J. (2016). Partial Replacement of River Sand with Volcanic Pyroclastics as Fine Aggregates in Concrete Production. *IOSR-Journal of Mechanical and Civil Engineering*. *13* (5), 41-45. DOI: 10.9790/1684-1305034145

[8] Odera, B.J., Mutuku, R.N. & Kabubo, C.K. (2015). Mechanical Characteristics of Normal Concrete Partially Replaced with Crushed Clay Bricks. *International Journal of Civil Engineering and Technology (IJCIET)*. *6* (1), 62-75. http://www.iaeme.com/citearticle.asp?Ed=4478&Jtype=IJCIET&VType=6&Itype=1

[9] Nigussie, L.F., Muge, M.M. & Ghebrab, T. (2019). Recycled Fine Aggregate from Demolished Hollow Concrete Block for Green Concrete in Ethiopia. *Global Journal of Engineering Science. 3* (2): 2019. GJES.MS.ID.000559. DOI: 10.33552/GJES.2019.03.000559

[10] Lemma. *Study of Partial Replacement of Sand with Wanza Sawdust to Produce Concrete*. Msc. Thesis. Addis Ababa University, 2019. http://213.55.95.56/bitstream/handle/123456789/19551/Getish%20Lemma.pdf?sequence=1&isAllowed=y

[11] Gemeda & Alemu (2020). Water Rubber Tires: A Partial Replacement of Coarse Aggregate in Concrete Floor Tile Production. *American Journal of Civil Engineering*. *8* (3), 57-63. *DOI:* 10.11648/j.ajce.20200803.12

[12] Getahun, M.A., Shitote, S.M. and Gariy, Z.C.A. (2018). Experimental Investigation of Engineering Properties of Concrete Incorporating Reclaimed Asphalt Pavement and Rice Husk Ash. *Buildings*, 8:15 DOI:10.3390/buildings8090115

[13] Mrema & Mboya. Feasibility of LightWeight Aggregate Concrete for Structural & Non-structural Works in Tanzania [Electronic Version]. University of Dar es Salaam Research Repository- 2013.

[14] Philips, E.S., Mutuku, R.N. & Mwero, J.N. (2017). Palm Kernel Shell as Partial Replacement of Normal Weight Aggregate in Concrete. *Civil & Environmental Research (CER). 9* (11). https://iiste.org/Journals/index.php/CER/article/download/39565/40686

[15] Djima, M.O.A., Mang'uriu, G.N. & Mwero, J.N. (2018). Experimental Investigation of Lime Treated Palm Kernel Shell and Sugercane Bagasse Ash as Partial Replacement of Coarse Aggregate and Cement Respectively in Concrete. *Open Journal of Civil Engineering*, 8, 358-372. DOI:10.4236/ojce.2018.84027

[16] Dorr, B.J., Kanali C.L., & Onchiri R.O. (2019). Effects of Recycled Tyre Steel Fibres on the Compressive, Splitting Tensile and Flexural Strenghts of Structural Lightweight Concrete Using Palm Kernel Shells as Partial Replacement of Coarse Aggregates [Electronic Version]. *Civil and Environmental Research (CER), 11* (6). PP 35-41. July, 2020. Institutional repository, Technical University of Mombasa. DOI: 10.7176/CER

[17] Almaleeh, M.A., Shitote, S.M., & Nyomboi, T. (2017). Use of Waste Rubber Tyres as Aggregate in Concrete. *Journal of Civil Engineering and Construction Technology*. 8 (2), pp 11-19. DOI: 10.5897/JCECT2016.0421

[18] Mang'uriu, G.N., Karugu, C.K., Oyawa, W.O., Aboudha, S.O., & Mulu, P.U. (2013). Partial Replacement of Natural River Sand with Crushed Sand in Concrete Production [Electronic Version]. *Global Engineering and Technologist Review*. http://www.jkuat.ac.ke/departments/civil/wp-content/uploads/2013/10/1.-PARTIAL-REPLACEMENT-OF-NATURAL-RIVER-SAND-WITH-CRUSHED-ROCK-SAND-Getview-manguriuoyawa.pdf

[19] Mang'uriu, G.N., Mutuku, R.N., Oyawa, W.O. & Aboudha, S.O. (2012). Properties of Pumice

Light Weight Aggregate. *Civil and Environmental Research. 2* (10), https://iiste.org/Journals/index.php/CER/article/view/3540/3588

[20] Mutabaruka, J.D. & Pranesh, M.R. (2016). Assessing Suitability of Volcanic Rock of Rwanda as an Aggregate Based on the Engineering Characteristics. *International Journal of Civil Engineering and Technology*. *7* (6), 449-459

[21] Koech (2017). Full Replacement of Fine Aggregate in Concrete with Crushed Ceramic Waste. *Global Journal of Environmental Science and Technology*. *5* (6), 488-520.

[22] Mbereyaho, L., Amini, F., Bigirimana, F. & Isengwe R.C. (2019). The Use of Ceramic Tiles Waste in Concrete as Partial Replacement of Fine Aggregate. *Mediterranean Journal of Basic and Applied Sciences*. *3* (3). pp 122-130. http://mjbas.com/data/uploads/700011.pdf

[23] Abebaw, & Muhammed (2020). Effect of Sewage Sludge as Partial Replacement of Fire Aggregate in Concrete at Elevated Temperature: Compressive and Mass Loss Characteristic. *Global Scientific Journal.* 8 (4), pp 46-57. http://www.globalscientificjournal.com

[24] Makunza, J.K. (2014). Investigation of Fired Animal Bones as Aggregate Replacement in Concrete. RILEM International Workshop on Performance-Based Specification and Control of Concrete Durability, 11-13 June, 2014, Zagreb, Croatia.

[25] Azunnna S.U.(2019). Compressive Strength of Concrete with Palm Kernel Shell as Partial Replacement of Coarse Aggregate. *SN Appl. Sci.*1, 342. https://doi.org/10.1007/s42452-019-0334-6

[26] Okoroigwe E.C., Saffron C.M. & Kamdem P.D. (2014). Characterization of Palm Kernel Shell of Materials Reinforcement and Water Treatment. *Journal of Chemical Engineering & Material Science*. 5(1). pp 1-6. DOI: 10.5897/JCEMS 2014.0172

[27] Maina, K., Gwaya, A.O., & Koteng, D.O. (2018). Effects of Different Fine Aggregate on Concrete Strength. Proceedings of the sustainable research and innovation conference. 2-4 May 2018 (135-140). JKUAT Main Campus, Kenya.

[28] Tejiona, T.F.R. (2018). *Structural Performance of Sisal Fibers Reinforced Lightweight Concrete with Waste Plastic Pre-coat Volcanic Scoria Aggregates*. Msc. Thesis Jomo Kenyatta University of Agriculture and Technology-JKUAT, JKUAT Digital Repository.

[29] Odera, B.J. (2016). *Physical and Mechanical Properties of Normal Concrete with Recycled Clay Products and the Plastic Fibres as Coarse Aggregates.* Msc. Thesis Jomo Kenyatta University of Agriculture and Technology-JKUAT, JKUAT Digital Repository.

[30] Musembi T.M. *Laterized Quarry Dust and Recycled Concrete as Alternative Building Materials*. Msc. Thesis-2009 Jomo Kenyatta University of Agriculture and Technology-JKUAT, JKUAT Digital Repository. http://ir.jkuat.ac.ke/handle/123456789/1278/recent-submissions?offset=200

[31] Almaleeh A.M. Performance of Selected Waste Materials as Aggregates in Concrete. Msc. Thesis-2016 Jomo Kenyatta University of Agriculture and Technology-JKUAT, JKUAT Digital Repository.
http://ir.jkuat.ac.ke/bitstream/handle/123456789/4007/M.Sc.%20THESIS.pdf?sequence=1&isAllowed=y

DOI: 10.1515/sspjce-2020-0015

Methodology of Research on Transparent Wood in Architectural Constructions

Viktor Karľa

Technical University of Košice, Slovakia
Faculty of Civil Engineering, Institute of Architectural Engineering
e-mail: viktor.karla@tuke.sk

Abstract

The article describes methodology of research on transparent wood in architectural constructions which is to be held at Faculty of Civil Engineering at Technical University in Košice. The goal is to set multiple stages of research to be able to obtain samples of transparent wood of different species and to evaluate them and subsequently to design constructions suitable for the properties of the obtained material. The aim is to be for the constructions of façade systems and beams of composite cross-section, possibly with the focus on "I" section beams made of transparent wood, but different approaches will also be considered. First, the designs will be evaluated and adjusted using suitable software and after, they will be built and experimentally tested. As the technology at the university will not allow the production of full scale models, some models in scale shall be produced and evaluated in Košice during the upcoming months.

Key words: transparent wood, façade systems, composite cross-section beams, veneers, lignin, cellulose

1 Introduction

Transparent wood was first mentioned in the article Transparent Wood – A New Approach in the Functional Study of Wood Structure by German scientist Sigfried Fink in 1992 [1]. In his research he turned wood samples transparent in order to be able to better observe specific three dimensional structures of wood. In his attempt he was inspired by a Spalteholz, who in 1914 introduced a technique to make thick body organs transparent for analytical purposes using organic liquids with appropriate refractive indexes.
Between 2015 and 2016, two teams at Swedish KTH Royal Institution of Technology and at University of Maryland rediscovered Fink's invention and started their research on properties of transparent wood and suggested its possible applications for lightweight low-cost structures in light-transmitting buildings, transparent solar cell windows, furniture, or as structural material in automobiles and optoelectronics [2][3]. While at Maryland, their research of transparent wood is part of their ongoing research of super wood structures, in KTH they

focus solely on transparent wood, therefore have published more articles related to this content and have come up with interesting innovations considering the concepts of its fabrication and enhancing its properties.
So far, there are some interesting facts discovered about transparent wood and its production has been refined over the couple of years of research, but is still has its limits. Only small samples were created up until this date, but at KTH they are now recruiting more people to work on fabrication of large transparent wood samples.
Research at Technical University in Košice shall be focused on applying the newly discovered composite material in building industry in architectural constructions while considering its limits, advantages and disadvantages. All of the previous research conducted at KTH and Maryland will be considered and incorporated, so it will be possible to best tune the process of fabrication of transparent wood for the intended constructions.

2 Creation of transparent wood samples

The first stage of research at TUKE, of course, is to be creation of samples of transparent wood. Multiple veneers of various wood species and thicknesses shall be used for the creation. All of them shall be bought from a local supplier. Species considered are balsa, pine, spruce, birch, maple, ash, lime, walnut, oak and beech which are available in thicknesses of 0.60, 0.90, 1.40 and 2.50 mm. During all stages, an environmental product declaration (EPD) will be created, so it will be possible to compare transparent wood structures to those made of glass and thus to finally determine, whether constructions made of transparent wood are in reality more ecological or it is only a misleading presumption.

2.1 Lignin modification

To create transparent wood, the first step is to remove or modify lignin. As the lignin modification produces more stable samples, it was chosen as the better method for the purpose. Optical properties are very similar compared to delignification method, although slightly weaker. The great advantage of lignin modification compared to delignification is better ecology, as fewer chemicals are required to produce such samples and these samples also show better mechanical properties [4].
The lignin modification solution shall be prepared using a recipe published by KTH mixing chemicals in the following order: deionized water, sodium silicate Na_2SiO_3 (3.0 wt %), sodium hydroxide solution NaOH (3.0 wt %), magnesium sulfate $MgSO_4$ (0.1 wt %), diethylenetriaminepentaacetic acid DTPA (0.1 wt %), and then hydrogen peroxide H_2O_2 (4.0 wt %). The wood substrates will then be submerged in the solution at 70 °C until the veneers become white. The samples shall then be thoroughly washed with deionized water and kept in water until use [4].

2.2 Polymer infiltration

After lignin modification, samples will be ready for polymer infiltration to become transparent. Various kinds of polymers have been used to create transparent wood. At KTH, they mainly used poly (methyl methacrylate) PMMA, while in Maryland, they used epoxy

resins. The important factor is the refractive index of polymer, which should be close to a value of 1.61, which is the refractive index of lignin to achieve maximum transparency.
As there is another research held at Technical University in Košice using epoxy resins, they are chosen for this particular case because of their availability.
Epoxy resin will be infiltrated into lignin-modified samples using OV301 Precision Curing Oven (as it is part of the equipment of robotic laboratory at Faculty of Arts of Technical University in Košice) at a temperature specified by epoxy resin supplier under repeated vacuum and de-vacuum (the complete infiltration should be achieved after about three times the process of vacuum and de-vacuum is performed) [3].

2.3 Evaluation of obtained samples

Once the polymer will be infiltrated, the veneer samples will become transparent. At this point, the evaluation process shall begin. Their optical, thermal and mechanical properties will be researched. Optical transmittance and haze will be of interest considering optical properties. Thermal conductivity coefficient will be measured to determine thermal properties of transparent veneer samples. The steady-state technique method will be used to measure it. After consultations with authorities at the faculty, it has been determined that samples will be sent to Slovak Academy of Sciences in order to measure its thermal properties. Strength and modulus will be revealed to set their mechanical properties. For this the samples with the normative shapes are to be created and are to be tested. The samples will be evaluated for compressive strength, tensile strength and bending in all directions to determine their orthotropic properties. The standard according to which the tests are to be undertaken is EN408:2010 to determine its modulus of elasticity in bending, shear modulus, bending strength, modulus of elasticity in tension parallel to the grain, tension strength parallel to the grain, modulus of elasticity in compression parallel to the grain, compression strength parallel to the grain, modulus of elasticity in tension perpendicular to the grain, tension strength perpendicular to the grain, modulus of elasticity in compression perpendicular to the grain, compression strength perpendicular to the grain and shear strength.

3 Design of transparent wood architectural constructions

Based on the measured properties, the design of architectural constructions from transparent wood shall follow. The focus will be on façade systems and beams.

3.1 Façade systems

Transparent wood will not be suitable for the use on façades in the form of a solid wall, because the thickest achieved sample, so far, has only been of 10 mm [5]. It is possible to go slightly thicker, but not too much, as transparency in much thicker samples is unachievable, at least, at the current state of technology of production of transparent wood.
If thermal conductivity of transparent wood is considered as 0.17 W/mK (a guess based on thermal conductivity of all the components of the composite materials and their respective percentage shares), a solid transparent wood wall would have to be 285 mm thick to satisfy European standards that will come to be valid after year 2021. As 285 mm thick transparent

wood wall is not going to happen, a different approach must be taken. The inspiration might come from double and triple glazing systems with inert gases filled between transparent panes. To create transparent wood façades, an inspiration must be taken from double and triple glazing systems in order to make them valid as a construction material. To make the façade system as transparent as possible, 1.5 mm thick transparent wood panes should be used. Double pane transparent wood façade with a usual 16 mm thick layer of argon would have a U value of 1.1 W/m^{2}K. To satisfy the current standard, 18 mm thick layer should be used, but to reach the standard after 2021, a 30 mm thick layer of argon would have to be used. It is different with krypton, as only 17 mm thick layer would satisfy the standard after 2021. To satisfy the current standard, only 10 mm thick layer of krypton would be necessary. The usual thickness of krypton layer in glazing systems is 12 mm, which makes TW façade's U value of 0.82 W/m^{2}K.
Triple pane transparent wood façade with usual 16 mm thickness of argon layers would have its U value of 0.55 W/m^{2}K. This is even more efficient than the standard after 2021 requires. To satisfy this standard, only 15 mm thick layers of argon are necessary. For the current standard it would only be 9 mm thick layers of argon. With the usual 12 mm thick layers of krypton in a triple pane transparent wood façade system, the system would have its U value of 0.41 W/m^{2}K. For the satisfaction of the standard valid after 2021, only 9 mm thick layers of krypton would be necessary and to satisfy the current standard, only 5 mm thick layers of krypton would be required. All the options of façade set ups mentioned above are summarized in Table 1 [6].

Table 1: Summary of U values of different transparent wood façade set ups [6].

Facade type	**Thickness of layer(s) (mm)**			**U (W/m^{2}K)**
	Transparent wood	**Ar**	**Kr**	
Solid wall	170	-	-	1
	285	-	-	0.6
Double pane	2x1.5	16	-	1.1
	2x1.5	18	-	0.98
	2x1.5	30	-	0.59
	2x1.5	-	10	0.98
	2x1.5	-	12	0.82
	2x1.5	-	17	0.58
Triple pane	3x1.5	2x9	-	0.97
	3x1.5	2x15	-	0.59
	3x1.5	2x16	-	0.55
	3x1.5	-	2x5	0.97
	3x1.5	-	2x9	0.55
	3x1.5	-	2x12	0.41
	satisfies current EN standard			
	satisfies EN standard after 2021			

Thermal conductivity of transparent wood was considered as 0.17W/mK

Having an actual thermal conductivity value of transparent veneers might lead into different conclusions, but if it were remotely close to a predicted value, it might lead to a considerable

savings of material, as transparent wood layer could be thinner than glass and inert gasses could be used in shorter spans, therefore would be of lower volumes compared to standard glazing systems.
In a Physibel software, critical details of construction will be evaluated and final design will adapt to conclusions produced by the program. Various façade set ups might emerge during the process.

3.2 Beams

To achieve the best results, the thinnest possible elements must be incorporated into the design of beams made of transparent wood. There are few ways to achieve this. Composite cross-section beams are the most obvious solution. Firstly, "I" beams will be designed, where the web of those beams is to be made of thin transparent wood and flanges are to be made either of a laminated veneer lumber or thick transparent wood members. To achieve a better mechanical properties, the member might also be created by lamination as transparent plywood [7]. This is the lightest possible version of transparent wood beams in the means of appearance. Architectonically, a structure made using such beams would almost seem to be floating or levitating in space, which might become much desired (Figure 1) [8].

Figure 1: Transparent wood I beam rendering [8]

Another option is to create box beams. They would be created in a similar fashion as "I" beams. Flanges could again be made of laminated veneer lumber or thick transparent wood members and webs would be made of thin transparent wood panels. Again, transparent plywood can be used. These beams are not as light (although still pretty light), but can support bigger weights. The variation of the box beams is to create a Vierendeel truss (again, either by using natural or thick transparent wood) and add a thin transparent wood panels at its both sides (Figure 2). Out of all the mentioned it is a least light variant, but the firmest [8].

Figure 2: Transparent wood Vierendeel box beam rendering [8]

Transparent wood trusses are yet another way to use transparent wood structurally (Figure 3). Of course, the thicker members will have to be used to create them, but not as thick, as it would require a single massive beam. So, compared to that, it is still a lighter structure. Such trusses can be all transparent wood, or only a flange would be made of transparent wood and it would then work together with steel cable to

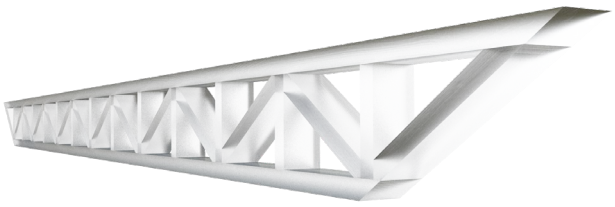

Figure 3: Transparent wood truss rendering [8]

achieve a much lighter structure overall [8].
As mentioned before, massive transparent wood beams are not possible to create, because transparency cannot be achieved in very thick samples. However, there might be a chance to create massive beams inspired by parallam structures. Parallams are created using wood stands. They are of a scale that can be turned transparent. Strands would then be bonded by the same polymer which is used in the infiltration process of polymer into lignin-modified wood. This way, even massive transparent wood beams might see the light of day.
The designs will be evaluated in software for structural analysis available at the university and modified according to the obtained results to achieve the best performance.

4 Building and testing scaled models

Once designed, façades and beams shall be built in scale, as there is not a technology at the university to create the full scale models. After, they will be tested experimentally, whether their properties match those obtained during the software analysis.
The great challenge, considering transparent wood façades will be to secure inert gasses to not leak from the construction, because it is yet unclear, whether transparent wood is not too porous for such construction. If it is, some other way will have to be thought of to make transparent wood façades possible or first, to create delignified samples for the façades and test the leakage. In the case leakage would not be a problem, critical details will be tested in climatic chamber and/or in situ.
Beams in scale will be evaluated in the VUKONZE laboratories at Technical University in Košice and their mechanical properties shall be put to the test.

5 Conclusion

Transparent wood is still a very new material with properties that have still not been fully researched. The research of its applications in architectural constructions has never been done before, but its properties and appearance predetermine it for such use. This is why this research is to be undertaken at Technical University in Košice in the near future. The research shall be done methodologically as described in this article focused on façade and beam constructions. Its results will then be reviewed and published.

Acknowledgements

This contribution is supported by the Scientific Grant Agency and project KEGA 046TUKE-4/2019 supported by the Cultural Grant Agency of the Ministry of Education, Science, Research and Sport of the Slovak Republic and the Slovak Academy of Sciences. This paper was elaborated with financial support project with ITMS code: 26220220182 (TECHNICOM).

References

[1] Fink, S. (2009). Transparent Wood – A New Approach in the Functional Study of Wood Structure. Holzforschung - International Journal of the Biology, Chemistry, Physics and Technology of Wood, 46(5), pp. 403-408.

[2] Yuanyuan Li, Qiliang Fu, Shun Yu, Min Yan, and Lars Berglund, Optically Transparent Wood from a

Nanoporous Cellulosic Template: Combining Functional and Structural Performance, *Biomacromolecules* 2016 *17* (4), 1358-1364,

[3] Mingwei Zhu, Jianwei Song, Tian Li, Amy Gong, Yanbin Wang, Jiaqi Dai, Yonggang Yao, Wei Luo, Doug Henderson, Liangbing Hu (2016), Highly anisotropic, highly transparent wood composites. Advanced Materials, 28(26), 5181–5187

[4] Li, Y., Fu, Q., Rojas, R., Yan, M., Lawoko, M., & Berglund, L. (2017). A new perspective on transparent wood: Lignin-retaining transparent wood. ChemSusChem.

[5] Li, Y., Yang, X., Fu, Q., Rojas, R., Yan, M., & Berglund, L. (2018). Towards centimeter thick transparent wood through interface manipulation. Journal of Materials Chemistry A, 6(3), 1094-1101.

[6] Karľa, V., (2019) Update of Research on Transparent Wood, YS2019 - Young Scientist 2019: proceedings of the 11th International Scientific Conference of Civil and Environmental Engineering for PhD. Students and Young Scientists. - Bristol (UK): IOP Publishing p. 1-8 [online]. - ISSN 1757-8981.

[7] Fu, Q., Yan, M., Jungstedt, E., Yang, X., Li, Y., & Berglund, L. A. (2018). Transparent plywood as a load-bearing and luminescent biocomposite. Composites Science and Technology.

[8] Katunský, D., Kanócz, J., Karľa, V., (2018) Structural Elements with Transparent Wood in Architecture, International Review of Applied Sciences and Engineering = IRASE. - Budapest (Hungary): Akadémiai Kiadó Roč. 9, č. 2 (2018), s. 101-106 [print]. - ISSN 2062-0810

DOI: 10.1515/sspjce-2020-0016

Equilibrium isotherm studies of copper and zinc removal from model solutions using natural and alkaline treated hornbeam sawdust

Zdenka Kováčová[1], Štefan Demčák[2], Magdaléna Bálintová[1]

[1]Technical University of Košice, Faculty of Civil Engineering, Institute of Environmental Engineering, Slovakia
e-mail: zdenka.kovacova.2@tuke.sk, magdalena.balintova@tuke.sk
[2] University of Prešov, Faculty of Management, Department of Environmental Management, Slovakia
e-mail: stefan.demcak@unipo.sk

Abstract

In the present study, sawdust an industrial by-product available in large quantities as sorbent material was studied. The removal adsorption capacity of Cu(II) and Zn(II) from aquatic solutions was obtained. The batch experiments were carried out to determine the effect of initial concentration of copper/zinc solution at pH=4.0 onto natural hornbeam and hornbeam modified with NaOH and KOH. The Fourier transform infrared spectroscopy (FTIR) determined the changes in functional groups after the modification of sawdust. The equilibrium data were fitted with four isotherm models - Langmuir, Freundlich, Tempkin and Dubinin–Radushkevich. The Langmuir model was found to be most suitable and the maximum adsorption capacity obtained for modified hornbeam sawdust was 2 to 4-times higher as in natural one for both heavy metals.

Key words: copper, zinc, sorption, wooden sawdust, adsorption isotherm, FTIR spectroscopy

1 Introduction

In the last decades, the chemical and biological pollution of water sources has become a serious environmental problem affecting people's health. The pollution of water can be released naturally by geological and biological activity, but the human activity associated with urban development, energy use, pesticides and fertilizers, industrial waste, sewage water, mining and others has a significant impact on environmental contamination [1-3].
Wastewaters from industry production can be harmful and caused severe and long-time issues for surface and underground water sources due to significant low value of pH and increased concentration of heavy metals that transcends many times the maximum acceptable concentration defined by legal regulations (SR Government Regulation 269/2010 Coll. which stipulates criteria for achieving good water balance – limit values for zinc and copper discharged waste water are 2.0 and 0.5 mg/L, respectively) [4, 5] .
The conventional methods using for heavy metals removal from wastewaters are reverse

osmosis, precipitation, ion exchange, chemical oxidation or reduction, ultrafiltration, extractions, electrodialysis. These techniques can be sensitive to operation conditions, produce of a large amount of sludge, and have high cost and energy consumption [6-8]. The adsorption onto low-cost sorbents can be a promising technique for removal of pollutants from aquatic solutions because it's effective, cheap and environmental friendly. The natural materials, industrial and agricultural waste products have potential to be used as sorbents due to their low price, availability in large quantities and easy disposed without long regeneration [9]. Lots of low cost materials such as cocoa shells [10], cashew nut shells [11], cactus leaves and pine needles [12], green tea waste [13], olive stone [14], rice husk [15], zeolite [16], juniper bark [17], sawdust [18] are investigated as a sorbents for the removal of heavy metals.
The wooden sawdust is one of the most attractive agricultural by-products available in large quantities in lumber mills as solid waste. It consists mainly of lignin, cellulose and hemicelluloses, which easily traps impurities present in wastewater [19-21].
The aim of this paper has been to determine the sorption capacity of hornbeam sawdust in its natural and chemically activated state using potassium and sodium hydroxide to adsorb Cu(II) and Zn(II) from aquatic solutions. Both kinds of sawdust were characterized by FTIR spectroscopy to determine functional groups involved in the process of adsorption. The experimental data are fitted to the Langmuir, Freundlich, Tempkin and Dubinin–Radushkevich isotherm with the purpose to find best model describing process.

2 Materials and methods

2.1 Sawdust preparation

The raw hornbeam sawdust (particle size less than 2.0 mm) was obtained from locally available wood and used in the experiments.
Chemical modifications of sorbent were realized using 200 mL of 1.0 M solution of hydroxide sodium/potassium with 20 g of hornbeam sawdust for 24 h. Subsequently the sawdust was filtered, washed with demineralised water and dried.

2.2 Metal solution preparation

The stock solution of copper and zinc were prepared by dissolving predefined amounts of copper sulfate pentahydrate ($CuSO_4 \cdot 5H_2O$) and zinc sulfate heptahydrate ($ZnSO_4 \cdot 7H_2O$), respectively in distilled water to achieve concentration of 10,000 mg/L in each flask. The initial concentrations (10, 30, 50, 70, 110, 130 and 150 mg/L) of Cu(II) and Zn(II) were obtained by diluting the stock solution. The initial concentration was chosen based on previous research of Bulut and Tez [22] and kinetic study realized in previous research [23]. The pH was adjusted using 0.1 M sulfuric acid to the value 4.0.

2.3 Experimental procedures

Sorption assays were carried out at constant temperature by adding 0.5 g of hornbeam wood sawdust with or without modification to the breakers containing 50 mL of copper/zinc

synthetic solution. The suspensions in all sorption experiments were left for 24 h and then filtered through filtrate paper. Initial and final concentrations of Cu(II) and Zn(II) were determined by Colorimeter DR 890 (HACH LANGE, Germany). The final pH value was measured by FiveGo pH meter FG2 (Mettler Toledo, Switzerland).
The amount of heavy metals removal by the hornbeam sawdust and the percentage removal of were calculated by the following Equations (1) and (2), respectively.

$$q = \frac{(C_o - C_e) \cdot V}{m} \tag{1}$$

$$\%\, Efficiency = \frac{(C_0 - C_e) \cdot 100}{C_o} \tag{2}$$

where, q is the sorption capacity (mg/g), C_0 and C_e are the initial and equilibrium concentration (mg/L), V is the volume of solution in mL and m is the total amount of sawdust (g).

2.4 FTIR spectroscopy

Fourier transform infrared spectroscopy is using for:

- studying wood decay chemistry,
- characterizing the chemistry of wood,
- determination of lignin content in pulp and wood and
- analysis of chemical and structural changes in wood components due to NaOH and KOH treatments [24].

The FTIR spectroscopy of the natural and modified wood sawdust was recorded in Bruker Alpha Platinum-ATR spectrometer (BRUKER OPTICS, Germany) with the wavenumber ranging of 4000 to 400 cm^{-1} to observe functional groups involved in decontamination process. FTIR analysis was performed to investigate the reaction the change of the functional groups of sawdust due to base modification.

2.5 Adsorption models

Adsorption isotherms express the relationship between the concentration of a contaminant in a liquid and the amount of that contaminant bound to a unit weight of sorbent at a constant temperature. They are important to describe the mechanism of elimination process and to obtain the adsorption capacity of sorbent for contaminates removal. In general, all sorption models are characterized by specific constants that represent the surface properties and the affinity of the tested sorbents materials towards pollutant removal.
Four isotherm models Langmuir, Freundlich, Tempkin and Dubinin–Radushkevich (D-R) are described in the following sections, where the differences between them and the significance of the characteristic parameters of each sorption model are indicated.

2.5.1 Langmuir isotherm

The Langmuir isotherm [25] is used in case of homogenous monomolecular layer adsorption. This model assumes the same affinity at all adsorption sites and that sorption at one site does not affect adsorption at an adjacent site. The maximum adsorption capacity is obtained from complete coverage of the adsorbent surface in monolayer and is given by the Eq. (3):

$$q_e = \frac{q_m \cdot K_L \cdot C_e}{1 + K_L \cdot C_e} \tag{3}$$

where q_e is amount of metal ions adsorbed per specific amount of adsorbent (mg/g), C_e is equilibrium concentration (mg/L), q_m is quantity of heavy metal ions necessary to form a single monolayer on unit mass of sorbent (mg/g) and K_L is Langmuir equilibrium constant which is related to the apparent energy of sorption process (dm^3/mg).
The separation factor R_L indicates the isotherm shape and is given by Eq. (4):

$$R_L = \frac{1}{1 + K_L \cdot C_0} \tag{4}$$

where C_o is initial concentration of contaminant in solution. The values of separation factor are in Table. 1.

Table 1 Values of sorption factor

Separation factor	Sorption process
$R_L = 0$	irreversible
$0 < R_L < 1$	favourable
$R_L = 1$	linear
$R_L > 1$	unfavorable

2.5.2 Freundlich isotherm

Freundlich isotherm [26] considered empirical isotherm assumes that the ratio of the amount of solute bound onto a given quantity of sorbent at different solute concentrations is not constant. In many processes, the heat of adsorption decreases with increasing the extent of adsorption. For sorption from solution, the isotherm is expressed by Eq. (5).

$$q_e = K_F \cdot C_e^{1/n} \tag{5}$$

where K_F is Freundlich equilibrium constant which describe the relative sorption capacity related to the bonding energy ($(mg/g)\cdot(L/mg)^{1/n}$) and n is Freundlich coefficient the or heterogeneity factor which indicates the deviation from linearity of process.

2.5.3 Tempkin isotherm

Tempkin isotherm [27] equation assumes that the heat of sorption of all the molecules in the layer decreases linearly with the coverage of molecules and the process of adsorbate is evenly distributed. Unlike the Freundlich isotherm, the decrease in heat of adsorption is more linear than logarithmic and is given by Eq. (6):

$$q_e = \frac{R \cdot T}{b_T} \cdot \ln(A_T \cdot C_e) \tag{6}$$

where T is the absolute temperature (K), R is the universal gas constant (8.314 J/ mol·K), b_T is the constant which is related to the heat of sorption (J/mol), K_T is the equilibrium constant which describes the maximum binding energy (dm^3/mg).

2.5.4 Dubinin–Radushkevich (D-R) isotherm

Dubinin and Radushkevich [28] (D-R) isotherm is applied to estimate the free energy of sorption (E), if 0 < E < 16 kJ/mol is the physical adsorption and if E > 16 kJ/mol chemisorption prevails. The form of D–R equation is given by Eq. (7):

$$q_e = q_m \cdot exp(-K_{D-R} \cdot \varepsilon^2) \tag{7}$$

where K_{D-R} (mol^2/kJ^2) is a constant which describe the adsorption energy and ε can be calculated from Eq. (8):

$$\varepsilon = R \cdot T \cdot \ln\left(1 + \frac{1}{C_e}\right) \tag{8}$$

3 Results and discussion

3.1 Infrared spectra

The heavy metal removal from contaminated aquatic solutions by natural sorbents as sawdust is closely linked to the surface structure where functional groups such as –OH, –COOH, –NH, –NH2, and –NH3 are presented [18].

The FTIR spectrum of natural and modified sawdust with NaOH and KOH are shown in Figure 1. The alkaline treatment with NaOH significantly intensified the wide peak of the hydroxyl functional group results in stretching at wavenumber 3331 cm^{-1}.

The band at 2892 cm^{-1} corresponded to the C–H stretch. Presence of C=O from the acetyl groups at 1731 cm^{-1} band was attributed to the characteristic of the hemicelluloses. Some new strong peak at 1593 cm^{-1} was attributed to the C–C stretch and that at 1320 cm^{-1} to the C–O stretch. The band at 1690 cm^{-1} represents aldehydes and ketones.

Aromatic skeletal vibrations in the lignin components were assigned to 1503, 1454, 1321 cm^{-1}. The absorbance near 1422, 1369, 1321, 1156 and 1031 and 897 cm^{-1} was attributed to the cellulose. Wavenumbers at 830 cm^{-1} were determined as functional groups of aromatics, carboxylic acids and alkyl halides [29-31].

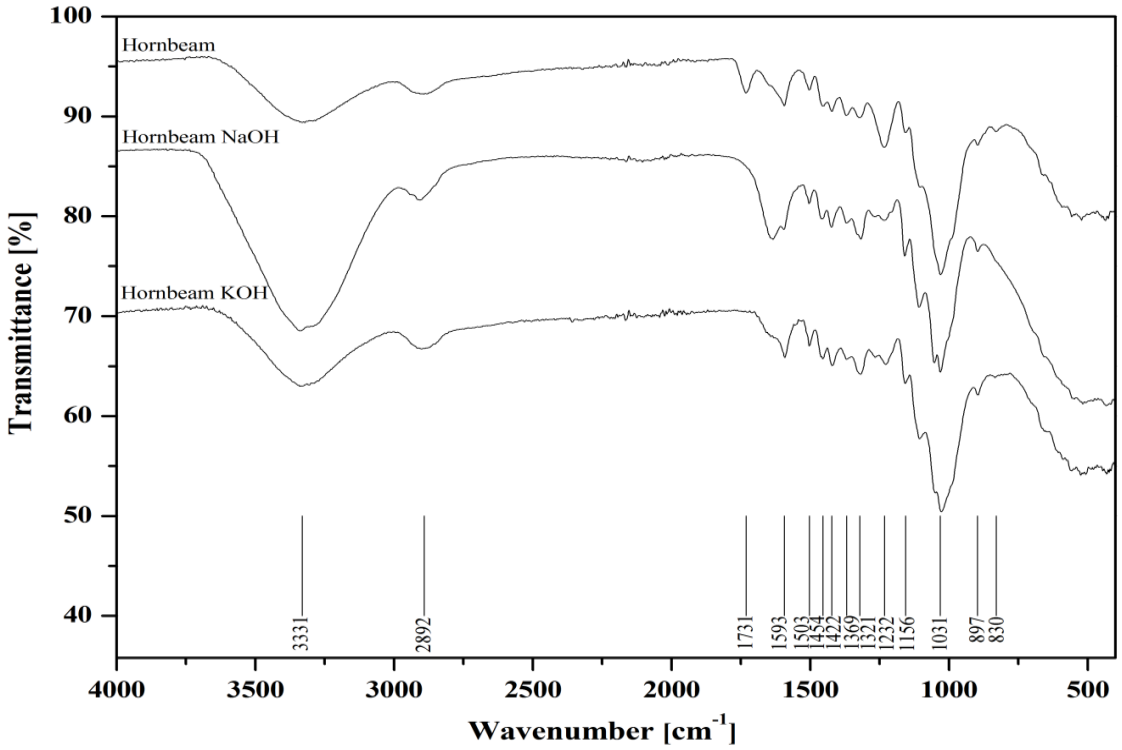

Figure 1 FTIR spectrum of raw and modified sawdust

3.2 Sorption isotherm study

Sorption isotherms are important to describe the mechanism of elimination process and to obtain the adsorption capacity of sorbent for contaminates removal. In general, all sorption models are characterized by specific constants that represent the surface properties and the affinity of the tested sorbents materials towards pollutant removal. The isotherm data using the Langmuir, Freundlich, Temkin and Dubinin-Radushkevich equation for copper and zinc removal are shown in Figure 2. Table 2 shows the values of corresponding isotherm parameters together with their correlation coefficients (R^2).

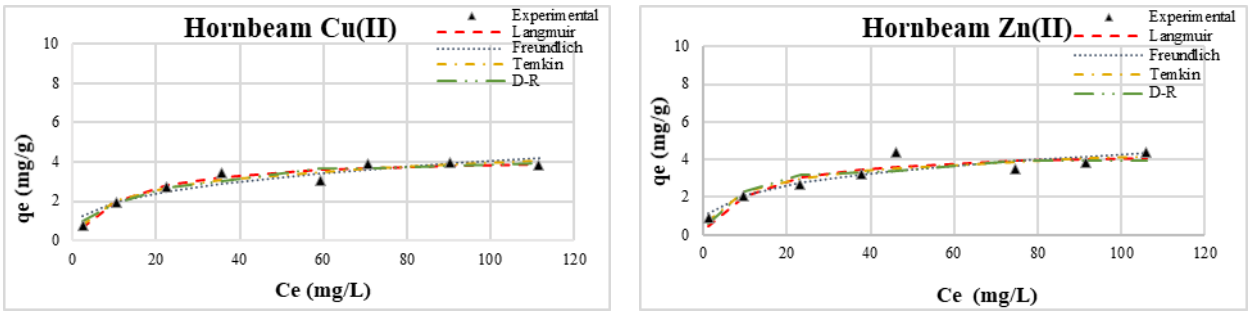

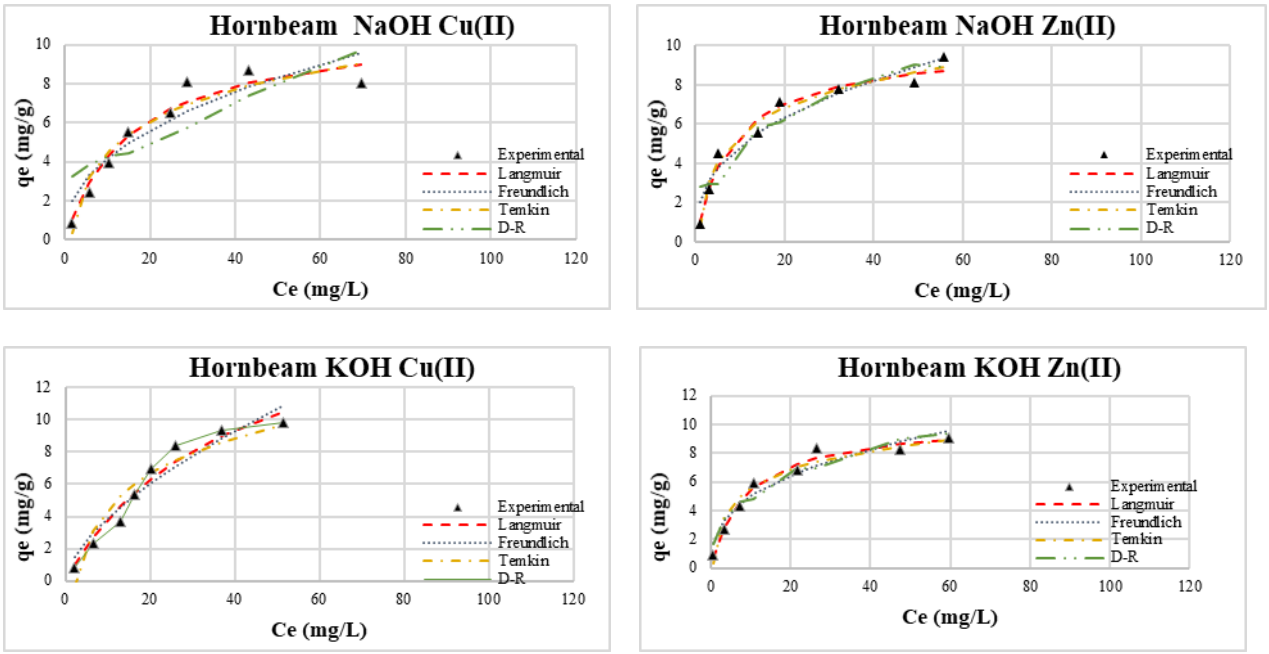

Figure 2 Isotherm data of natural and modified hornbeam sawdust

Correlation coefficient (R^2) (Figure 2 and Tables 2 & 3) are derived by fitting experimental data into the Langmuir, Freundlich, Temkin and the Dubinin-Radushkevich isotherm model. The highest value of R^2 for copper was reached by hornbeam (0.956), hornbeam NaOH (0.954) and hornbeam KOH (0.964) fitting to Langmuir model. In case of zinc adsorption the highest values of R^2 was achieved by hornbeam (0.889), hornbeam NaOH (0.978) and hornbeam KOH (0.082) following Langmuir isotherm.

Table 2 Isotherm constants for isotherm models sawdust for adsorption of Cu(II) on sawdust

Model	Parameter	Sawdust		
		Hornbeam	Hornbeam NaOH	Hornbeam KOH
Langmuir	q_m (mg/g)	4.318	11.064	18.181
	K_L (dm^3/mg)	0.082	0.062	0.027
	R^2	0.956	0.954	0.964
Freundlich	K_F ((mg/g)(L/mg)$^{1/n}$)	0.944	2.282	0.905
	n	3.167	1.568	1.583
	R^2	0.903	0.867	0.931
Tempkin	K_T (dm^3/mg)	1.101	0.682	0.400
	b_T (J/mol)	1.934	5.378	7.383
	R^2	0.950	0.875	0.920
Dubinin–Radushkevich	q_m (mg/g)	4.170	12.537	10.429
	K_{D-R} (mol^2/KJ^2)	0.114	0.073	28.643
	R^2	0.922	0.675	0.957

Table 3 Isotherm constants for isotherm models sawdust for adsorption of Zn(II) on sawdust

Model	Parameter	Sawdust		
		Hornbeam	Hornbeam NaOH	Hornbeam KOH
Langmuir	q_m (mg/g)	4.539	10.015	10.309
	K_L (dm^3/mg)	0.086	0.120	0.110
	R^2	0.889	0.978	0.982
Freundlich	K_F ((mg/g)(L/mg)$^{1/n}$)	1.075	2.015	2.125
	n	3.329	2.612	2.713
	R^2	0.869	0.945	0.936
Tempkin	K_T (dm^3/mg)	1.998	1.471	1.873
	b_T (J/mol)	1.790	4.648	4.361
	R^2	0.884	0.971	0.957
Dubinin–Radushkevich	q_m (mg/g)	4.196	11.608	11.550
	K_{D-R} (mol^2/KJ^2)	0.077	0.044	0.042
	R^2	0.826	0.864	0.919

As shown, the values of maximum adsorption capacity for Cu(II) removal determined using Langmuir model was 4.318, 11.064 and 18.181 mg/g for hornbeam, hornbeam NaOH and hornbeam KOH, respectively. For zinc removal was maximum adsorption capacity, and for hornbeam (4.539 mg/g), hornbeam NaOH (10.015 mg/g) and hornbeam KOH (10.309 mg/g). The values correspond closely to the Langmuir model, which indicates the copper and zinc removal process might be realized as the monolayer adsorption and dominate ion exchange mechanism [22]. From the results (Tables 2&3) it can be assumed that the adsorption ability for cooper is better as zinc one in case of alkaline treated sawdust, the similar results was publicized by Bozic et al [3].

4 Conclusion

Utilization of wooden sawdust for the removal of Cu(II) and Zn(II) from the synthetic solutions was investigated. Sawdust was found to be a promising adsorbent because consist of lignin, cellulose and hemicelluloses which are capable of catch pollutants from waters.
FTIR spectra demonstrated the existence of groups responsible for heavy metal ions binding, where NaOH modification intensified the wide peak of the strong broad -OH stretching at wavenumber 3331 cm^{-1}. The equilibrium adsorption data was fitted with four isotherm models - Langmuir, Freundlich and Tempkin, Dubinin–Radushkevich. The equilibrium data are best fitted with Langmuir isotherm model (due to highest value of R^2) which confirms the monolayer adsorption of heavy metals ions onto the natural and modified hornbeam sawdust.
The treatment with NaOH and KOH increased the sorption capacity for both metals from 2.5 to 4.2 times for copper and about 2.2-times for zinc in comparison to untreated sawdust.
The maximum adsorption capacity for Cu(II) is obtained with the Langmuir isotherm model as 4.318 mg/g, 11.064 mg/g and 18.181 mg/g for hornbeam, hornbeam NaOH and hornbeam KOH, respectively. The adsorption capacity is better with modified sawdust as in natural one. In case of zinc removal, the maximum adsorption capacity was reached by Langmuir isotherm for hornbeam (4.539 mg/g), hornbeam NaOH (10.015 mg/g) and hornbeam KOH (10.309 mg/g). Hornbeam sawdust with modification of NaOH and KOH can be used as sorbent to

copper and zinc removal from aquatic environments.

Acknowledgements

This article was elaborated in the framework of the project VEGA - Scientific Grant Agency of the Ministry of Education, Science, Research and Sport of the Slovak Republic and the Slovak Academy of Sciences, grant number 1/0419/19. The work has been supported by GAMA - Grant Agency for Research in Management at the Faculty of Management of University of Prešov in Prešov (GAMA/20/3).

References

[1] Pavolová, H., Lacko, R., Hajduová, Z., Šimková, Z., & Rovňák, M. (2020). The Circular Model in Disposal with Municipal Waste. A Case Study of Slovakia. *International Journal of Environmental Research and Public Health*, 17(6), 1839. https://doi.org/10.3390/ijerph17061839

[2] Crini, G., & Lichtfouse, E. (2019). Advantages and disadvantages of techniques used for wastewater treatment. *Environmental Chemistry Letters*, *17*(1), 145–155. https://doi.org/10.1007/s10311-018-0785-9

[3] Očenášová, M., Seňová, A., Pavolová, H., Rovňák, M., & Muchová, M. S. (2020). A Systematic Approach to Occupational Safety and Health Focusing on Prevention of Damaging Aspects and Risk Categories in Mining Company. In *New Approaches in Management of Smart Manufacturing Systems* (pp. 187-206). Springer, Cham. https://doi.org/10.1007/978-3-030-40176-4_12

[4] Božić, D., Gorgievski, M., Stanković, V., Štrbac, N., Šerbula, S., & Petrović, N. (2013). Adsorption of heavy metal ions by beech sawdust – Kinetics, mechanism and equilibrium of the process. *Ecological Engineering*, *58*, 202–206. https://doi.org/10.1016/j.ecoleng.2013.06.033

[5] SR Government Regulation 269/2010 Coll. which stipulates criteria for achieving good water balance – limit values for zinc and copper discharged waste water

[6] Abdel-Ghani, N. T., El-Chaghaby, G. A., & Helal, F. S. (2013). Simultaneous removal of aluminum, iron, copper, zinc, and lead from aqueous solution using raw and chemically treated *African beech* wood sawdust. *Desalination and Water Treatment*, *51*(16–18), 3558–3575. https://doi.org/10.1080/19443994.2012.750806

[7] Renu, Agarwal, M., & Singh, K. (2017). Heavy metal removal from wastewater using various adsorbents: A review. *Journal of Water Reuse and Desalination*, *7*(4), 387–419. https://doi.org/10.2166/wrd.2016.104

[8] Pavan Kumar, G. V. S. R., Malla, K. A., Yerra, B., & Srinivasa Rao, K. (2019). Removal of Cu(II) using three low-cost adsorbents and prediction of adsorption using artificial neural networks. *Applied Water Science*, *9*(3), 44. https://doi.org/10.1007/s13201-019-0924-x

[9] Tribedia, P., Singh, S., & Pandey, L. (2015). Removal of zinc from synthetic waste water by saw dust as an adsorbent. *International Journal of Innovative Science, Engineering & Technology, 2*(6), 120-127.

[10] Meunier, N., Laroulandie, J., Blais, J. F., & Tyagi, R. D. (2003). Cocoa shells for heavy metal removal from acidic solutions. *Bioresource Technology*, *90*(3), 255–263. https://doi.org/10.1016/S0960-8524(03)00129-9

[11] Kumar, P. S., Ramalingam, S., Kirupha, S. D., Murugesan, A., Vidhyadevi, T., & Sivanesan, S. (2011). Adsorption behavior of nickel(II) onto cashew nut shell: Equilibrium, thermodynamics, kinetics, mechanism and process design. *Chemical Engineering Journal*, *167*(1), 122–131. https://doi.org/10.1016/j.cej.2010.12.010

[12] Dakiky, M., Khamis, M., Manassra, A., & Mer'eb, M. (2002). Selective adsorption of chromium(VI) in industrial wastewater using low-cost abundantly available adsorbents. *Advances in Environmental Research*, *6*(4), 533–540. https://doi.org/10.1016/S1093-0191(01)00079-X

[13] Yang, S., Wu, Y., Aierken, A., Zhang, M., Fang, P., Fan, Y., & Ming, Z. (2016). Mono/competitive adsorption of Arsenic(III) and Nickel(II) using modified green tea waste. *Journal of the Taiwan Institute of Chemical Engineers*, *60*, 213–221. https://doi.org/10.1016/j.jtice.2015.07.007

[14] Moubarik, A., & Grimi, N. (2015). Valorization of olive stone and sugar cane bagasse by-products as biosorbents for the removal of cadmium from aqueous solution. *Food Research International*, *73*, 169–175. https://doi.org/10.1016/j.foodres.2014.07.050

[15] Krishnani, K. K., Meng, X., Christodoulatos, C., & Boddu, V. M. (2008). Biosorption mechanism of nine different heavy metals onto biomatrix from rice husk. *Journal of Hazardous Materials*, *153*(3), 1222–1234. https://doi.org/10.1016/j.jhazmat.2007.09.113

[16] Holub, M., & Balintova, M. (2014). Using of zeolite for copper and zinc removal under acidic conditions. *Pollack Periodica*, *9*, 141–149. https://doi.org/10.1556/Pollack.9.2014.2.14

[17] Shin, E. W., Karthikeyan, K. G., & Tshabalala, M. A. (2007). Adsorption mechanism of cadmium on juniper bark and wood. *Bioresource Technology. Vol. 98 (2007): Pages 588-594.* https://www.fs.usda.gov/treesearch/pubs/27105

[18] Demcak, S., Balintova, M., Demcakova, M., Csach, K., Zinicovscaia, I., Yushin, N., & Frontasyeva, M. (2019). Effect of alkaline treatment of wooden sawdust for the removal of heavy metals from aquatic environments. *DESALINATION AND WATER TREATMENT*, *155*, 207–215. https://doi.org/10.5004/dwt.2019.24053

[19] Memon, S. Q., Memon, N., Solangi, A. R., & Memon, J.-R. (2008). Sawdust: A green and economical sorbent for thallium removal. *Chemical Engineering Journal*, *140*(1–3), 235–240. https://doi.org/10.1016/j.cej.2007.09.044

[20] Shukla, A., Zhang, Y.-H., Dubey, P., Margrave, J. L., & Shukla, S. S. (2002). The role of sawdust in the removal of unwanted materials from water. *Journal of Hazardous Materials*, *95*(1–2), 137–152. https://doi.org/10.1016/S0304-3894(02)00089-4

[21] Argun, M. E., Dursun, S., Ozdemir, C., & Karatas, M. (2007). Heavy metal adsorption by modified oak sawdust: Thermodynamics and kinetics. *Journal of Hazardous Materials*, *141*(1), 77–85. https://doi.org/10.1016/j.jhazmat.2006.06.095

[22] Bulut, Y., & Tez, Z. (2007). Removal of heavy metals from aqueous solution by sawdust adsorption. *Journal of Environmental Sciences*, *19*(2), 160–166. https://doi.org/10.1016/S1001-0742(07)60026-6

[23] Kovacova, Z. (2019). Study of zinc removal from water solutions using hornbeam wooden sawdust. *IOP Conference Series: Materials Science and Engineering*, *566*, 012019. https://doi.org/10.1088/1757-899X/566/1/012019

[24] Bodirlau, R., & Teaca, C. (2009). Fourier transform infrared spectroscopy and thermal analysis of lignocellulose fillers treated with organic anhydrides. 54, 93–104.

[25] Langmuir, I. (1918). THE ADSORPTION OF GASES ON PLANE SURFACES OF GLASS, MICA AND PLATINUM. *Journal of the American Chemical Society*, *40*(9), 1361–1403. https://doi.org/10.1021/ja02242a004

[26] Freundlich, H.M. (1906) Over the Adsorption in Solution. Journal of Physical Chemistry A, 57, 385-470.

[27] Tempkin, M. J., & Pyozhev, V. (1940). *Kinetics of ammonia synthesis on promoted iron catalyst*. Acta Physiochim URSS *12*, 217-222.

[28] Dubinin, M.M. and Radushkevich, L.V. (1947) The Equation of the Characteristic Curve of Activated Charcoal. Proceedings of the Academy of Sciences, Physical Chemistry Section, 55, 331.

[29] Owen, N. L., & Thomas, D. W. (1989). Infrared Studies of “Hard” and “Soft” Woods. *Applied Spectroscopy*, *43*(3), 451–455. https://doi.org/10.1366/0003702894202760

[30] Zhu, G., Xing, X., Wang, J., & Zhang, X. (2017). Effect of acid and hydrothermal treatments on the dye adsorption properties of biomass-derived activated carbon. *Journal of Materials Science*, *52*(13), 7664–7676. https://doi.org/10.1007/s10853-017-1055-0

[31] Demcak, S., Balintova, M., Hurakova, M., Frontasyeva, M. V., Zinicovscaia, I., & Yushin, N. (2017). Utilization of poplar wood sawdust for heavy metals removal from model solutions. *Nova Biotechnologica et Chimica*, *16*(1), 26–31. https://doi.org/10.1515/nbec-2017-0004

DOI: 10.1515/sspjce-2020-0017

Recycled aggregate amount variation of fraction 4/8 mm and 8/16 mm in the concrete mixture

Jozef Junák and Natália Junáková

Technical University of Košice, Slovakia
Faculty of Civil Engineering, Institute of Environmental Engineering
e-mail: jozef.junak@tuke.sk, natalia.junakova@tuke.sk

Abstract

The introductory part of the paper is devoted to the classification of aggregates according to various criteria, one of them is the geographical origin of aggregates. From the point of view of the circular economy, the use of recycled aggregates comes to the fore, mainly from the ecological point of view but also from the economic point of view.
The paper summarizes the results of research focused on the variation of the amount of 2 Recycled concrete aggregate fractions in concrete, followed by an evaluation of the effect of the presence of recycled material in the mixture on the selected property, specifically compressive strength. The highest compressive strength 34.7 MPa after 28 days hardening reached sample containing 100% recycled fraction 4/8 mm, and 60% recycled fraction 8/16 mm. This value is only slightly different from the compressive strength of the reference sample (34.4 MPa).

Key words: waste, utilization, filler, compressive strength

1 Introduction

Aggregates are the important constitutes of the concrete, which give body to the concrete and also reduce shrinkage. Aggregates occupy 70 to 80% of total volume of concrete. So, we can say that one should know definitely about the aggregates in depth to study more about concrete. Aggregates can be classified in many ways [1-6]:

I. Classification of aggregates based on grain size:
   a. Fine,
   b. Coarse.

II. Classification of aggregates based on density:
   a. Lightweight,
   b. Standard,
   c. High density.

III. Classification of aggregates based on shape:
- a. Rounded,
- b. Irregular,
- c. Angular,
- d. Flaky,
- e. Elongated,
- f. Flaky and Elongated.

IV. Classification of aggregates based on geographical origin:
- a. Natural,
- b. Manufactured,
- c. Recycled,
- d. Reuse by-product.

Recycled concrete aggregate (RCA) is generally produced by crushing of demolished concrete, and screening and removal of contaminants such as reinforcement, paper, wood, plastics and gypsum. Concrete made with such recycled concrete aggregate is generally called Recycled aggregate concrete [7].

When demolished concrete is crushed, a certain amount of mortar and cement paste from the original concrete remains attached to stone particles in recycled aggregate. This attached mortar is the main reason for the lower quality of RCA compared to natural aggregate [8].

Technology of RAC production is different from the production procedure for concrete with natural aggregate. Because of the attached mortar, recycled aggregate has significantly higher water absorption than natural aggregate. Therefore, to obtain the desired workability of RAC it is necessary to add a certain amount of water to saturate recycled aggregate before or during mixing, if no water-reducing admixture is applied. One option is to first saturate recycled aggregate to the condition - water saturated surface dry, and the other is to use dried recycled aggregate and to add the additional water quantity during mixing. The additional water quantity is calculated on the basis of recycled aggregate water absorption in prescribed time [9, 10].

Different researches were devoted to providing solutions in using of waste for natural aggregate replacement because aggregates represent about 60-70% per volume of concrete mixture. In our experiment of strength properties of concrete based on natural aggregate compensation by selected fractions of recycled concrete were investigated.

2 Materials and methods

In our experiment, Portland cement CEM II 32.2 R, recycled concrete aggregate (RCA) and natural aggregate were used as raw materials.

Used recycled concrete aggregate was created as a crushed and sorted waste from demolition building and roads. This material was obtained from recycling plant Rail and Transport Buildings, Ltd. Kosice, Slovakia. RCA, fraction 4/8 and 8/16 mm was used as natural aggregate replacement in concrete mixtures.

Three different fractions of natural aggregate (0/4 mm, 4/8 mm and 8/16 mm) from company

VSH, a.s. (Turna nad Bodvou, Slovakia) was used for concrete samples preparing. Natural aggregate was evaluated according to the Slovakian standard [11].

To manufacture of concrete samples was used Portland slag cement CEM II/B-S 32.5 R from company Povazska cementaren, a.s., Ladce, Slovakia [12].

Table 1 shows proposal composition of 1 m^3 concrete and was designed for strength class C 16/20 (C 16/20 XC1, (SK) CL - 0,4 D_{max16}, S3). As an additive to concrete samples was used plasticizer Stacheplast. It is a plasticizer based on lignin, which specifically regulates the hardening of concrete samples with a strong plasticizing effect.

Table 1: Composition of experimental concrete

Composition	1 m^3
CEM II/ B-S 32,5 R [kg]	300
Water [l]	160
0/4 mm [kg]	955
4/8 mm [kg]	210
8/16 mm [kg]	710
Plasticizer [l]	2,15

Ten different mixtures based on recycled concrete aggregate (called C0-C9) with solid/liquid ratio of 0.55, including admixture Stacheplast was performed in our study. Sample C0 was reference sample prepared only with natural aggregate. In the other mixtures (C1-C9) natural aggregate fractions, 4/8 and 8/16 mm were replaced by recycled concrete aggregate. The replacement variation in the experimental mixtures was in range 0 to 100%, as it is shown in Table 2.

Table 2: Percentage variation of natural aggregate by Recycled concrete aggregate in the experimental mixture

Sample	RCA	
	4/8 mm [%]	8/16 mm [%]
C0	0	0
C1	100	20
C2	100	40
C3	100	60
C4	100	80
C5	100	100
C6	20	100
C7	40	100
C8	60	100
C9	80	100

After a careful mixing of the all components concrete mixture were placed into cleaned plastic forms. Thus, prepared forms were then over 15s compacted on a vibrating table. After

filling, cubic forms were labelled and placed on a flat surface next 48 hours. After 48 hours, the cube bodies were removed from the forms and then placed in a water bath. Time hardening of samples contained recycled concrete aggregate was 2, 7, 14 and 28 days (Table 3) and was performed on samples shaped cubes with dimensions 150 x 150 x 150 mm according to the standard [13]. Monitoring of strength after 2 and 7 days was to detected possible anomalies in the development of sample strengths.

Table 3: Compressive strength testing intervals for samples with RCA

Sample	Testing interval after			
	2 days	7 days	14 days	28 days
C0	■	■	■	■
C1	■	■	■	■
C2	-	-	■	■
C3	-	-	■	■
C4	-	-	■	■
C5	■	■	■	■
C6	■	■	■	■
C7	-	-	■	■
C8	-	-	■	■
C9	-	-	■	■

3 Results and discussion

Values of compressive strength samples prepared with recycled concrete aggregate after 2, 7, 14 and 28 days of hardening shows Figure 1. The four concrete samples (C0, C1, C5 and C6) was monitored start-up compressive strength after 2, 7 and 28 days of hardening. Figure shows, that samples C0 and C1 after 7 days meeting the minimum strength of 20 MPa according to [14], but samples C5 and C6 fulfills this requirement after 28 days.

From Figure 1 it is evident that all samples met the requirement of a standard (strength 20 MPa), and already after 14 days setting. Highest compressive strength after 28 days of hardening reached sample C3 (34.7 MPa; 100% recycled fraction 4/8 mm, and 60% recycled fraction 8/16 mm), but these are only slightly different from the strength of the reference sample C0 (34.4 MPa). The lowest strength only 27.4 MPa reached sample C7 (40% recycled fraction 4/8 mm, and 100% recycled fraction 8/16 mm). However, it should be noted that sample C8 (60% recycled fraction 4/8 mm, and 100% recycled fraction 8/16 mm) reached a compressive strength value of 27.6 MPa, which is essentially the difference in the level of measurement error. On this basis, it can generally be stated that the samples containing 100% replacement of the natural aggregate fraction 8/16 mm with recycled material reached after 28 days hardening lowest values of compressive strength.

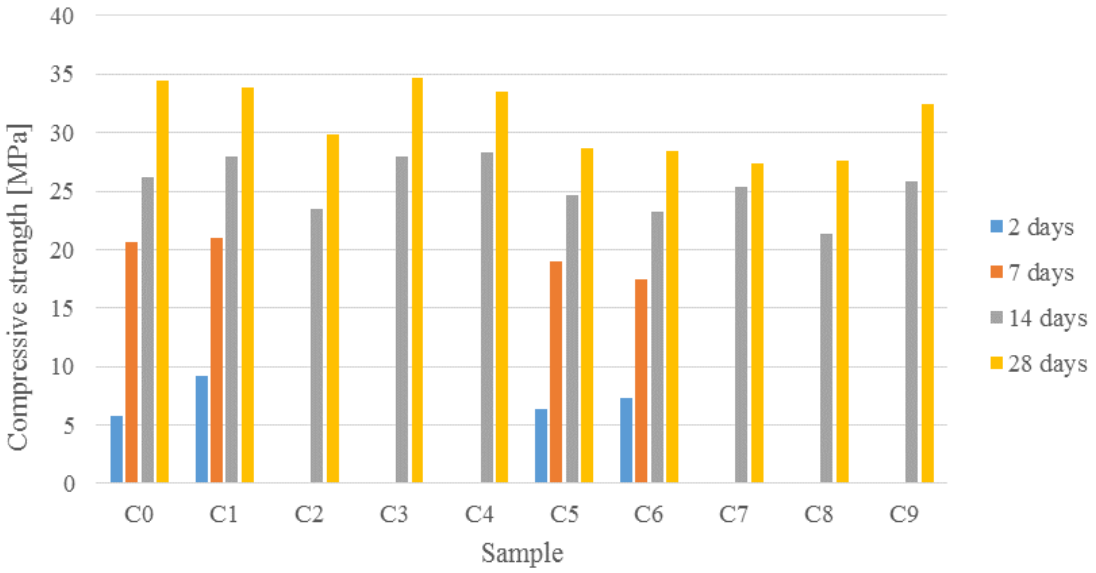

Figure 1: Values of compressive strength samples containing RCA after 2, 7, 14 and 28 days of hardening

4 Conclusion

Recovery way of construction waste is most important for our environment. Recycling will help to conserve natural resources and waste is used in further constructions. Recycling technologies are from year to year more modern and more powerful. Recycling of concrete waste generated and the subsequent use of recycled materials in the production of new concrete now has an increasing trend.

Results show that it is possible to replace the two fractions (4/8 mm and 8/16 mm) of natural aggregate by recycled concrete aggregate to making of recycled aggregate concrete with lower strength classes. Thus, concrete meet standardized requirements for final compressive strength (28 days). From the point of view of evaluating the obtained results of the resulting compressive strengths, it seems more advantageous to replace the 4/8 mm fraction of natural aggregate by RCA, whereas the obtained values are at the level of 35 MPa. On the other hand, the strength values of the samples with a fraction of 8/16 mm lag really little behind. More relevant information to the problem would be provided by monitoring the samples in the longer term (365 days and more).

Acknowledgements

This research has been carried out within the project of Slovak Cultural and Education Grant Agency (contract No. 073TUKE-4/2015).

References

[1] Oikonomou, N.D. (2005). Recycled Concrete Aggregates. *Cement & Concrete Composites*. *27*, 315-318.

[2] McNeil, K. & Kang, T.H.-K. (2013). Recycled Concrete Aggregates: A Review. *International Journal of Concrete structures and Materials*. *7*, 61-69.

[3] The Constructor. (2020). *Classification of Aggregates as per Size and Shape-Coarse and Fine Aggregates*. 2.11.2020, https://theconstructor.org/building/classification-of-aggregates-size-shape/12339/

[4] Hintons. (2018). *Classification of Aggregates*. 2.11.2020, https://www.hintonswaste.co.uk/news/classification-of-aggregates/#origin

[5] Baricova, D., Pribulova, A., Demeter, P., Bulko, B. & Rosova, A. (2012). Utilizing of the Metallurgical Slag for Production of Cementless Concrete Mixtures. *Metalurgija*. *51* (4), 465-468.

[6] Singh, D. & Singh, S.P. (2020). Influence of recycled concrete aggregates and blended cements on the mechanical properties of pervious concrete. *Innovative Infrastructure Solutions*. *5* (3), Art. No. 66.

[7] Taffese, W.Z. (2018). Suitability Investigation of Recycled Concrete Aggregates for Concrete Production: An Experimental Case Study. *Advances in Civil Engineering*. 2018, 1-11.

[8] Obe, R.K.D., de Brito, J., Silva, R.V. & Lye. C.Q. (2019). 5 - Properties and Composition of Recycled Aggregates, *Sustainable Construction Materials* (89-141). Woodhead Publishing Series in Civil and Structural Engineering.

[9] Dvorsky, T., Vaclavik, V., Simicek, V., Brenek, A. (2015). Research of the Use of Waste Rigid polyurethane Foam in the Segment of Lightweight Concretes. *Inzynieria Mineralna*. *2*, 51-56.

[10] Rashid, K. et al. (2020). Multi-criteria Optimization of Recycled Aggregate Concrete Mixes. *Journal of Cleaner Production*. *276*, Art. No. 124316.

[11] Slovak Office of Standards, Metrology and Testing. (2008). Aggregates for concrete. STN EN 12 620+A1. Slovakia.

[12] Slovak Office of Standards, Metrology and Testing. (2012). Cement. Part 1: Composition, specifications and conformity criteria for common cements. STN EN 197-1. Slovakia.

[13] Slovak Office of Standards, Metrology and Testing. (2013). Testing hardened concrete. Part 1: Shape, dimensions and other requirements for specimens and moulds. STN EN 12390-1. Slovakia.

[14] Slovak Office of Standards, Metrology and Testing. (2017). Concrete. Specification, performance, production and conformity. STN EN 206-1+A1. Slovakia.

DOI: 10.1515/sspjce-2020-0018

Reducing the carbon footprint in the foundations structures of masonry family houses

Marcela Ondová, Adriana Eštoková, Martina Fabianová

Technical University of Kosice, Slovakia
Civil Engineering Faculty, Institute of Environmental Engineering
e-mail: marcela.ondova@tuke.sk

Abstract

Nowadays, the environmental assessment becomes more and more of interest as an additional tool for the decision-makers. The researchers in civil engineering focus on building materials, structures as well as whole buildings environmental evaluation. Analysis of the environmental impact of particular structures may be helpful for selecting building materials, with regard to the environmental performance of buildings in the early project phase. The aim of this paper is presentation of an environmental evaluation of the rarely assessed particular structures – building foundations and the analysis of the share of the building foundations to the overall environmental impact of building as well. The obtained data point to the need to include the environmental impacts of foundations when assessing the buildings, because of it is a necessary part of any type of family house. One kilogram of built-in foundations materials was responsible for emissions of 0.092 kg of greenhouse gases expressed by carbon dioxide (CO_2). Embodied energy was calculated as equal to 1.14 MJ per 1kg of foundations materials and 832.2 MJ/m^2 per building floor area. The foundation materials of houses contributed to the total environmental impact of the whole buildings by, on average, 15.0 and 22.8 % for embodied energy and global warming potential, respectively.

Key words: primary energy, sustainability, greenhouse gases, LCA

1 Introduction

Sustainability has attracted increasing attention of general public in recent years. The sustainability challenges we face today are mainly related to environmental threats [1-3]. The construction industry is an important contributor to these negative threats. The construction of buildings consumes a lot of energy, produces a lot of pollutants and solid waste, consumes renewable as well as non-renewable raw materials for the production of building materials and consumes water throughout the building's life cycle. According to UNEP-SCBI, buildings consume about 40% of the energy, 25% of the water and 40% of the resources available on Earth, while producing 30% of greenhouse gases [4]. Therefore, the construction sector is a field with immediate need for reducing environmental impacts. Many companies have found

it advantageous to explore ways of moving beyond compliance, using pollution prevention strategies and environmental management systems, to improve their environmental performance [5]. The enforcement of energy efficient building is considered as the most successful strategy for CO_2 emission reduction and energy saving during the life cycle of the building, while the application of suitable green building products plays an important role in facilitating energy efficient building promotion [6].

New environmental perceptions and sustainability approaches have led to the development of a number of environmental methods that contribute significantly to reducing environmental degradation. Monitoring the environmental performance of building materials (which can be expressed by different environmental parameters), gives us the impact of construction products and buildings on the environment during total or part of the life cycle. As a result, the degree of environmental damage can be determined. Currently, the most popular environmental impact assessment tool is method "Life Cycle Assessment" (LCA). LCA is an environmental approach that considers all the aspects of resource use and environmental releases associated with an industrial system. Specifically, it is a holistic view of environmental interactions that covers a range of activities, from the extraction of raw materials from the Earth and the production and distribution of energy, through the use, and reuse, and final disposal of a product [7]. LCA methodology is standardized in ISO14040 [8] and 14044-2006 [9] and consists of four principle steps. Nowadays, it can be used in various fields of building assessment from building material [10] and operation phase – energy consumption [11] to apartment house [12] and residential buildings [13]. When LCA is applied to a building, the product studied is the building itself, and the assessment runs in previously determined system boundaries. Because a balance is desired between practicability of the study and validity of the results, it is possible to say an LCA presents an accurate estimate of the quantities and timing of environmental impacts, it provides a solid basis for identifying the benefits of changes in the construction of a building or its operation.

The results show that over 80 % of greenhouse gases emissions take place during the operational phase of buildings, when energy is used for heating, cooling, ventilation, lighting, appliances and other applications [14]. A smaller percentage of the energy consumed is for materials manufacturing and transportation, construction, maintenance renovation and demolition. The significant environmental impact, especially as a result of the high quantity of harmful materials used for building structures, is not negligible. Author McHendry [15] reported that embodied energy is between 17 % and 25 % of the estimated lifetime energy demands of a building. Sartori claimed that the embodied energy in materials varied between 9 % and 46 % of the overall energy used over the building's lifetime when dealing with low energy consumption buildings i.e. with good insulation, adequate orientation, passive conditioning, etc., and between 2 % and 38 % in conventional buildings [16]. Based on the available information, it is clear that, embodied energy in conventional buildings can be reduced by approximately 10–15 % through proper selection of building materials with low environmental impacts [17].

The goal of this paper was to analyse the environmental impacts of five Slovak masonry family houses paying special regard to the foundations materials. Environmental analysis was focused on the calculation of embodied energy (primary energy) and global warming potential in order to determine the share of foundation materials in the overall environmental impact of the building.

2 Material and methods

Masonry family houses with commonly used building materials were selected for an evaluation of the environmental impacts of building foundations. The configurations of five assessed houses are stated in Table 1.

Table 1: Purposeful space configurations of the houses

Space configuration	H1	H2	H3	H4	H5
Total built-up area [m^2]	192.4	158.7	148.9	101.9	461.4
Calculated built-up area [m^2]	185.5	110.3	112.5	95.1	440.5
Total useful area [m^2]	468.6	168.6	182.4	140.7	370.6
Calculated useful area [m^2]	468.6	147.4	164.6	110.5	340.8
Living area [m^2]	235.8	114.7	87.0	80.4	155.9
Floor area [m^2]	518.7	220.6	220.2	171.1	440.5
Built-up volume [m^3]	2 393	612.5	611.6	636.7	1987
Heated area [m^2]	435.0	138.6	131.7	110.1	155.9
Heated volume [m^3]	1 131	530.0	507.0	286.2	623.6

Next Table (2) presents an overview of used building materials.

Table 2: Representation of used materials in the assessed houses – weight [kg]

Groups of used materials	H1	H2	H3	H4	H5
Bulk materials	18,144	2,718	63,684	882	117,684
Reinforced concrete (0.7 wt.% of steel)	103,468	210,890	99,307	130,811	187,072
Ceramics	107,877	34,625	31,207	152,186	65,744
Wood	2,275	35,885	7,630	46,623	5,099
Lime cement plaster	3,600	8,388	10,271	21,983	24,401
Gypsum materials	-	1,275	1,832	1,053	-
Laminate	-	84,841	576.6	331.2	300.9
Glass	731.0	148.2	661.0	704.0	466.1
Other metals	-	521	5,841	-	4,159
Mineral insulation	-	2,561	-	-	-
PS insulation	24.8	1,285	814.1	1,315	1,430
PVC materials	-	270.0	383.8	62.5	426.0
∑	236,121	383,398	222,207	313,990	406,781

- Bulk materials included: gravel, sand and soil constituting a layer below the concrete foundations. Reinforced concrete, containing 0.7 wt. % of steel, was used for horizontal structures of bond beams and girders, slabs and capping as well as pillars or staircase material.
- Concrete hollow blocks were also used as wall footings.
- Ceramics representing: ceramic bricks, blocks and tiles were used for load-bearing walls (perforated ceramic bricks for external and internal walls), partitions and floor surfaces as well as roof components (ceramic roof tiles).

- The material group Wood included: wood and wood products used in ceilings, slant roof or shuttering and vapour barrier (OSB boards) and floor covering.
- Other metals (copper, aluminium) were used rarely, e.g. the damp proof course was constructed of bitumen-aluminium sheet.
- Mineral insulation (mineral wool, rock wool, mineral foam) was applied on facades (insulation of walls) and ceilings. PS insulation (polystyrene insulation) represented by expanded polystyrene EPS and extruded polystyrene XPS was used for thermal insulation of walls and foundation strips (XPS) or in floors on the ground (EPS). PVC materials were used for frame and sash construction (windows, doors).
- Lime cement plasters were used for interior surface covering.
- Gypsum materials including plaster, plasterboard and gypsum fiber boards were used for interior plastering or lower ceiling.
- Laminate materials represented floor coverings.
- Glass materials were applied in transparent or semi-transparent in-fill materials (as double or triple glazed windows or doors).

The houses evaluated are built on concrete slabs. Concrete, gravel, asphalt and polyvinylchloride were the most used materials in the foundations of the evaluated houses.

2.1 Methodology

The environmental evaluation of house foundations was based on the calculation of the environmental impacts of building materials used in five selected buildings. The overall environmental impact was calculated with aim to obtain the load of the foundations in comparison with the total building impacts. Environmental impacts were expressed in terms of two main important environmental indicators with respect to embodied energy (primary energy intensity - PEI) and embodied carbon emissions (global warming potential GWP [18].

- Primary energy indicates in general the level of depletion of natural resources within boundaries of evaluated product life cycle and is usually expressed in MJ or kWh.
- Global warming potential represents in a parallel manner to PEI the greenhouse gases emissions (GHGs) through the life cycle of the product or building. The strength of global warming potential is used to refer to CO_2 emissions equivalent and measured in $kgCO_2eq$; this is then an equivalent to the impact category of Global warming potential. The GWP of the analysed building materials was calculated considering the data for 100-year time horizon.

Unit environmental indicators per 1 kg of building materials were calculated in boundaries "cradle to gate" [19]. The data used for the calculation of environmental performance of the used materials originated from a broadly used IBO database.

3 Results and discussion

Figure 1 presents the calculated environmental indicators (PEI and GWP) of evaluated house foundations. Embodied energy (PEI) of concrete slab foundation materials ranged from 122 to 220 GJ and corresponded to the results reported for concrete bay (213 GJ) by Griffin et al.

[20].

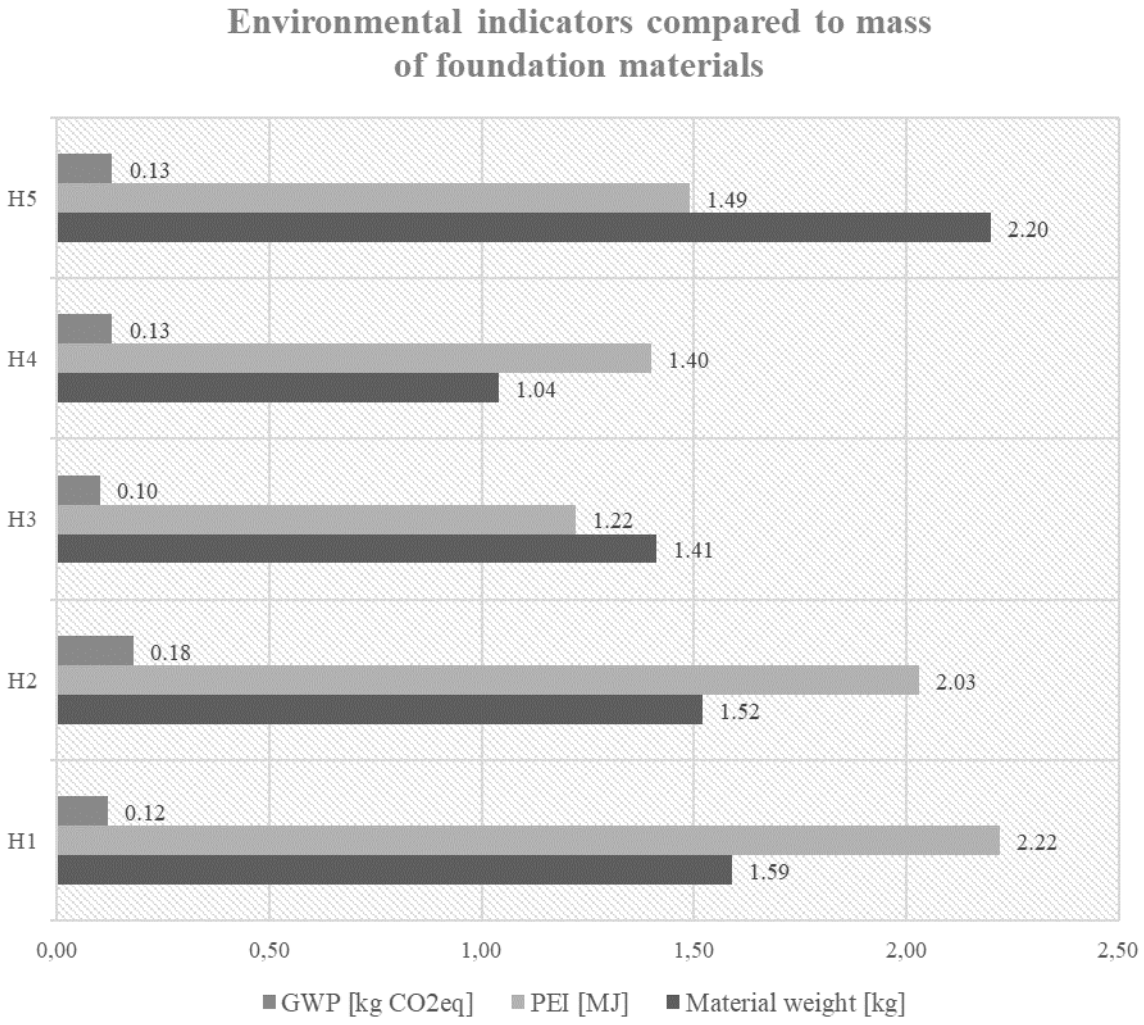

Figure 1: Environmental indicators (PEI and GWP) of house foundations (all expressed as x 10^5)

As seen in Figure 1, the highest PEI was not calculated for the house with the highest mass of foundation materials. In comparison, House 5 representing the highest weight of foundation building materials was responsible for PEI impact which was less than the average value (167 GJ).

Global warming potential (GWP) has been calculated in a range 0.10×10^5–0.18×10^5 kg CO_2eq with an average value of 0.13×10^5 kg CO_2eq. The highest and the lowest GWP values correlated to the highest and the lowest PEI values (House 3 and House 2, respectively). Environmentally suitable foundation alternatives, mentioned by Magwood and Feigin [21], reached, similarly to PEI, much lower values of embodied carbon dioxide emissions for the rammed earth tire foundations, for the stone foundations and for earth bag foundations).

Nemry et al. [22] observed that the basement (foundations), the exterior walls and floors/ceilings are important relating to the contribution of the individual construction

elements to the environmental impacts of family houses. Interior walls, roof and windows play a minor role only.
In comparing the results of the house foundations' environmental impacts with the total environmental impacts of the whole houses, the highest contribution was observed for embodied carbon dioxide emissions. The average GWP of foundations was 1.3×10^4 kg CO_2eq, while the average GWP of the whole building was equal to 6.5×10^4 kg CO_2eq, which means that the foundations contribute by 1/5 to total global warming potential.
The share of foundation material impacts of the overall impacts differed. Foundation materials represented: 9.0–18.1 % of the embodied energy (PEI) and 12.5–28.0 % of the global warming potential (GWP) obtained for the whole buildings. The calculated values of foundations were also converted into normalised values per 1 m^2 of floor area. The findings revealed that the normalised embodied energies of house foundations are in a wide range of 427.74–919.42 MJ/m^2 having an average value of 718.5 MJ/m^2 and embodied carbon dioxide emissions (GWP) normalised per floor area ranged from 22.59 to 83.33 kg CO_2eq/m^2. The highest normalised values of all evaluated indicators converted to floor areas have been found for House 2 and the lowest for House 1.
Based on summarising of results is obvious, that one kilogram of the foundation materials used in the study is responsible for emissions of 0.092 kg CO_2eq and energy for production of one kilogram of foundation is equal to 1.14 MJ. Also applies that the CO_2 contribution of the concrete slab foundations can be reduced by changing the materials used, e.g. by using non-conventional materials and implementation of sustainable building materials and technologies such as a rammed earth tire foundation.

4 Conclusion

In this study, the environmental impacts of the foundations materials of five family houses in Slovakia were examined regarding the embodied energy of materials (PEI) and global warming potential (GWP). As can be seen from the results of the study, the calculated environmental impacts presented depend strongly on the material base used in the evaluated houses and this may vary under various conditions (geographical, climatic, economic, cultural, etc.).
The findings revealed that the share of the foundation materials of the overall environmental impact of masonry building has been the relatively high, especially on global warming potential, draws attention to the optimization of foundation materials with similar material basis.
The proposed approach of the optimalisation is focused to the harmonization between environmental and structural criteria with aim to include environmental criteria in the decision-making process of building design, thus fostering a more efficient use of resources throughout the life cycle of buildings and reducing the environmental impacts of construction works.

Acknowledgements

This paper has been prepared with a support of the Scientific Grant Agency of the Ministry of Education, Science, Research and Sport of the Slovak Republic and the Slovak Academy of Sciences (VEGA Grant No. 1/0648/17) and Slovak Grant Agency for Science Slovak Cultural and Education Grant Agency (Contract No. 073TUKE-4/2018).

References

[1] Johnston, P.; Everard, M.; Santillo, D.; Robèrt, K. (2007). Reclaiming the Definition of Sustainability. *Environ. Sci. Pollut. Res. 14*, 60–66.

[2] Benoît, C.; Mazijn, B. Guideline for Social Life Cycle Assessment of Products; United Nations Environment Programme: Paris, France, 2009; ISBN 9789280730210.

[3] Onat, N.C.; Kucukvar, M.; Halog, A.; Cloutier, S. (2017). Systems Thinking for Life Cycle Sustainability Assessment: A Review of Recent Developments, Applications, and Future Perspectives. *Sustainability 9*, 706.

[4] UNEP/SETAC Life Cycle Initiative. Global Guidance Principles for Life Cycle Assessment Databases – A basis for greener processes and products – Shonan Guidance Principles. Output of the UNEP/SETAC „Global Guidance for LCA Databases“ workshop. Shonan, Japan.

[5] Curran, M. A. (2004). The status of life-cycle assessment as an environmental management tool. *Env Progress 23* (4), 277-283.

[6] Huang, M., Wang, B. (2014). Evaluating green performance of building products based on gray relational analysis and analytic hierarchy process. *Env Progress & Sust Energy 33* (4), 1389-1395.

[7] Curran, M. A. (2016). Life Cycle Assessment.Kirk-Othmer Encyclopedia of ChemicalTechnology. 1–28.

[8] Environmental management. Life cycle assessment - Principles and framework (ISO 14040:2006)

[9] Environmental management. Life cycle assessment - Requirements and guidelines (ISO 14044:2006)

[10] Abeysundara, Y., Babel, S. (2010). A quest for sustainable materials for building elements in Sri Lanka: Foundations. *Env Progress & Sust Energy 29* (3), 370-381.

[11] Velagapudi, S., Kumar, A., Spivak, A., Franchetti, M. (2014). Comparison of pollution prevention assessments for the facilities with and without energy star certification. *Env Progress & Sust Energy 33* (4), 1366-1372.

[12] Keun, H. Y., Tae, H. K., Seung, J. R. (2015). Analysis of lifecycle CO_2 reduction performance for long-life apartment house. *Env Progress & Sust Energy 34* (2), 555-556.

[13] Li, D.Z., Chenb, H.X., Huic, E.C.M., Zhanga, J.B., Lia, Q.M. (2013). A methodology for estimating the life-cycle carbon efficiency of a residential building. *Build Environ 59*, 448-455

[14] UNEP Sustainable Buildings & Climate Initiatives (2009) Buildings and climate change: Summary of decision-makers, UNEP DTIE Sustainable Consumption & Production Branch, Paris

[15] McHendry, S. (2013). The Embodied Energy and Carbon of Passive House, University of Strathclyde Engineering, Master study.

[16] Sartori, I., Hestnes, A.G. (2007). Energy use in the life-cycle of conventional and low-energy buildings: a review article. *Energ Buildings 39*, 249–257.

[17] Thormark, C., (2006). The effect of material choice on the total energy need and recycling potential of a building. *Build Environ 41*, 1019–1026.

[18] Ondova, M.; Estokova, A. (2016). Environmental impact assessment of building foundation in masonry familyhouses related to the total used building materials. *Environ. Prog. Sustain.*

Energy 35, 1113–1120.

[19] Waltjen, T. (2008). Passive House - Parts Catalogue. Details for passive houses: A catalogue of ecologically rated constructions (in German), Vienna, Austria: Springer.

[20] Griffin, C.T., Reed, B., Hsu, S. (2010). Comparing the embodied energy of structural systems in buildings. Proceedings of the 1st International Conference on Structures & Architecture (ICSA2010). Guimarães, Portugal, July 2010.

[21] Magwood, C., Feigin, J. (2014). Making better buildings: A comparative guide to sustainable construction for homeowners and contractors, 1th ed. (p. 441), Gabriola Island, Canada: New Society Publishers.

[22] Nemry, F., Uihlein, A., Colodel, C.M., Wittstock, B., Braune, A., Wetzel, C., Hasan, I., Niemeier, S., Frech, Y., Kreißig, J., Gallon, N. (2008). Environmental improvement potentials of residential buildings (IMPRO-Building), Luxembourg: Office for Official Publications of the European Communities, European Communities.

DOI: 10.1515/sspjce-2020-0019

Single case study photovoltaic panels within water heating system

Richard Baláž

Technical University of Košice, Slovakia
Faculty of Civil Engineering, Institute of Architectural Engineering
e-mail: richard.balaz@tuke.sk

Abstract

The submitted article offers one of the possible options of a usage of photovoltaic panels for a domestic hot water preparation with an option to extra heating a heating system, and following recalculation of a produced electric energy amount in regards of a total return of the assembled system. An electric heating boiler combined with a heating option working on solid propellant was chosen for the experiment. The most frequently used combined electric storage tank was chosen as a classic option to heat domestic hot water.

Key words: photovoltaic panels, heating system

1 Introduction

Solar energy systems include photovoltaic (PV) materials and devices that convert sunlight into electric energy; PV cells are commonly called solar cells [1].
A large study in California completed by Lawrence Berkeley National Laboratory com-pared sales of homes with PV and without to determine what premium, if any, existed on homes sold with PV systems. Their results indicated that depending on whether the home was new construction, or existing, the price per watt premium varied between $ 2.30 - $ 2.60 /watt, and $ 3.90 and $ 6.40 /watt, respectively for homes with PV systems, as com-pared to comparable homes without PV.
Sample Comparison of Energy Savings Value to better understand some factors that affect energy savings, and therefore value to the consumer, an example follows comparing identical 5 kW PV systems—one in Colorado and one in Louisiana. This example illustrates the difference in energy savings as a function of production potential, utility electricity rates, and typical electricity consumption patterns. The example uses average conditions and is only intended as an illustration, not a real-world scenario. According to US Energy (2011) the typical Colorado household uses around 711 kWh of electricity per month that is approximately 8532 kWh/year.
Information Administration (EIA) data.16 Using the typical PV system size of 5 kW, a PV

system in Denver will produce approximately 7.594 kilowatt-hours (kWh) in the first year, 17 offsetting approximately 89 % of the household usage. Using average electricity rates in Denver of 11.1 cents/kWh, 18 the price typically paid by the homeowner is around $ 947/year, and the value of electricity produced by the PV system is approximately $843 in the first year (11.1 cents/kWh × 7.594 kWh), effectively reducing the amount paid by the homeowner from $ 947 to $ 104 in the first year, an 89 % reduction [2].
A photovoltaic system by itself and its behaviour should be introduced at the beginning. The article will follow the characteristics of the system's equipment. Subsequently, we will evaluate amount of produced electric energy used on a production of domestic hot water and amount of produced electric energy used for additional heating-up the heating system, also with calculation of payback from designed solution for heating [3].
The photovoltaic is a technical section, which concerns with a process of a direct transformation of light into the electric energy. The term is derived from a word photo (light) and volt (electric current unit). The transformation process runs in a photovoltaic cell. The photovoltaics were discovered by Alexander Edmond Becquerel in 1839. The photovoltaic cells for energy production in cosmic programs were used for the first time in 1958. Since then, it becomes inseparable part of the cosmic program. The article will not analyse a transformation process more deeply [4].
The basis of the photovoltaic (PV) systems is the photovoltaic (PV) cells merged into the photovoltaic (PV) panels. The most popular photovoltaic panels are made from silicium. The different ways of silicium treatment can create monocrystalline, polycrystalline and amorphous (non crystalline) photovoltaic cells. The monocrystalline cell is black octagon and the polycrystalline cell is a blue square.
The monocrystalline cells are more efficient than polycrystalline, however, the usage of an area in the polycrystalline cells is not so perfect according to its shape, so both types has similar performance in the conclusion.
The polycrystalline cells effectivity is 12-14 %. The monocrystalline cells effectivity is 12-16 %. Price and durability are the same. The photovoltaic panels are capable to produce an electric energy without a direct sunlight based on diffuse equipment, which is dominant in the Slovakia.

2 2. Designed system

The designed system is with a direct connection. This system was chosen due to its quick payback, what was the initiative though of a system design.

- Used system elements: Photovoltaic (PV) panels Kyoto 275 kWp – 16 pieces
- MPPT regulators DC/AC designed for PV system – 2 pieces
- Combined boiler Mora k 120 L 2 x 1000 W or 2 x 1800 W
- Storage tank Regulus 200 L
- Electric heating spirals 2 x 2000 W

Existing heating system that combined electric boiler and heating by a solid propellant. It is necessary to mention, that the photovoltaic system was installed into the existing fully functional system of domestic water heating. It was ensured by an electric energy from the network in a summer and the heat exchanger connected to the heating system in a winter.
The combined boiler was used MORA K 120 L by reason of having dry spirals installed in

the flange with changeable input power 2 x 1000 W or 2 x 1800 W /LD TOPTEL/. The combination of the spirals settings 2 x 1000W was used during connection to the network 230 V/ ~50 Hz, combination 2 x1800 W was used during connection of the MPPT / MPPT Stands for Maximum Power Point Tracking is a technique for tracking and regulate the output energy from the solar panel to the battery. The MPPT detects the solar panel output voltage and current in real-time and continuously track the maximum power (P=U*I), regulates the output voltage correspondingly so that the system can always charge the battery with the maximum power./ regulators DC/AC determined for medium solar PV system in a number of 2 pieces. They are connected to the photovoltaic panels in number of 8 pieces with a performance 275 Wp by piece on every regulator, what gives together approximately 4.4 kWp (Figure 1).

Fig. 1: photovoltaic panels

3 3. Measurement of the consumption of an electric energy taken from the network

I did not measure the real consumption of an electric energy from the network. I keep up to the information from manufacturer, who officially indicate 7.64 kWh with input power 2 x 1000 W and temperature up to 65 °C from initial entry temperature of water 15 °C (Figure 1). This information is sufficient for a functionality demonstration and a payback of the whole system. It is possible to measure the real consumption of an electric energy with given type of the boiler and boundary conditions in a case of deeper examination (Table 1).

It is required to mention the spirals connection to the boiler 2 x 1000 W was changed to 2 x 1800 W to use the most input power from the photovoltaic panels in the shortest time. We watched it as an advantage during winter, when there is a less sunlight.

3.1 Display of the system connection:

The domestic hot water heating system is solved by 16 pieces of the photovoltaic panels FV Kyoto 275 kWp, which are connected by 8 pieces in a series with 2 pieces of regulators MPPT SOLARECO. The panels are directly connected into to the regulators, where a switch

is designed by a capillary thermometer in a case of overheating the combined boiler. An excessive energy after overheating of the combined boiler goes straight to the heating system via resisting heating spirals assembled to the storage tank connected to the existing heating system. The excessive energy after overheating the combined boiler will be discussed some other time. The combined boiler is directly connected to the MPPT SOLARECO regulators with classic 16A plug box, although there is a change against the classical electric energy network. The dry spirals with a performance 2 x 1000 W were changed for the heating device for contact heating LD-TOPTEL, cartridge heater with caliber 12.5 mm, L = 400 mm, and outlet length Lv = 250 mm, U = 230 V and performance 1800 W for one piece [8].

Table 1: Technical parameters of energy consumption

TYPE	K 120 L
Volume (l)	120
Pressure (MPa)	0.6
Weight / filled with water (kg)	62/66
Anticorrosive protection	Enamel / Mg anode
Input power (W)	2 x 1000
Voltage	230 V ~
Protection class	I.
Protection level	IP25
Time to heat water to 65 °C (h)	3.82
Energy consumption to temperature 65 °C (kW)	**7.64**
Quantity of water with 40 °C (l)	228
Heat loss (kWh / 24 h)	1.77

3.2 Measurement methodology

The basis of my research is the question: “Will the given photovoltaic system fulfil needs of a domestic hot water with correct operation and without any feeling of missing comfort due to lack of hot water, or any necessary physical switching to a classical electric network?” The measurement was designed for reading the values based on a boiler’s water temperature, which was set on a maximum operational temperature. The reading was always at 5 pm. The measurement of the really produced electric energy was made similarly; however, we will not represent it in this article. [9].

3.3 Payback of domestic water heating:

It is necessary to bring up that particular photovoltaic system would also run with a half number of panels and one regulator MPPT SOLARECO a half price of photovoltaic panels with accessories. However, my though was to design a heating system, which will still work during winter months – December, January. It could not be done with a system of 8 pieces of panels and only one regulator MPPT SOLARECO. The measurement implemented in 2016, 2017 and 2018 is presented in the Figure 2. Input requirements and total initial costs are specified in Table 2.

Fig. 2: Designed system [10].

Table 2: Input costs

Photovoltaic panels	140 € x 16	2 240 €
Connection accessories + cables		387€
regulator MPPT SOLARECO	2	300€
Cartridge heater	2	105€
Assembly material on the roof		274€
Total costs		**3285€**

Real consumption of an electric energy reported by a manufacturer multiplied by ratio 1.5, because of need of hot water was mostly more than 1 heat up of the combined boiler in a day 7.64 kW/h x 1.5= 11.46 kW/h x 365 day = 4182 kW/h.

Table 3: Calculation of a total electricity price

Distributive area	Product	Amount of energy import [kW/h]
East Slovakia	DD2*	1T/VT - 4 182.00
Invoicing items [€]	Yearly	Monthly
Payment for electricity	186.68	15.56
Fixed monthly payment – keeper	7.80	0.65
Fixed payment for distribution (breaker, emergency capacity)	50.83	4.24
Variable payment for distribution	105.80	8.82
Loss	25.05	2.09
System services	28.82	2.40
System operation	109.57	9.13
Nuclear fund	13.42	1.12
DPH	105.60	8.80
Total	**633.59** [€]	**52.80** [€]

* DD2 - Single-band rate for consumption points with higher electricity consumption

The payback of the whole system after total calculation of all costs is 5.18 year. However, with half number of the panels and only one regulator is payback 2.59 year.

4 Conclusion

The photovoltaic system for a hot water heating was design with a thought to speed up money payback from initial capital. The time of 5.18 year might look long, yet, we did not focus on an excessive energy after overheating the combined boiler. This energy could be used to heat water in a heating system, though this topic will be discussed in some other article.

4.1.1 References

[1] Office of Energy Efficiency and Renewable Energy, "Energy Basics—Photovoltaics" (Washington, DC: US Department of Energy), http://energy.gov/energybasics/articles/photovoltaics

[2] Bikos Nikolaos, Laochoojaroemkit Kittima, Department of Architecture - CHALMERS UNIVERSITY OF TECHNOLOGY GÖteborg, Sweden, 2012 Report No. 46

[3] http://www.energybulletin.net/node/17219, Energy Payback of Roof Mounted Photovoltaic Cells by Colin Bankier and Steve Gale

[4] GEOFFREY T. KLISE, JAMIE L. JOHNSON, AND SANDRA K. ADOMATIS, *SRA,* Valuation of Solar Photovoltaic Systems Using a Discounted Cash Flow Approach, Appraisal Journal, Fall/2013

[5] B. HOEN, R. WISER, P. CAPPERS, AND M. THAYER, "An Analysis of the Effects of Residential Photovoltaic Energy Systems on Home Sales Prices in California," LBNL-4476E, Lawrence Berkeley National Laboratory, April 2011

[6] Barbose, G., Darghouth, N., & Wiser, R. (2012). Tracking the Sun V: An Historical Summary of the Installed Price of Photovoltaics in the United States from 1998 to 2011. Lawrence Berkeley National Laboratory, Energy Analysis & Environmental Impacts Department. Berkeley, CA: University of California. Retrieved from http://emp.lbl.gov/sites/all/files/LBNL-5919e-REPORT.pdf

[7] Ben Hoen, Ryan Wiser, Peter Cappers, and Mark Thayer, An Analysis of the Effects of Residential Photovoltaic Energy Systems on Home Sales Prices in California (Lawrence Berkeley National Laboratory, LBNL-4476E, April 2011), available at http://emp.lbl.gov/sites/all/files/lbnl-4476e.pdf.

[8] http://www.ld-toptel.sk/index.php?page=uvod

[9] http://www.energybulletin.net

[10] https://www.solareco.sk/fotovoltaicky-ohrev-vody-sk

DOI: 10.1515/sspjce-2020-0020

Behaviour of Sediments in Water Structures

Natália Junáková, Jozef Junák

Technical University of Košice, Slovakia
Faculty of Civil Engineering, Institute of Environmental Engineering
e-mail: natalia.junakova@tuke.sk, jozef.junak@tuke.sk

Abstract

Bottom sediments are a natural part of aquatic ecosystems. They are increasingly contributing to the deterioration of watercourses and reservoirs and are an undesirable material that causes various serious environmental and technical problems. The most significant problems include the instability of riverbeds, the transport of chemicals, nutrients and organic compounds, the supply of sediments to water reservoirs. Bottom sediments have the ability to bind to their surface various predominantly harmful substances such as heavy metals, radionuclides, nutrients and organic substances. Such sediments pose a risk to the water system in terms of possible remobilization of pollutants into the water.

This paper is focused on the study of behavior of sediments in the Hervartov small water reservoir located in the east of Slovakia and their ability to adsorb phosphorus at the sediment-water interface. The results show that the efficiency of sorption of phosphorus from the aqueous environment by fine and coarse-grained sediments is the highest at the lowest input concentrations of phosphorus in solution, or at low concentrations in surface water above the sediment. At these concentrations, the amount of sorbed phosphorus by fine-grained sediments was up to almost 99%. The coarse-grained sediments sorbed phosphorus at a level of up to 84%. Increasing the concentration of phosphorus in the solution leads to a decrease in the sorption efficiency of the sediment, while at high concentrations of the sorbate, the sorption process is significantly stabilized due to reaching the maximum sorption capacity of bottom sediments.

Key words: sediment, reservoir, sorption, nutrient

1 Introduction

Bottom sediments are an important component of the ecosystem of watercourses and reservoirs. Depending on the type of water, the natural content of substances, the grain composition and also the proportion of anthropogenically influenced components change in sediments. After deposition, they become an important habitat, they are inhabited by macro- and microorganisms, which, among other things, participate in their transformation [1,2,3].
Sediments accumulate substances that can significantly affect the quality of the water with which they are in contact, both in the water body itself and in the waters infiltrating through

the sedimentation layer. For this reason, bottom sediments should be seen as a source of possible pollution of both water types [4].
Sediments deposited at the bottom of reservoirs pose the largest reservoir of phosphorus in most water structures, which can contribute to its high concentrations in water. Because increased concentrations of nutrients (nitrogen and phosphorus) cause water eutrophication, one of the most studied mobilization processes at the sediment-water interface is the study of phosphorus sorption by bottom sediments [5,6].
In the sediment matrix, phosphorus is mostly found in adsorbed (particulate) form [7]. Storage of phosphorus within the sediments potentially reduces eutrophication by reducing its bioavailability [8]. Most of the adsorbed phosphorus is not easily desorbed. The amount that is desorbable decreases with the age of the phosphorus complex adsorbed on the sediment [9]. Desorption of phosphorus from sediments is thought to contribute approximately 10 percent of the total amount of phosphorus in lakes [10]. However, resuspension of phosphorus from the sediment into the water column can be essential in the case when there is no supply of phosphorus from external inlets, or supply is not significant [11]. Other factors and reservoir conditions that may support phosphorus mobilization are critical.
Several authors have studied the phosphorus sorption by sediments, where they found that the sediment grain size, organic content and content of iron and aluminum are the main factors influencing sorption process [12-17].
Therefore, it is necessary to know the behavior of sediments, because quality of sediments is an important indicator of water pollution in water bodies, it allows to detect and locate sources of pollution in the river basin and thus also allows taking the necessary revitalization measures in water basins and reservoirs.

2 Material and methods

Sediment behaviour and the study of their ability to adsorb phosphorus at the sediment-water interface were carried out under laboratory conditions on samples of fine-grained (SF, under 63 μm) and coarse-grained (SC, above 63 μm) in order to demonstrate the influence of different sediment properties (especially their grain size, Fig. 1) on sorption processes. Sediments with different physical and chemical properties were taken from the Hervartov small water reservoir.

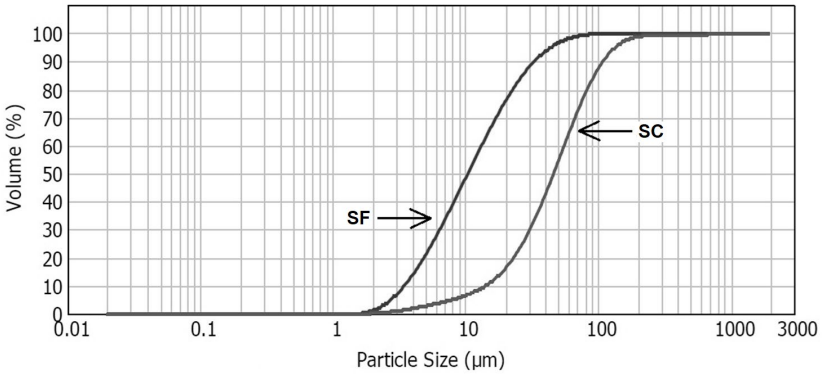

Figure 1: Particle size distribution of fine (SF) and coarse-grained (SC) sediments (Mastersizer 2000, Malvern UK)

Air-dry fine-grained and coarse-grained sediments were used to study the phosphorus sorption process at the sediment-water interface. Two grams of sediments were agitated in 50 ml of 0.01 M $CaCl_2$ solution that is used in adsorption/desorption testing, containing sorbate of various concentrations. As a sorbate, a solution of KH_2PO_4 in the range of 0 ~ 24 mg P/L was used in the experiments. The mixture of sediment and solution was stirred for 24 hours at a constant temperature in order to reach adsorption equilibrium. The suspension was then filtered and the equilibrium phosphorus concentration was determined in the separated aqueous solution using a DR 890 colorimeter (Hach Lange, Germany). The concentrations of total phosphorus adsorbed on the sediment (q_e) were calculated as the difference between the initial concentration of phosphorus in solution (C_0) and its amount in solution after contact with sediment at the end of the experiment (C_e) according to equation (1):

$$q_e = \frac{(C_0 - C_e) \times V}{m} \qquad (1)$$

where q_e is the amount of P adsorbed by the sediment after reaching equilibrium (mg P/kg), C_0 is the initial concentration of P in solution (mg/L), C_e is the equilibrium concentration of P in solution (mg P/L), m is the mass air-dry sediment (kg) and V is the volume of the KH_2PO_4 (L) solution.

The following equation was used to calculate the phosphorus removal efficiency from solution at different initial concentrations for both sorbents (2):

$$\% \text{ Sorption} = \frac{(C_0 - C_e)}{C_0} \times 100 \qquad (2)$$

3 Results and discussion

The results of the study of the sediment behaviour through the research of their ability to adsorb phosphorus at the sediment-water interface are given in Table 1.

Table 1: Phosphorus content sorbed by fine (SF) and coarse-grained sediment (SC) at equilibrium and their sorption efficiency

C_0 (mg P/L)	$C_{e,SF}$ (mg P/ L)	$q_{e,SF}$ (mg P/kg)	Sorption efficiency,$_{SF}$ (%)	$C_{e,SC}$ (mg P/ L)	$q_{e,SC}$ (mg P/kg)	Sorption efficiency,$_{SC}$ (%)
0	0.13*	3.25*	-	0.08*	2.00*	-
1.18	0.14	26.01	98.90	0.26	22.99	84.02
1.60	0.20	34.90	95.51	0.50	27.56	73.67
6.36	0.53	145.86	93.79	2.77	89.68	57.59
11.12	1.13	249.73	91.00	6.46	116.59	42.61
17.68	4.83	321.90	73.43	12.36	132.90	30.50
23.87	10.99	322.05	54.51	17.45	160.62	27.23

Note: * desorption was observed

The results show that the efficiency of sorption of phosphorus from the aqueous environment

by fine and coarse-grained sediments is the highest at the lowest input concentrations of phosphorus in solution, or at low concentrations in surface water above the sediment. At these concentrations, the amount of sorbed phosphorus by fine-grained sediments was up to almost 99%. The coarse-grained sediments sorbed phosphorus at a level of up to 84%. However, when no sorbate is used, phosphorus is released from the sediment into the water, as shown by the results of leachability tests in our previous research [18]. The amount of phosphorus released into water was recorded at 0.15% for fine-grained and 0.25% for coarse-grained sediment.

Increasing the concentration of phosphorus in the solution leads to a decrease in the sorption efficiency of the sediment, while at high concentrations of the sorbate, the sorption process is significantly stabilized due to reaching the maximum sorption capacity of bottom sediments (Fig. 2).

Maximum sorption of phosphorus by fine and coarse-grained sediments was observed at the highest concentrations of phosphorus in solution [19] with a maximum phosphorus sorption capacity of 325 mg P/kg for fine-grained sediment and 207 mg P/kg for coarse-grained sediment (Fig. 3).

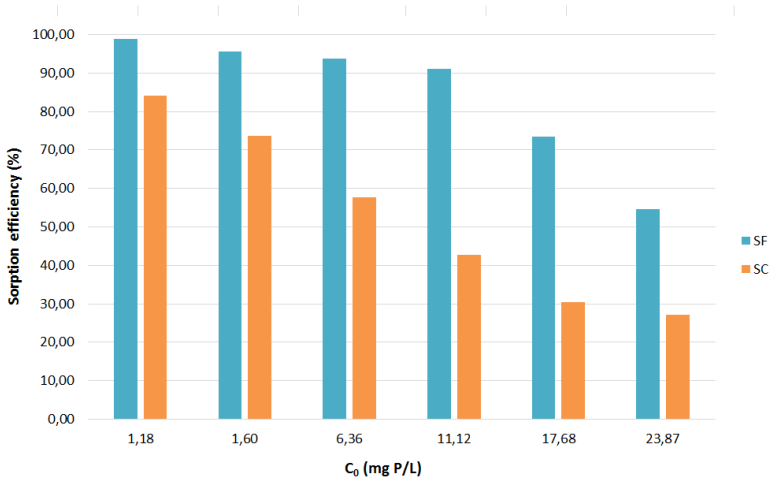

Figure 2: Phosphorus sorption efficiency by bottom sediments depending on their particle size

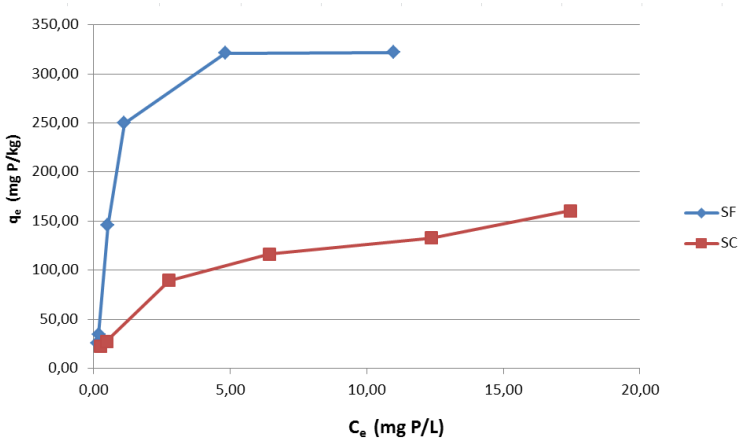

Figure 3: The development of phosphorus sorption by fine (SF) and coarse grained (SC) sediments in the aquatic environment

The study shows that fine-grained sediment has a higher sorption capacity and can bind

higher amounts of phosphorus than coarse-grained sediment, which is probably related to the granularity and consequently higher specific surface area of fine-grained bottom sediments.

4 Conclusion

In this research, the mechanism of phosphorus adsorption behaviour on the fine and coarse-grained sediments in the Hervartov small water reservoir (in Slovakia) due to the different particle grain size was investigated.
The study demonstrated the ability of phosphorus sorption by sediments. The fine-grained sediment with a higher specific surface area was able to sorb a double amount of phosphorus compared to the coarse-grained sediment with a lower specific surface area. With increasing concentration of added sorbate, the amount of phosphorus sorbed by the sediments decreased, indicating that the sorption efficiency decreased with increasing sorbate concentration. A significantly higher sorption capacity was demonstrated by the fine-grained sediment, which implies that the grain composition and the associated specific surface area play an important role in the sorption properties of bottom sediments.
In terms of the ability of bottom sediments to bind nutrients, it is appropriate to apply them after extraction to the soil, in compliance with the requirements set out in Act no. 188/2003 Coll. on application of sludge and bottom sediments into the land.

Acknowledgements

This research has been supported by the Slovak Grant Agency for Science (Grant No. 1/0419/19) and by the Slovak Cultural and Education Grant Agency (Grant No. 073TUKE-4/2018).

References

[1] Bartram J., Ballance R. & Ongley E. (1996). *Water Quality Monitoring - A Practical Guide to the Design and Implementation of Freshwater Quality Studies and Monitoring Programmes*. London: WHO.

[2] Jurík Ľ., Húska D. & Baszo R. (2009). Historical basins sediments (in Slovak). In Sediments of watercourses and reservoirs: Proceedings of a conference with foreign participation (in Slovak), 13. – 14. May 2009 (231-240). Bratislava: SVHS ZSVTS.

[3] Hucko P. (2008). Phosphorus interactions between water and sediments in reservoirs (in Slovak). In Drinking water 2008: Proceedings of the conference. 9th continuation of conferences Drinking water from valley reservoirs (in Czech) (53-58). České Budějovice: W&ET Team

[4] Hucko P. (2009). Sediment quality of selected reservoirs. In Sediments of watercourses and reservoirs: Proceedings of a conference with foreign participation (in Slovak), 13. – 14. May 2009 (251-262). Bratislava: SVHS ZSVTS.

[5] Lee G. F. & Jones R. A. (1992). Water Quality Aspects of Dredging and Dredged Sediment Disposal. In J. Herbich (Ed.) *Handbook of Dredging Engineering* (9-23 to 9-59). New York: McGraw-Hill.

[6] Environmental Protection Agency. (1999). *A review of contaminant occurrence in public water*

systems. Report numer EPA/816/R-99/006. USA, Washington, D.C: U.S. Environmental Protection Agency, Office of Water.

[7] Junáková N., Bálintová M., Vodička R. & Junák J. (2018). Prediction of Reservoir Sediment Quality Based on Erosion Processes in Watershed Using Mathematical Modelling. *Environments*. Vol. 5, no.1, 2018, 1-12.

[8] Pacini N., Harper D.M. & Higler L.W.G. (2009). Dynamics and cycling of materials in river systems. In Dooge J.C.I. (Ed) *Fresh surface water - Volume II, Encyclopedia of life support systems* (196-221). UK: Eolss Publishers.

[9] National Research Council (Committee on Long-Range Soil and Water Conservation, Board on Agriculture). (1993). *Soil and Water Quality: An Agenda for Agriculture.* USA, Washington, D.C: National Academy Press.

[10] Sharpley A.N. & Menzel R.G. (1987). The impact of soil and fertilizer phosphorus on the environment. *Advances in Agronomy*. Vol. 41, 297-324.

[11] Carneiro Ch., Gutseit K.C., Andreoli C.V. & Lima R.L.D. (2014). Sediment. In Carneiro Ch., Andreoli C.V., Cunha C.L.N., Gobbi E.F. (Eds) *Reservoir Eutrophication: Preventive Management: An applied example of Integrated Basin Management Interdisciplinary Research* (191-216). UK: IWA Publishing.

[12] Sundareshwar P.V. & Morris J.T. (1999). Phosphorus sorption characteristics of intertidal marsh sediments along an estuarine salinity gradient. *Limnol. Oceanogr*. Vol. 44(7), 1693–1701.

[13] Tamatamah R.A. (2005). Phosphorus sorption in relation to soil grain size and geochemical composition in the Simiyu and Kagera river basins, Tanzania. *Tanz J Sci.* Vol. 31(2), 31-39.

[14] Wang Y., Shen Z., Niu J. & Liu R.: Adsorption of phosphorus on sediments from the Three-Gorges Reservoir (China) and the relation with sediment composition. *J Hazard Mater*. Vol. 162, 92-98.

[15] Jalali M. & Peikam E.N.: Phosphorus sorption–desorption behaviour of river bed sediments in the Abshineh river, Hamedan, Iran, related to their composition. *Environ Monit Assess.* Vol. 185, 537–552.

[16] Xiao Y., Zhu X., Cheng H., Li K., Lu Q., & Liang D. (2013). Characteristics of phosphorus adsorption by sediment mineral matrices with different particle sizes. *Water Sci Engineer*. Vol. 6(3), 262-271.

[17] Zhu H., Wang D., Cheng P., Fan J. & Zhong B. (2015). Effects of sediment physical properties on the phosphorus release in aquatic environment. *Sci China-Phys Mech Astron*. Vol. 58(2), 1-8.

[18] Junáková N. & Bálintová M. (2013). Nutrient leaching from reservoir bottom sediments. *Chemical Engineering Transactions*. Vol. 35, 1141-1146.

[19] Junáková N., Bálintová M. & Smolakova M. (2017). Influence of granularity of sediment from a water reservoir on phosphorus sorption processes. *Environmental processes*. Vol. 4, Supplement 1, S239–S249.

DOI:10.1515/sspjce-2020-0021

Investigation of the use of various materials for the construction of an enthalpy exchanger

Pavol Kozák, Danica Košičanová

Technical University of Košice, Slovakia
Civil Engineering Faculty, Institute of Environmental Engineering
e-mail: pavol.kozak@gmail.com, danica.kosicanova@tuke.sk

Abstract

Considering the current gradual depletion of non-renewable primary sources, it is necessary to address the reduction of energy consumption in ventilation and air conditioning systems. Although heat recovery alone reduces the energy intensity of these systems, if moisture recovery is considered as well, the contribution in reducing energy consumption is significant. These are mainly the devices designed primarily for spaces where people stay permanently, which do not allow large fluctuations in temperature and humidity. In cooperation with the manufacturer of heat recovery exchangers, we determined our own method of comparing different types of materials that could be used to design an exchanger which would also allow moisture recovery. These results in a significant reduction in energy consumption used to humidify the air in ventilation and air conditioning systems. It is one of the possible ways how to compare individual samples that are being measured. This article primarily deals with the comparison of three different types of materials, out of the total number of twelve measured samples.

Key words: enthalpy exchanger, permeability, moisture recovery, air handling unit, ventilation and air conditioning unit

1 Introduction

The current global situation, rapid economic development and industrial growth of individual countries result in accelerated depletion of primary energy sources, which threatens the future of any life on our planet. This state is simply not sustainable. Primary energy sources are not renewable and therefore, it is in the interest of each and every one of us to look for a solution how to prevent it, how to reverse this situation, slow it down or stop it completely. People cannot pretend it is not their responsibility. All these primary sources are being used for human needs; therefore, everyone should have their energy consumption under control and try to use energy as economically as possible. It basically does not matter if it is a household, a residential agglomeration, an industrial or agricultural operation. Attention must be paid to the

sustainability aspect of primary energy sources. In many cases, humanity needs to learn how to save energy. It has a huge impact on our future and the future of the next generations.

The primary legislative document for the energy performance of buildings is [1]. It defines the minimum requirements for new and renovated buildings, requirements for energy certification, requirements for heating and air conditioning systems control, and electromobility. There should be a focus on comparing the primary energy consumption and the method of evaluating its accuracy and evaluation errors [2, 5]. Optimization of primary energy consumption in HVAC systems is of great importance. There is a significant attention on the research in this area [3, 4, 6].

The potential savings when using model predictive control (MPC) to monitor temperature and humidity are discussed in [7].

Research and development in the energy consumption sector is moving in the direction of a search for possibilities to use renewable energy sources as much as possible. This applies not only to ventilation and air conditioning systems, but almost too all the areas that need energy sources. The goal is to gradually build "green buildings" [8].

Cho, K., Cho, D., and Kim, T. researched the reduction of electricity consumption in the ventilation and recuperation unit. The results of the experiments conducted in this study demonstrated that the bypass and room control modes of HRVS can result in an annual fan energy saving up to ~ 10.76% –61.84% [9].

By using renewable resources, reducing energy consumption, and increasing the efficiency of ventilation and air conditioning equipment, people could contribute to the preservation of the earth's primary energy sources for the future generations. The use of renewable energy sources has the greatest potential in this area, be it solar, water, wind, or air energy. One of the possibilities is to store thermal energy and to use it subsequently [10].

Another view on reducing energy consumption is the economic aspect, as energy prices are constantly rising, and the overall tendency is even less favorable. From this point of view, it can be assumed that if the society wants to maintain the same standard of living in the future as it currently enjoys, it will be much more financially demanding in the future. Therefore, it is appropriate to invest in renewable energy sources already in the present. In many countries these are already supported by the state subsidies. In this way, low operating costs for energy can be achieved in the future and at the same time, the environment would not be burdened.

Technological progress is currently focused on product improvement and work efficiency in the production process. Last but not least, there is an effort to achieve automation of production processes, robotization and minimization of errors, which results in increased quality and efficiency of individual products. The aim of the manufacturers is to minimize production costs, while maintaining the highest possible production quality. Production processes become fully automated, with minimal human intervention. By minimizing the human labor the production process becomes more error-free, reliable, faster and efficient. Robotization and automation ultimately bring manufacturers not only an increase in production capacity, simplification of the entire production process (from design, through production process itself, to dispatch), but also simplification of warranty and post-warranty service of individual products. Bar codes and QR codes speed up the identification of equipment and components, which also has a significant impact on the production process.

Based on the Paris Agreement under the United Nations Framework Convention on Climate, and the subsequent European Green Deal currently being negotiated, [11] the European Union has set a goal to achieve climate neutrality by 2050. The Paris Agreement of 2015 requires all the signatories to commit to reducing greenhouse gas emissions. Every five years, each signatory shall increase the obligations under this Agreement, except for developing countries for which a transitional period applies. It is in developing countries where the fulfillment of the commitments is the most difficult. However, a tiny developing country, Bhutan, which was already carbon neutral, or rather, carbon negative in 2009, can serve as an example for all the countries in the world. With the help of its natural resources, this small country manages to sequester three times more CO2 per year than it produces [12]. It is an example worth following. Achieving this neutrality will include a transformation of the European society and economy, but in a fair and effective manner. This agreement assumes that in the second half of the century, European countries will produce only as much emissions as nature is able to sequester, thus achieving carbon neutrality.

Currently, the European Parliament intervenes in the field of ventilation and air-conditioning in a rather significant way by the means of the European Commission´s regulation No. 1253/2014 from 7 July 2014, implementing the directive 2009/125/ES of the European Parliament and of the Council [13] concerning the eco-design of ventilation units. This regulation significantly increases the energy efficiency of the ventilation equipment meeting the requirements of this directive. Ventilation devices receive energy labels, based on which they can be compared in a relevant way. Each device must indicate under which operating parameters it complies with the afore-mentioned directive.

Manufacturers are striving to come up with the most economical ventilation and air conditioning systems. They invest a lot of money in research and development, thus trying to increase the efficiency of their devices.

The analysis of topics in heating, ventilation and air conditioning is presented in [14]. Energy-saving fans exhaust air heat recovery devices, heat pumps, high-efficiency heat exchangers, humidification and dehumidification units and various filtration devices are installed in the equipment. The casing of the device itself is designed and manufactured to have minimum heat loss and the greatest possible tightness. All these measures increase the efficiency of individual devices. The aim is also to achieve the smallest possible error rate of individual HVAC systems, for example in the use of automated fault detection and diagnostics. (The application of automated fault detection and diagnostics (FDD) under HVAC predictive maintenance programs requires the development of simulation models able to accurately compare the faulty operation with respect to nominal conditions) [15].

Each of these components is subject to continuous research and development, whether on an academic or competitive basis. This results in high-efficiency devices with minimal energy consumption. It should be everyone´s goal to ensure comfort of the environment for which the air handling unit is designed.

Much attention is being paid to research in this area. A possible increase in the efficiency of HVAC systems is mentioned in [16, 17].

The measurement and mutual comparison of two enthalpy exchangers is discussed in [18].

Zhang focuses on a specific laboratory space and possible savings in energy consumption by

using an HPHX (Heat Pipe Heat Exchanger) [19, 20].

An alternative to a countercurrent enthalpy exchanger is a rotary exchanger. Its analysis can be found in [21, 22].

Most units are designed and manufactured for use in areas where people move and breathe the air treated in these devices. Therefore, it is paramount to approach the research, development, production, installation, operation and maintenance of these devices thoroughly. Several parameters affecting the thermal comfort in space have been addressed in [23].

Indoor air quality based on CO2 concentration depending on ventilation is investigated in [24]. Lowering of indoor air quality and subsequent recommendation of forced ventilation with heat recovery is discussed in [25].

2 Experiment

Humidity can be expressed in several ways [26].
- Absolute air humidity, a=ϱd. It is the actual water vapor density in the air (kg/m^3)
- Partial water vapor pressure, pd. It is most frequently determined by measuring with a dry and wet thermometer
- Relative humidity, Rh. It characterizes the degree of air saturation (%)
- Specific humidity, X. It is the weight of water vapor per 1 kg of dry air (kg/kg)
- Dew point temperature - the temperature at which the air is saturated when being cooled by water vapor
- The wet bulb temperature, tm. It is the equilibrium temperature at which the heat needed to evaporate water from a wet surface is supplied from the air. It is used to measure air enthalpy.

Relative humidity is an important parameter not only when expressing thermal comfort in interiors, but it is also an important parameter from the hygienic point of view. When assessing the thermal state of the environment according to the air temperature, humidity can be ignored only if the relative humidity in summer is less than 60%. At higher relative humidity, the great partial pressure of water vapor makes it difficult to evaporate sweat, which results in disturbed thermal comfort [27]. Maintaining humidity under optimal conditions is, therefore, very important. In Slovakia, the binding limits valid for certain types of operations are defined in particular in [28] [29].
Measuring of permeability can also be done according to the norm ASTM E96-00 [30], which is experimentally elaborated in detail [31]. For this reason we chose our own methodology of measuring and evaluating the possible use of different types of materials in the research of moisture transfer by different materials, as well as their possible use in an enthalpy exchanger, i.e. an exchanger enabling the transfer of heat energy and moisture. There are many materials that could be used to build an enthalpy exchanger; however, considering the achieved results from measurements, not all of them are suitable. The selection of the measuring set took a long period of time, during which we, together with Atrea Company, tried to come up with a suitable methodology for comparing samples. The most suitable one seemed to be the comparison of the material of the same size, in the same (or comparable) boundary conditions.
The measurements took place in the span of one year, from May 2019 to June 2020, at not exactly regular intervals. The measurements were carried out in the laboratory of Atrea

Company, which provided measuring instruments, premises and valuable advice both in the construction of the measuring set itself and in the evaluation of individual values. However, due to the geographical distance from Atrea, which is based in Jablonec nad Nisou, Czech Republic, several measurements were carried out at home, since the measuring set is easily portable and takes a short time to prepare.

A modified aquarium served as a measuring set. It was gradually modified and improved in order to obtain the most accurate data from individual measurements. Also, the size and shape of the opening for the measured sample was gradually changed up to the final circular cross-section with a diameter of 100 mm, which subsequently allows easier calculation of the results. The result of the measurements determined the specific water vapor permeability of individual samples.

The main component of the measuring apparatus, "the aquarium", consists of a glass square container with an attached fitted, tightly sealed stainless steel frame with a rubber seal for fitting the cover with the measured sample. The container is closed with a tight double cover made of stainless steel, where the measured sample is installed between two stainless steel plates. The overall dimensions of the container including the sheet metal extension are 300 x 200 x 260 mm. The net weight of the measuring set is 4190 g. The tightness of the sample is ensured by a polymer-based sealant without solvents and isocyanates used in the automotive industry for car bodies. The plates with the measured sample are screwed together and the screws themselves are sealed again after tightening. The cover is placed on the aquarium and fastened with plier clamps. In addition, because of the weighing method of the whole apparatus as well as for better tightness, small wooden prisms are attached transversely along the shorter side of the aquarium. On these, a board containing assembly accessories is placed during weighing. A visual check confirms that it is fitted correctly with the container. At the beginning of measurements, a combination humidity and temperature sensor in the aquarium was also used. A 100% relative humidity is assumed during the experiment. In addition, to increase the efficiency of the measurement, a small fan from a computer with a safe voltage of 12V DC was installed in the set. This ensures the convection of water vapor during the experiment needed to bring the state in the aquarium closer to real conditions. The fan is mounted in a plastic baffle so that the flow is directed directly to the measured sample. The heater is a standard aquarium heater with a power of 50W and a thermostat with a 230V power supply, purchased in an aquarium shop. The accuracy of the thermostat on the immersion heater was in conflict with the actual water temperature, and this temperature difference was changing. Therefore, an additional informative immersion mercury thermometer was used to determine when the system is in a stabilized state with the ambient temperature, and thus it is possible to start measurement.

The measurement itself is performed as follows: the aquarium is filled with water so that the immersion electric heater itself is immersed. The sample is tightly attached in the opening in the cover which had been precisely cut out on a CNC machine, the container is closed, and all the mechanical joints are sealed with a sealant which is used in the automotive industry to seal car body parts. Subsequently, the water is heated to 23 C. This temperature is considered as a boundary condition in the steady state of the apparatus at the beginning of the measurement. Then, the measuring set is weighed with all the components: two small wooden prisms are placed on the cover of the apparatus. On these prisms, a plate made of PIR panel UNILIN for smart living is placed. This serves as a mechanical protection of the measured sample during weighing, and at the same time, as a surface on which the fixed assembly accessories are

placed. All cable wires from the built-in temperature and humidity sensors, the power line and the fan power supply, as well as the power supply of the electric immersion heater are placed on this PIR plate. The set- up is weighed ten times on a calibrated scale placed on a solid horizontal base, in our case a desk.

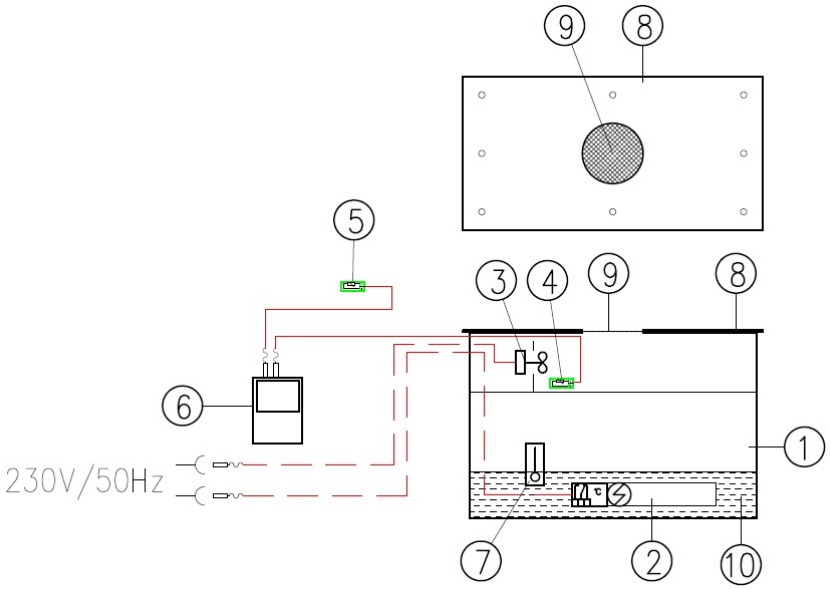

Figure 1: Measuring assembly scheme

①		aquarium –the main componet of the assembly
②		heater with thermostat, 230V/50Hz – 50W –water temperature adjustment in the assembly
③		AIREN Fan RedWings40 12V DC –ensuring air convection in the assembly
④		temperature sensor /AHLBORN ALMEMO 2690 instrument's probe –measuring the air temperature in the aquarium
⑤		temperature and humidity sensor /AHLBORN ALMEMO 2690 instrument's probe –measuring the air temperature and ambient moisture
⑥		AHLBORN ALMEMO 2690 measuring instrument –logging the temperature and humidity from the sensors in the assembly
⑦		informative submersible mercury thermometer –checking the steady state of the assembly before the start of the measurement
⑧		cap with an opening for the measured sample –the measured sample has been tightly attached here, joints sealed
⑨		measured sample –individual measured samples, sealed with putty
⑩		water –tap water heated to the ambient tempterature
		cable wiring –full line: sensor wiring, interrupted line: power supply

Figure 2: Table of the measuring assembly components

Each weighing takes place only after the water level has stabilized, which is monitored

visually. Then the measuring system is reconnected to the electric heater, the temperature and humidity sensors are connected to the measuring instrument and the fan adapter is switched on. The set is then left in a room with minimal fluctuations in ambient temperature, removed from the scale, placed on a flat surface, with heating on. The measurement time was dependent on the free time available. Some samples were measured for several hours, some for several days. The measurement time does not directly affect the specific permeability as can be seen in the graphical evaluation. At the end of the experiment, the measuring set is disconnected from the power supply, the sensors are disconnected and placed again on the PIR board on the wooden prisms, and weighed again ten times. The result is recorded. We then define the difference in humidity over the period of time on the specific area as the specific water vapor permeability in g / h / cm^2 of the measured sample.
The moisture transfer itself takes place in two areas. From the aquarium with 100% relative humidity to the lower edge of the measured sample, from there through the sample itself to the upper surface and from there to the surrounding air.

Permeability can be calculated according to [31]:

$$Per_{air} = \frac{\dot{m}}{P_{Sat}(R.H_{in} - R.H_{out})} \quad (1)$$

Air resistance to moisture transfer is calculated according to (Cengel [32]):

$$R_{air} = \frac{1}{Per_{air}}$$

Where:

Per_{air}	: Air permeability, kg/(m^2·s·Pa)
P_{Sat}	: Saturation pressure, Pa
$\dot{m}$	: Transferred moisture, (kg/m^2.s)
R	: Sample resistance to moisture transfer, m^2·s/kg
R_{air}	: Air resistance to moisture transfer, m^2·s·Pa/kg
H	: Enthalpy, J/kg

3 Description

Various materials were measured. A total of twelve samples were used for the measurement. Out of these, the focus is on three, for which there are the most documented individual measurements, which took place after the elimination of deficiencies in the measuring set and in the measurement and evaluation procedure. The whole process of measuring the vapor permeability of materials has gradually evolved; hence the results are more accurate towards the end of the recorded measurements. With regard to trademarks of industrial property, only the composition or a general description of individual materials is mentioned. As we do not have the permission of individual manufacturers, the names of the materials are intentionally not specified to avoid violation of industrial property laws.

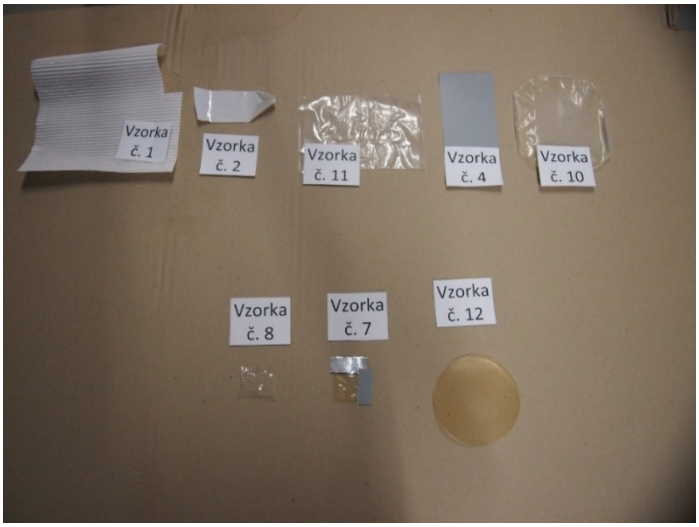

Figure 3: A photo of all measured samples

3.1 Sample No. 1

A piece of special patented paper, which has now been used in the production of enthalpy exchangers that allow both heat and moisture recovery for a long time. It serves as a comparison sample of the current functional material with new materials. This material is evaluated in this research paper.

Figure 4: Sample No. 1

3.2 Sample No. 2

It is a "semi-permeable membrane based on cross-linked polymer". This material is evaluated in the research paper.

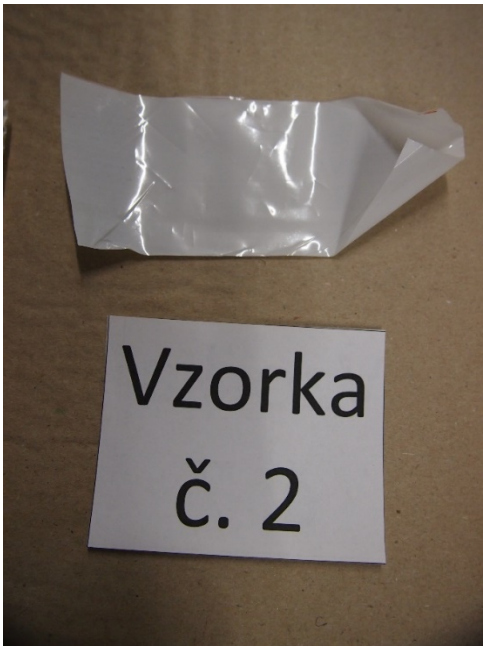

Figure 5: Sample No. 2

3.3 Sample No. 3, 5, 6, 10, 11

Different types and thickness of thermoplastic elastomer. This material is evaluated in the research paper.

3.4 Sample No. 4

The existing hPS Atrea material currently used to make standard heat recovery exchangers without moisture recovery – it was used to test the tightness of the measuring set.

3.5 Sample No. 7, 8, 9

It is a "semi-permeable membrane based on cross-linked polymer". This material is evaluated in the research another type of the sample no. 2 of different thickness. It is a "semi-permeable membrane based on a cross-linked polymer". This material is not evaluated in the work.

3.6 Sample No. 12

Copolymer resin. This material is evaluated in the work.

3.7 Measuring protocols

Due to the number of repeated measurements, samples no. 1, 2 and 12 were evaluated. Sample no. 4 served to continuously eliminate leaks and shortcomings of the measuring set since it is a material which is vapor-tight.

A measurement protocol was prepared for each measurement. The measurement protocol for the evaluated samples contains:

- Measurement date
- Start of measurement
- Initial assembly weight
- End of measurement
- Final assembly weight
- Steady water temperature
- Steady temperature inside the aquarium
- Relative humidity in the aquarium (assumption 100%)
- Absolute humidity inside the aquarium
- Ambient temperature
- Steady relative ambient humidity
- Absolute ambient humidity
- The difference between the absolute humidity in the aquarium and the absolute ambient humidity
- Permeability
- Sample area
- Specific permeability
- A note

Figure 6: Sample No. 12

4 Evaluation

Out of the total number of 47 measurements during the entire period of one year, a total of eleven measurements of 3 measured samples (no. 1, 2 and 12) were evaluated. These measurements were purposefully selected as the least affected by the error rate and by the gradual improvement of the measuring set. Individual descriptions of the measuring set modifications as well as control measurements with the sample no. 4, or repeated measurements are stated in individual measurement protocols. Because the heater in the aquarium was just a common one, there were inexplicable fluctuations in water temperature, +/- 1 °C. Thus, the measurement is affected by this deviation. However, in the long run, all measured samples had the same conditions, therefore, this error can be accepted. It does not affect the comparison of the specific permeability of water vapor significantly. At the beginning of the measurements, experiments were made with changing the water temperature as the "driving force" of the whole process, but these changes did not have a significant effect on the results, so the results were accepted with this inaccuracy. In the end it turned out that these fluctuations are caused by the thermostat in the heater device itself, and the temperature has since been additionally controlled by an immersion thermometer attached to the wall of the aquarium.
Another disadvantage of the measuring apparatus was the assumed leak, therefore, at the beginning of the measurements a value of 0.1 g/h was deducted from the value of water vapor

permeability. This leak also appeared in the leak test.
Gradual improvement of the measurement procedure, however, showed that the problem was not in the leakage of the measuring apparatus itself, but in the repeated weighing of the measured sample on the scale SOEHNLE QC Page Profi No. 67080. The scale was calibrated in 02/2018. For the first measurements, the assembly was weighed once, after the water level had completely stabilized on the scale. Then, however, the assembly was weighed ten times at the beginning of the measurement as well as at the end of the measurement. From these values, an arithmetic average was calculated. Its value was entered in the protocol as well as in the table, as the weight at the beginning and end of the measurement. In this way, a deviation in the measurements of +/- 1 g from the total weight of the weighed assembly, which was found in later measurements, was excluded. As a result, the value of 0.1 g/h was no longer deducted from the water vapor permeability.
Each measurement was performed in the same given manner described above.
The result of the measurements determines the specific water vapor permeability of the individual assessed samples and their mutual comparison in tables and graphs.

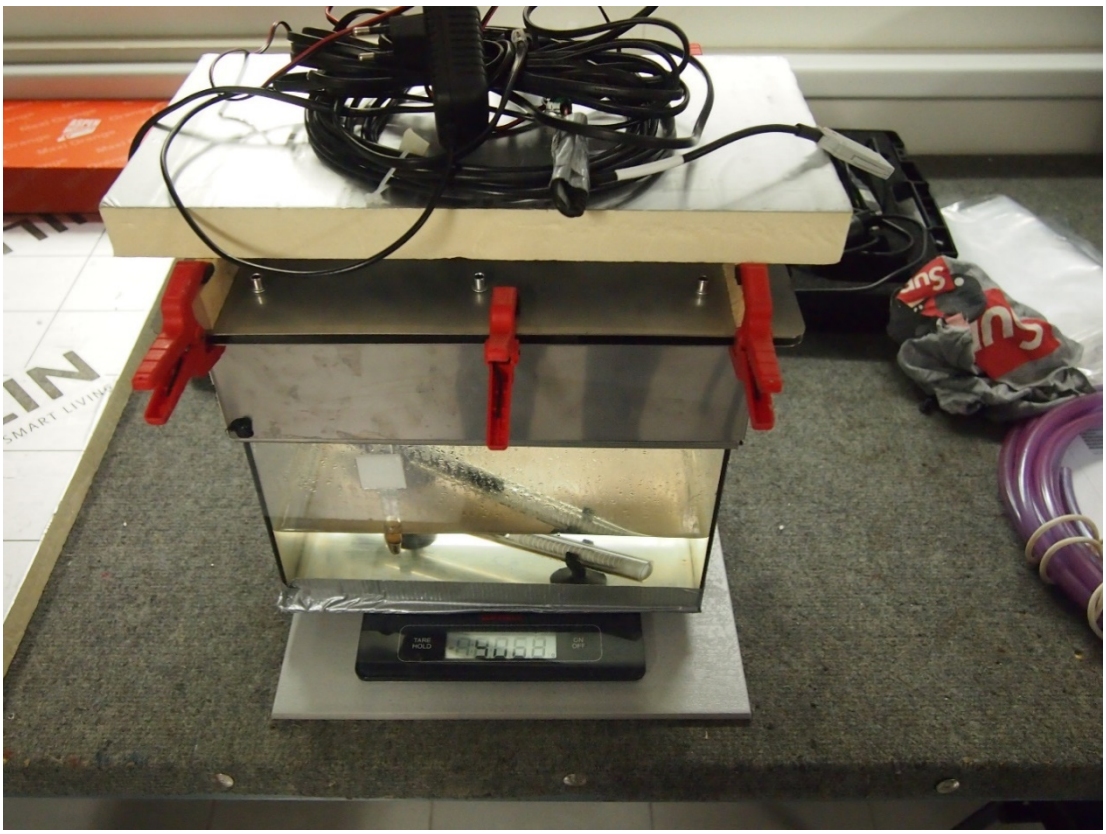

Figure 7: A photo of the measuring set while being weighed at the beginning of the measurement

Table 1: Measured and calculated data from the measurements

Measurement date	17. 2.	11. 3.	13. 3.	20. 3.	27. 3.	1. 6.	2. 6.	3. 6.	19.6.	26.6.	28.6
Measurement number	27	29	30	32	34	43	44	45	46	47	48
Material	Sample	Sample	Sample	Sample	Sample	Sample	Sample	Sample	Sample	Sample	Sample no. 12

	no. 1	no. 2	no.. 2	no.. 2	no. 2	no. 12	no. 12	no. 2	no. 1	no.1	
Thickness [mm]	1 vrstva					0,216+/-0,026	0,311+/-0,042				0,311+/-0,042
$m_{poč}$ [g]	9415	7431	7344	8578	11 292	9 189,5	9 153,4	8 157,9	9 084,3	9 124,3	9 110,0
Start of measurement	14. 2.	10. 3.	11. 3.	19. 3.	27. 3.	29. 5.	1. 6.	2. 6.	18.6.	25.6.	27.6.
	13:30:00	13:30:00	15:30:00	8:00:00	12:00:00	15:00:00	15:00:00	13:30:00	13:00:00	8:00:00	8:00:00
m_{kon}[g]	9298	7344	7207	8398	11 274	9 190	9 151,7	8 027,3	9 067,8	9 099,8	9 108,8
End of measurement	17. 2.	11.3.	13.3.	20. 3.	30. 3.	1.6.	2. 6.	3. 6.	19.6.	26.6.	28.6.
	7:00	15:30	10:30	15:30	7:00	10:00	11:30	11:30	9:00	10:00	8:00
Water temperature [°C]	23	25	23	23	23	23	23	23	28,5	28	23
Steady temperature inside the aquarium [°C]	28,90	19,90	19,70	25,00	26,60	26,50	26,50	24,80	26,40	26,00	26,50
Steady relative aquarium humidity [%]	100	89,5	87,7	99	99-61	assumption 100	assumption 100	assumption 100	assumption 100	assumption 100	assumption 100

Table 1: Measured and calculated data from the measurements (cont.)

Measured and calculated data from the measurements (cont.)											
Measurement date	17. 2.	11. 3.	13. 3.	20. 3.	27. 3.	1. 6.	2. 6.	3. 6.	19.6.	26.6.	28.6
Measurement number	27	29	30	32	34	43	44	45	46	47	48
Material	Sample no. 1	Sample no. 2	Sample no.. 2	Sample no.. 2	Sample no. 2	Sample no. 12	Sample no. 12	Sample no. 2	Sample no. 1	Sample no.1	Sample no. 12
Absolute humidity in aquarium [g/kg]	26,11	13,2	12,9	20	24	22,6	22,6	20,3	22,4	21,9	22,6
Ambient temperature [°C]	22,5	22,5	22,3	22	22	22,6	22,3	22,6	23,3	22,5	22,8
Steady relative ambient humidity [%]	48,3	29	35	36	26	41,3	46,6	46	49,4	50,1	47,5
Absolute ambient humidity [g/kg]	8,4	4,9	6	6,1	4,5	7	7,8	8	9	8,7	8,4
Difference absolute humidity [g/kg]	17,71	8,3	9,7	13,9	19,5	15,6	14,8	12,3	13,4	13,2	14,2
Permeability [g/h]	1,79	3,3	3,2	7,8	0,27	0	0,083	5,94	0,825	0,946	0,05
Sample area[cm^2]	97,7	594,5	594,5	594,5	13,5	0	78,5	z	78,5	78,5	78,5
Specific permeability [g/h·cm^2]	0,018	0,006	0,005	0,013	0,020	0	0,0011	0,01	0,011	0,012	0,0006

Based on the measured data, five dependencies which are being compared are determined:

- Dependency of specific permeability on the temperature inside the aquarium
- Dependency of specific permeability on the ambient temperature
- Dependency of specific permeability on the difference of absolute humidity's
- Dependency of specific permeability on the temperature difference
- Dependency of specific permeability on the amount of measurement time

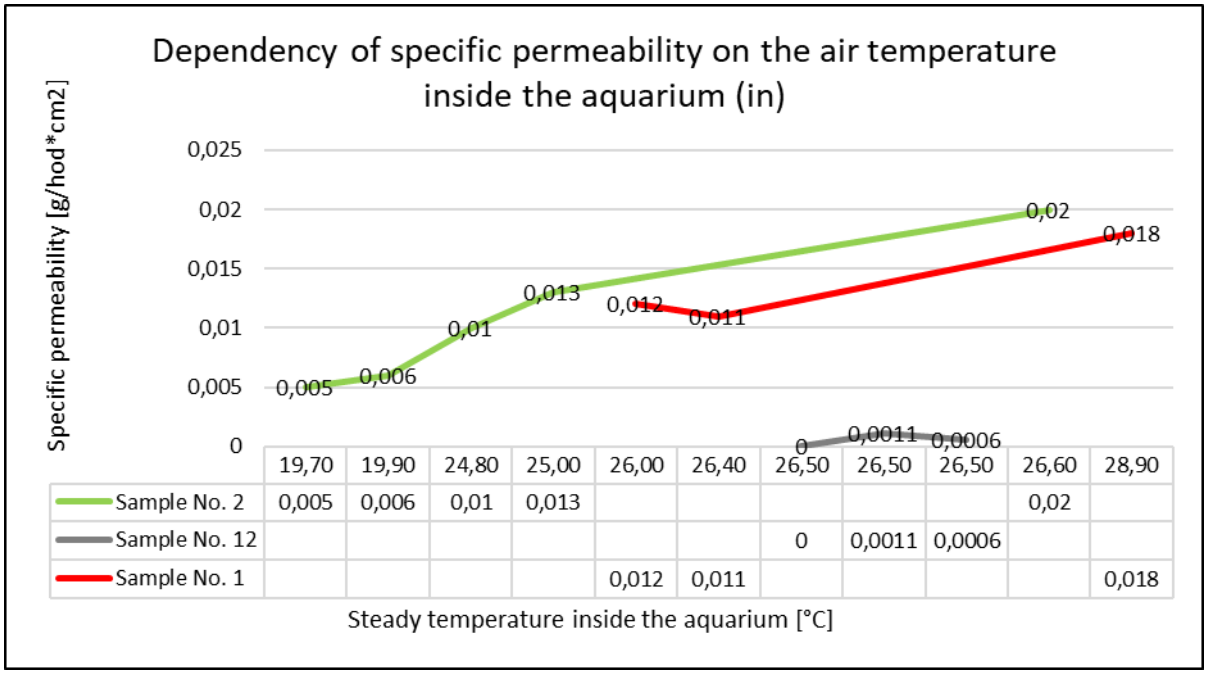

Figure 8: Dependency of specific permeability on the temperature inside the aquarium (in)

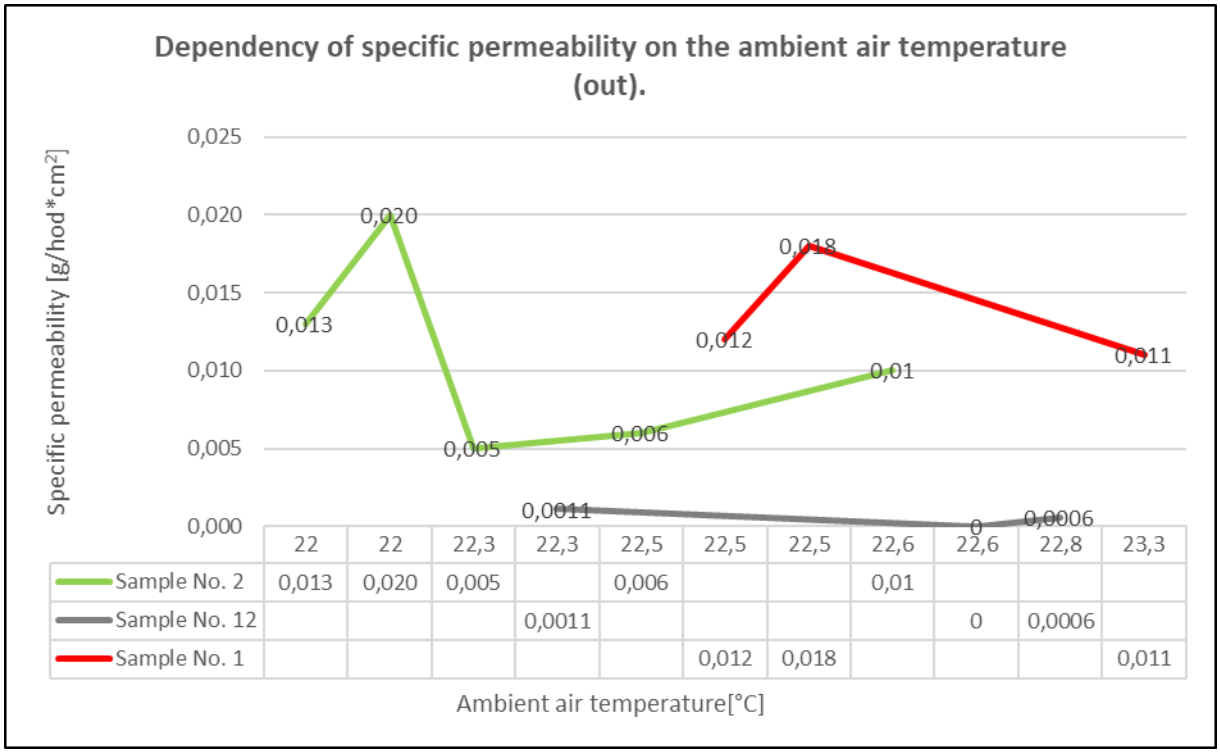

Figure 9: Dependency of specific permeability on the ambient temperature (out)

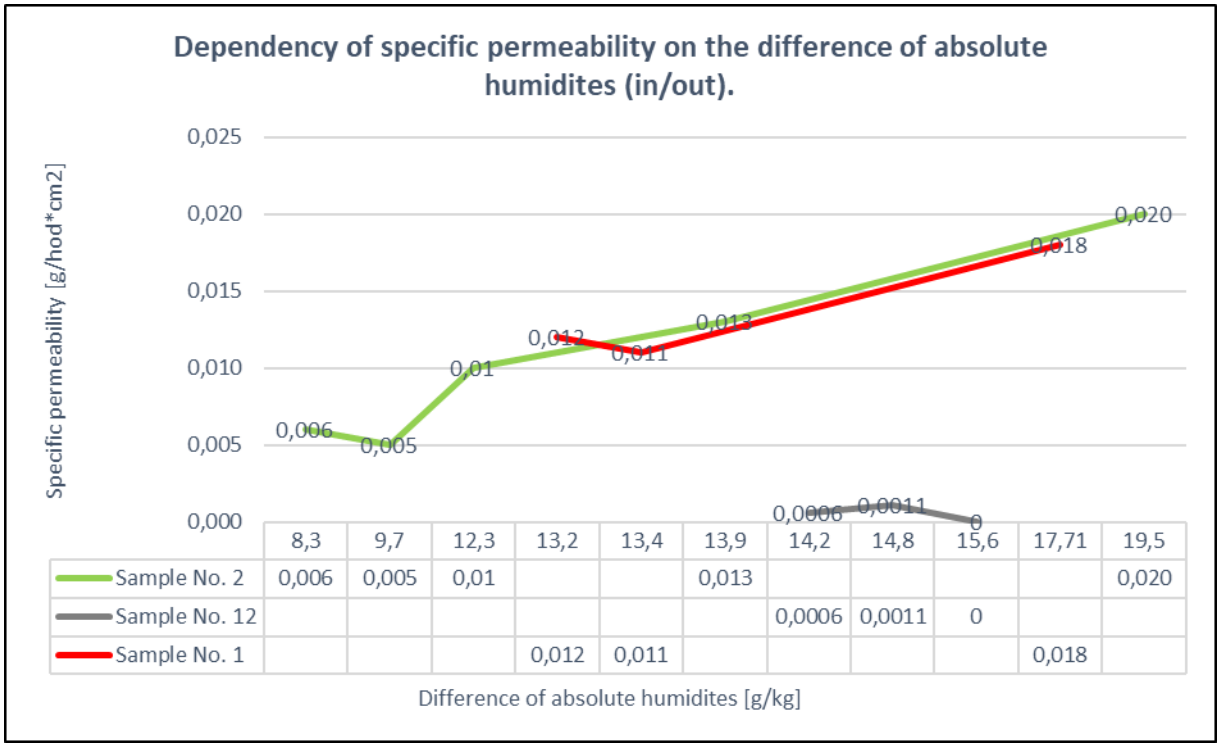

Figure 10: Dependency of specific permeability on the difference of absolute humidity's (in/out)

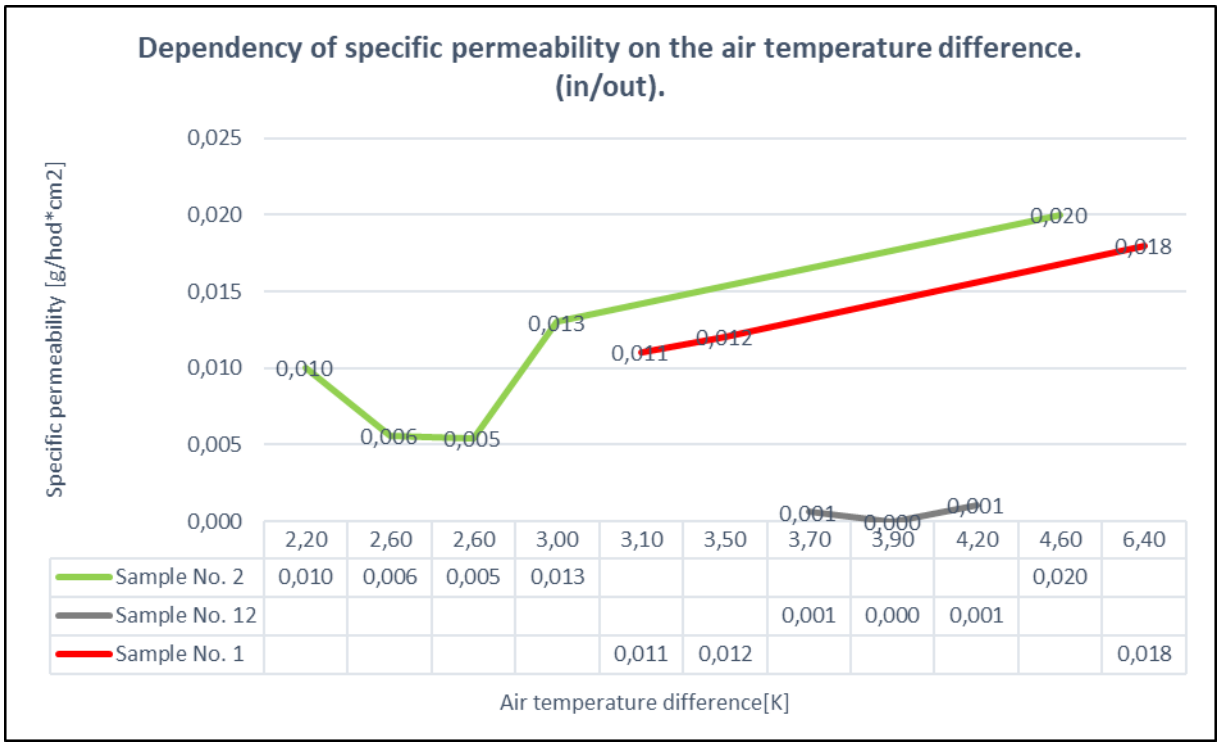

Figure 11: Dependency of specific permeability on the air temperature difference. (in/out)

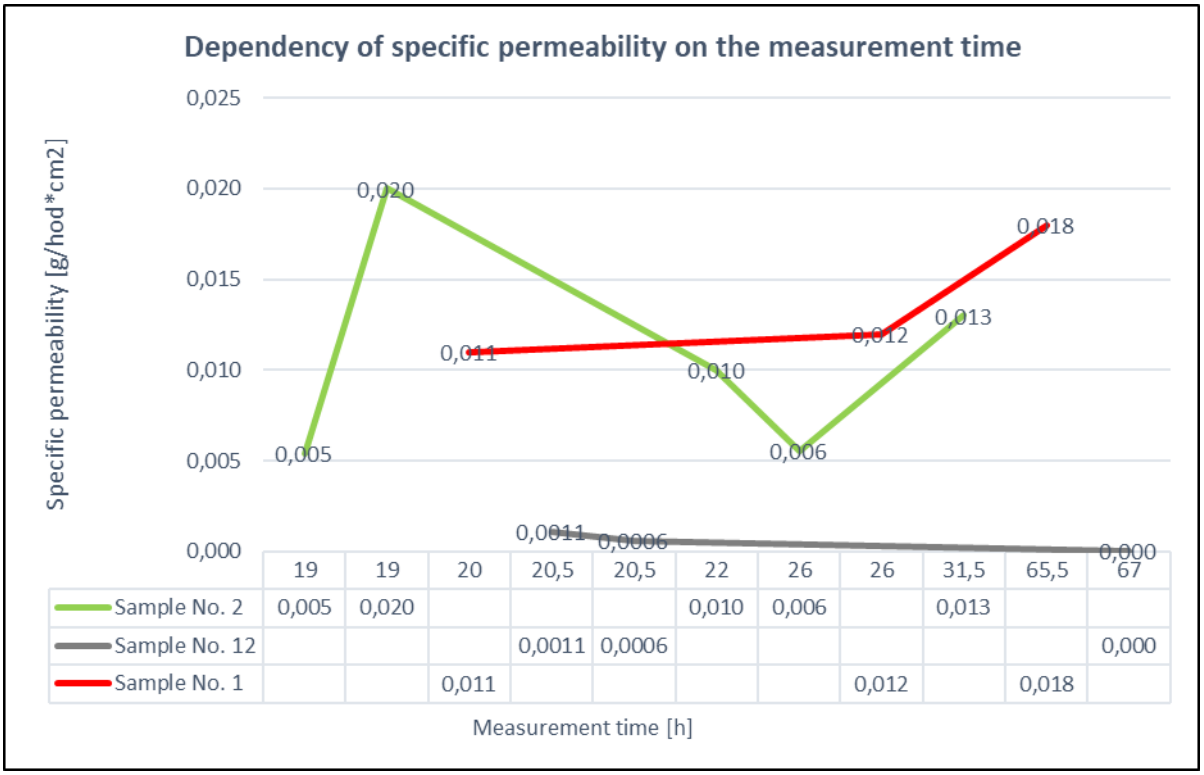

Figure 12: Dependency of specific permeability on the measurement time

The above graphs show that the highest specific permeability of water vapor is achieved by the sample no. 2 - whether concerning the dependency on the air temperature in the aquarium or on the ambient air temperature, and also on the difference in the absolute humidity's. However, the afore-mentioned material has the least prerequisites for use due to poor mechanical properties. In contrast, the material of the sample no. 12, which was assumed to be suitable for use, either from a mechanical or chemical point of view, had the most unfavorable parameters of all three evaluated samples.

The main idea of the measurements was to look for alternative materials for enthalpy exchangers, (heat exchangers capable of transmitting not only thermal energy, but also moisture) and subsequently to look for their use in ventilation and air conditioning systems. The benefit in our contribution is that the materials that are examined and compared are normally not usable/used for this purpose, i.e. according to the available sources, no one has yet explored their use in ventilation and air conditioning systems. Similar materials have been researched in [31]. This is also one of the reasons for not giving the names of individual materials. Therefore, only their general description or general chemical composition is mentioned, and all the materials are marked as a sample number 1 - 12. This was the reason for the chosen methodology of comparison with an already existing material, which has been used in the production of heat and moisture recovery exchangers the longest time. This specific method of mutual comparison makes it easy and realistic to compare the specific water vapor permeability of the individual materials.

Based on the specific permeability, we can determine, for instance, the size of the area of the enthalpy exchanger according to the parameters that are determined in advance (in this case it is how many grams of water vapor per hour needs to be transferred through the exchanger).

Given that theoretically, there are many suitable materials for use in the production of heat exchangers that allow heat and moisture recovery, this research is in its infancy. The ways to implement these materials in ventilation and air conditioning systems are still being researched. Of course, it is possible to use other methodologies to compare materials. Nevertheless, this method appears to be quite reliable once the deficiencies (either due to their design or the measurement procedure itself) were gradually eliminated. The measuring set is portable and relatively easy to construct. This made it possible to perform many measurements at home. Hence it is possible to measure other types of materials and compare them with each other. The only condition is to have a calibrated measuring device for measuring temperature and humidity, and a calibrated weight. During the measurements, the afore-mentioned device AHLBORN ALMEMO 2690 was used with a temperature sensor in the space inside the aquarium because the combination temperature and humidity sensor (which also measured humidity) was repeatedly flooded at 100% relative humidity and caused errors in displaying the sensor values. Hence it was not possible to record relative humidity and the right temperature. The combination temperature sensor was used to measure the temperature and humidity around the measuring set.
Other components are common ones and were purchased in the aquarium shop. The components made of stainless steel such as the cover (the lid that covers the measuring set) were made by Atrea Company on a CNC machine.

5 Conclusion

This research paper does not address the construction of the exchanger itself, as this topic would need a separate assessment methodology. This research focuses only on finding new materials for use in this area. Each measured sample has specific chemical, mechanical and thermo-technical properties. According to the results of the measurements, some samples change their shape, they stretch, shrink, deform, or return to their original shape, which has a major impact on the mechanical construction of the exchanger and its subsequent use in real life. The solution, after selecting a suitable material, could be adding additional reinforcement materials for mechanical strength, which would minimally restrict the actual air flow and the transfer of water vapor, and they would also maintain the optimal size of the heat and moisture recovery exchanger. An important aspect is also the hygienic aspect, resulting from the transfer of water vapor, which has not been assessed and evaluated here. One of the partial results was the "onion test". It was experimentally performed during a long-term test on some samples, in which the transfer of odors through selected measured samples is monitored. This test was performed at Atrea company premises. In this case, instead of water, a pan with fried onions is placed in the aquarium, the measuring set is closed and transferred to another room where respondents answer whether and how they perceive the smell of the onion. The respondents compared several samples, and it was interesting to see their perception. In some cases, the respondents even smelled the technical smell of the film, which can have a significant impact on the actual use in practice. Of course, this is influenced by the air temperature in the assembly, which, after inserting the hot pan, reaches higher values than in the common practice in air handling units. These outputs are presented in individual measurement protocols and in the overall table where there is a record of all the measurements, even those that are not compared and evaluated in this research paper. There is a need for separate research on this topic concerning hygiene, which is

also continuously processed and evaluated. An important finding was that the material that achieves the best results in water vapor transmission has the worst mechanical properties, when the future construction of an exchanger is considered. On the contrary, the material which was assumed to have excellent mechanical properties, and which was declared to have vapor permeable properties by the manufacturer, achieves the worst parameters of water vapor transmission. The research of water vapor transmission itself is not completed, as new materials are continuously made. Nevertheless, even the already existing materials such as, for example, the sample no. 12, are still being researched. We continue looking for their possible use, either by changing the thickness of the sample or its chemical composition, which would be able to increase the vapor permeability of the material itself. This currently limits it the most. With the sample no. 2, however, the problem is the opposite. More research on the mechanical properties of its material still needs to be conducted and a new way how to construct the exchanger needs to be found. Further research and evaluation criteria are needed in these areas; however, these are not addressed in this article.

Funding:

This work was financially supported by the Grant Agency of Slovak Republic to support project No. VEGA 1/0512/20: "Analysis of new approaches and certification of sustainable office buildings from the perspective of wellbeing and performance of employees."

References

[1] Directive of the European Parliament. (2018). *Directive (EU) 2018/844 of the European Parliament and of the Council of 30 May 2018 amending Directive 2010/31/EU on the energy performance of buildings and Directive 2012/27/EU on energy efficiency. Available online: http://data.europa.eu/eli/dir/2018/844/oj (acces 10. october* 2020).

[2] Airaksinen, M. (2011). *Energy Use in Day Care Centers and Schools.* Energies 2011, 4, 998-1009.

[3] Steen Englund, J.; Cehlin, M.; Akander, J.; Moshfegh, B. (2020).*Measured and Simulated Energy Use in a Secondary School Building in Sweden—A Case Study of Validation, Airing, and Occupancy Behaviour.* Energies 2020, 13, 2325.

[4] Wahid, F.; Fayaz, M.; Aljarbouh, A.; Mir, M.; Aamir, M.; Imran. (2020).*Energy Consumption Optimization and User Comfort Maximization in Smart Buildings Using a Hybrid of the Firefly and Genetic Algorithms*. Energies 2020, 13, 4363.

[5] Ruiz, G.R.; Bandera, C.F. (2017). *Validation of Calibrated Energy Models: Common Errors.* Energies 2017, 10, 1587.

[6] Wang, W.; Shan, X.; Hussain, S.A.; Wang, C.; Ji, Y. (2020). *Comparison of Multi-Control Strategies for the Control of Indoor Air Temperature and CO2 with OpenModelica Modeling.* Energies 2020, 13, 4425.

[7] Bahramnia, P.; Hosseini Rostami, S.M.; Wang, J.; Kim, G.-J. (2019).*Modeling and Controlling of Temperature and Humidity in Building Heating, Ventilating, and Air Conditioning System Using Model Predictive Control.* Energies 2019, 12, 4805.

[8] Dall'O', G.; Belli, V.; Brolis, M.; Mozzi, I.; Fasano, M. (2013). *Nearly Zero-Energy Buildings of the Lombardy Region (Italy), a Case Study of High-Energy Performance Buildings.* Energies 2013, 6, 3506-3527.

[9] Cho, K.; Cho, D.; Kim, T. (2020). *Effect of Bypass Control and Room Control Modes on Fan Energy Savings in a Heat Recovery Ventilation System.* Energies 2020, 13, 1815.

[10] Bendic, V.; Dobrotă, D. (2018). *Theoretical and Experimental Contributions on the Use of Smart Composite Materials in the Construction of Civil Buildings with Low Energy Consumption.* Energies 2018, 11, 2310.

[11] The European parliament (2019*) COMMUNICATION FROM THE COMMISSION TO THE EUROPEAN PARLIAMENT, THE EUROPEAN COUNCIL, THE COUNCIL, THE EUROPEAN ECONOMIC AND SOCIAL COMMITTEE OF THE REGIONS: The European Green Deal. COM/2019/640.* https://eur-lex.europa.eu/legal-content/EN/TXT/?uri=COM:2019:640:FIN

[12] Available online: https://ourworldindata.org/co2/country/bhutan?country=~BTN.

[13] European Commission´s. (2014). *European Commission´s regulation No. 1253/2014 from 7 July 2014, implementing the directive 2009/125/ES of the European Parliament and of the Council [3] concerning the eco-design of ventilation units.* Available online: https://eur-lex.europa.eu/legal-content/GA/TXT/?uri=CELEX%3A32014R1253

[14] Ding, Z.; Liu, R.; Li, Z.; Fan, C. A (2020). *Thematic Network-Based Methodology for the Research Trend Identification in Building Energy Management.* Energies 2020, 13, 4621.

[15] Rosato, A.; Guarino, F.; Filomena, V.; Sibilio, S.; Maffei, L. (2020). *Experimental Calibration and Validation of a Simulation Model for Fault Detection of HVAC Systems and Application to a Case Study*. Energies 2020, 13, 3948.

[16] Dong, J.; Winstead, C.; Nutaro, J.; Kuruganti, T. (2018). *Occupancy-Based HVAC Control with Short-Term Occupancy Prediction Algorithms for Energy-Efficient Buildings.* Energies 2018, 11, 2427.

[17] Kim, N.-K.; Shim, M.-H.; Won, D. (2018). *Building Energy Management Strategy Using an HVAC System and Energy Storage System.* Energies 2018, 11, 2690.

[18] Kassai, M.; Al-Hyari, L. (2019). *Investigation of Ventilation Energy Recovery with Polymer Membrane Material-Based Counter-Flow Energy Exchanger for Nearly Zero-Energy Buildings.* Energies 2019, 12, 1727.

[19] Zhang, L.; Zhang, Y.F. (2016). *Research on Heat Recovery Technology for Reducing the Energy Consumption of Dedicated Ventilation Systems: An Application to the Operating Model of a Laboratory.* Energies 2016, 9, 24.

[20] Zhang, L.; Zhang, Y.-F. (2014). *Research on Energy Saving Potential for Dedicated Ventilation Systems Based on Heat Recovery Technology.* Energies 2014, 7, 4261-4280.

[21] De Antonellis, S.; Intini, M.; Joppolo, C.M.; Leone, C. (2014). *Design Optimization of Heat Wheels for Energy Recovery in HVAC Systems.* Energies 2014, 7, 7348-7367.

[22] Al-Hyari, L .; Kassai, M. (2020). *Development and Experimental Validation of TRNSYS Simulation Model for Heat Wheel Operated in Air Handling Unit.* Energie 2020, 13, 4957.

[23] Fanger, P.O. (1970). *Thermal comfort. Analysis and applications in environmental engineering. In Thermal Comfort. Analysis and Applications in Environmental Engineering*. Danish Technical Press: Copenhagen, Denmark.

[24] Gładyszewska-Fiedoruk, K.; Zhelykh, V.; Pushchinskyi, A. (2019). *Simulation and Analysis of*

Various Ventilation Systems Given in an Example in the Same School of Indoor Air Quality. Energies 2019, 12, 2845.

[25] Mjörnell, K.; Johansson, D.; Bagge, H. (2019).*The Effect of High Occupancy Density on IAQ, Moisture Conditions and Energy Use in Apartments.* Energies 2019, 12, 4454.

[26] Chyský, J., and K. Hemzal. (1993). *Větrání a klimatizace.*Bolit.

[27] Székyová, Marta, Karol Ferstl, and Richard Nový. (2004). *Vetranie a klimatizácia*. Jaga group.

[28] *Vyhláška Ministerstva zdravotníctva Slovenskej republiky č. 259/2008 Z. z. o podrobnostiach o požiadavkách na vnútorné prostredie budov a o minimálnych požiadavkách na byty nižšieho štandardu a na ubytovacie zariadenia*. (č. 210/2016 Z. z., 124/2017 Z. z.). Official publication: Zbierka zákonov SR; Number: 105; Publication date: 17/07/2008

[29] Recknagel, Sprenger, Schramek. (1997).*Taschenbuch für Heizung+ Klimatechnik*. 67. vydanie.

[30] ASTME96. (2000).*American Standard Test Methods for Water Vapor Transmission of Materials, American Society for Testing and Materials*, pp. 842-849.

[31] Nasif, Mohammad Shakir, Graham L. Morrison, and Masud Behnia. (2005). *Heat and mass transfer in air to air enthalpy heat exchangers." Proceedings of the 6th World Conference on Experimental Heat Transfer, Fluid Mechanics, and Thermodynamics.* Matsushima, Japan.

[32] Yunus A. Çengel, Afshin J. Ghajar. (2011). Heat and mass transfer fundamentals and applications. McGraw-700 Hill Education 701. 52.

[33] Koester S.M., (2016). *Membrane-based Enthalpy Exchagers*, Von der Fakult¨at fur Maschinenwesen ¨ der Rheinisch-Westf¨alischen Technischen Hochschule Aachen zur Erlangung des akademischen Grades eines Doktors der Ingenieurwissen schaften genehmigte Dissertation.

DOI: 10.1515/sspjce-2020-0022

Lifecycle and ecomonical study of selected thermal solar installations

Jaroslav Košičan[1], Miguel Ángel Pardo[2], Silvia Vilčeková[3]

[1]Technical University of Košice, Faculty of Civil Engineering, Institute of Architectural Engineering, Slovakia
[2]University of Alicante, Department of Civil Engineering, Alicante, Spain
[3]Technical University of Košice, Faculty of Civil Engineering, Institute of Environmental Engineering, Slovakia
e-mail: jaroslav.kosican@tuke.sk, mpardo@ua.es, silvia.vilcekova@tuke.sk

Abstract

Creating a scheme of solar thermal installations is a mighty move forward to develop a suitable energy standards of residential buildings. In recent years were done many studies, which did a several energy simulations for residence buildings. If design of thermal installation is false, it can lead to rise in the expensive overall energy costs and unsatisfactory thermal comfort in the building. Nowdays, in Slovakia using solar thermal installations are increasing more than in recent years. This research investigates twelve modern solar water heating systems, formed on the roof of the family house. We tried to make analysis, where designed solar energy systems were appropriate and fulfill energy requirements of DHW and heating. The study deals with the best financial alternative of the prepared installations of the house. According to overall prices of installation, energy production of additional source for heating and total system efficiency and lifespan, we found out the best possible choice. Expected amount of the various energy contribution is simulated in specialized program. If we talk about midterm energy values, we can see the best possible choice for the alternatives. In this case we made analysis of these schemes for typical family house in Kosice. We set the limits of the building and analyzed which scheme is the best for need of the yearly average water consumption and heating.

Key words: solar thermal energy; cost analysis; domestic hot water

1 Introduction

Building integration has long been recognized as a promising approach for a more successful dissemination of solar thermal systems for domestic hot water and space heating. An improved architectural and constructional quality of the installation can increase the acceptance among architects and end-users and at the same time reduce the system cost thanks to synergic effects [1]. The application technologies of renewable energy have developed rapidly around the world; the solar hot water system is the most basic application of solar energy, and currently has rather obvious economic benefits. The solar energy

technology has many advantages and disadvantages comparing to others energy. The potential advantages are: it works on noiseless environment; it does not produce any unwanted waste such as radioactive materials; it has high performance and reliable system; it uses clean technology – it does not produce any toxic waste or radioactive material; it has highly credible system with life span expectation, between 20 and 30 years; it has a low maintenance system [2]. New Renewable energy supply allows achieving long-term sustainability by limiting the impact on future generations. Efficiency improvement refers to increasing the efficiency of energy conversion equipment, which results in less primary energy use during energy generation and delivery procedures. Demand energy reduction requires a social behavior change. Renewable energy generated from regenerative energy sources such as hydro, solar, wind, geothermal and biomass remains a prime objective in the RED policy [3]. Concentrating solar power (CSP) refers to the technology that collects solar energy and converts it into high-temperature thermal energy for heat transfer fluid (HTF), which is then converted into electrical energy using a conventional thermal engine or other forms of power generation technology. Utilizing solar power to generate thermal energy is an effective method for realizing grid-scale dispatch able power generation and replacing conventional energy, which may bring revolutionary solutions to serious energy problems [4]. The solar-thermal conversion is another superb approach for utilization of solar energy, in which the solar energy can be harvested and stored in heat storage materials as thermal energy. The conversion efficiency of solar to thermal energy can reach as high as 80% proving that this approach tends to be a promising direction for the future development of solar energy utilization [5]. 84% of the heating and cooling energy consumption in the EU is still based on fossil fuels while only 16% is provided by the renewable energy sector [6].
This paper deals with evaluating the twelve schemes with five solar panels and other differences and overall cost over the lifetime of the system. Proposed schemes were simulated using program “T*SOL”. This software returns the energy from auxiliary heating, the energy delivered to collectors, the solar contribution to heating and DHW for every choice. There is calculated the net present value for the new ST system for their lifespan and ranked alternatives from the best alternative solar energy installation to the worst. In short, the greater the revenues after the installation lifespan, the better the alternative. We used climate conditions for city Košice (Slovakia) for twelve cases.

2 Materials and Methods

Input data of experimental house are used in TSOL software, such a location of building, thermal installation, latitude and outside and inside temperatures of house. For the following simulations we also needed characteristics of solar panel system and his equipment. One of the important input data are also consumption of domestic hot water (DHW) and characteristic of space heating. For successful study is appropriate to have an economic data such as price of total solar system installations and prices of fuel, energy, pellets etc. In this article we divided our solution into these steps: first step we need to input data of house and solar installation to software. In step two we designed alternatives and got the midterm results of energy delivered by solar thermal panels, which are based on additional heat source. In next part we compared results from software to results in reality. Another step is to do an economic research based on prices of systems and prices of energy from additional sources.

Penultimate step is to make a summarization based on overall investments and yearly savings. After all these results, we did the final step, which is the total life cost.

2.1 Simulation software characteristics and midterm results

We used simulation software TSOL 2018 (Valentin Software GmbH, 10243 Berlin, Germany, which is created for modelling various solar thermal installations. Software contains most of the schemes, which are used around the world. Results are based on outside conditions such as location etc., and energy values such as heat load, type of space heating. Yearly results, which we need are for each alternative are:

- Energy from solar thermal collectors (kWh),
- Total energy produced by system which contains energy to DHW and energy to space heating (kWh),
- Energy produced by additional heat source (kWh),
- Saving by wood boiler (kg), gas savings (m^3), CO_2 emissions avoided by additional source- heat pump (kg).

3 Case study

For this case we used experimental house which is located in Košice, Slovakia. Designed house has one floor, usable area is 53 m^2, indoor temperature 20°C, heat load 5 kW, specific heat load 94.34 W/m^3, specific annual energy supply 163.585 W/m^3. Latitude is 48.7°, longitude -21,3°, total annual global irradiation 1144.4 kWh/m^2, diffuse radiation percentage 53.90%, mean outside temperature 9.8°C, lowest outside temperature is -13°C.
Solar thermal panels have active surface of 1.78 m^2, gross collector area is 2.03 m^2, orientation is on south - 180°, inclination 45° and azimuth angles is 0°. Figure 1 shows each alternative contains and numbers presents following:

1 - Solar collector Thermosolar Žiar TS 300;
2 - Solar preheating tank, 200 liters;
3 - DHW (Domestic hot water) standby tank, 120 liters;
4 - Gas boiler, 15 kW;
5 - Combination tank, 1000 liters;
6 - Dual coil indirect water tank, 300 liters;
7 - space-heating buffer tank, 500 liters;
8 - Heat exchanger;
9 - Floor heating;
10 - DHW consumption;
11 - Heat pump, 14 kW;
12 - Wood fired-boiler 14kW.

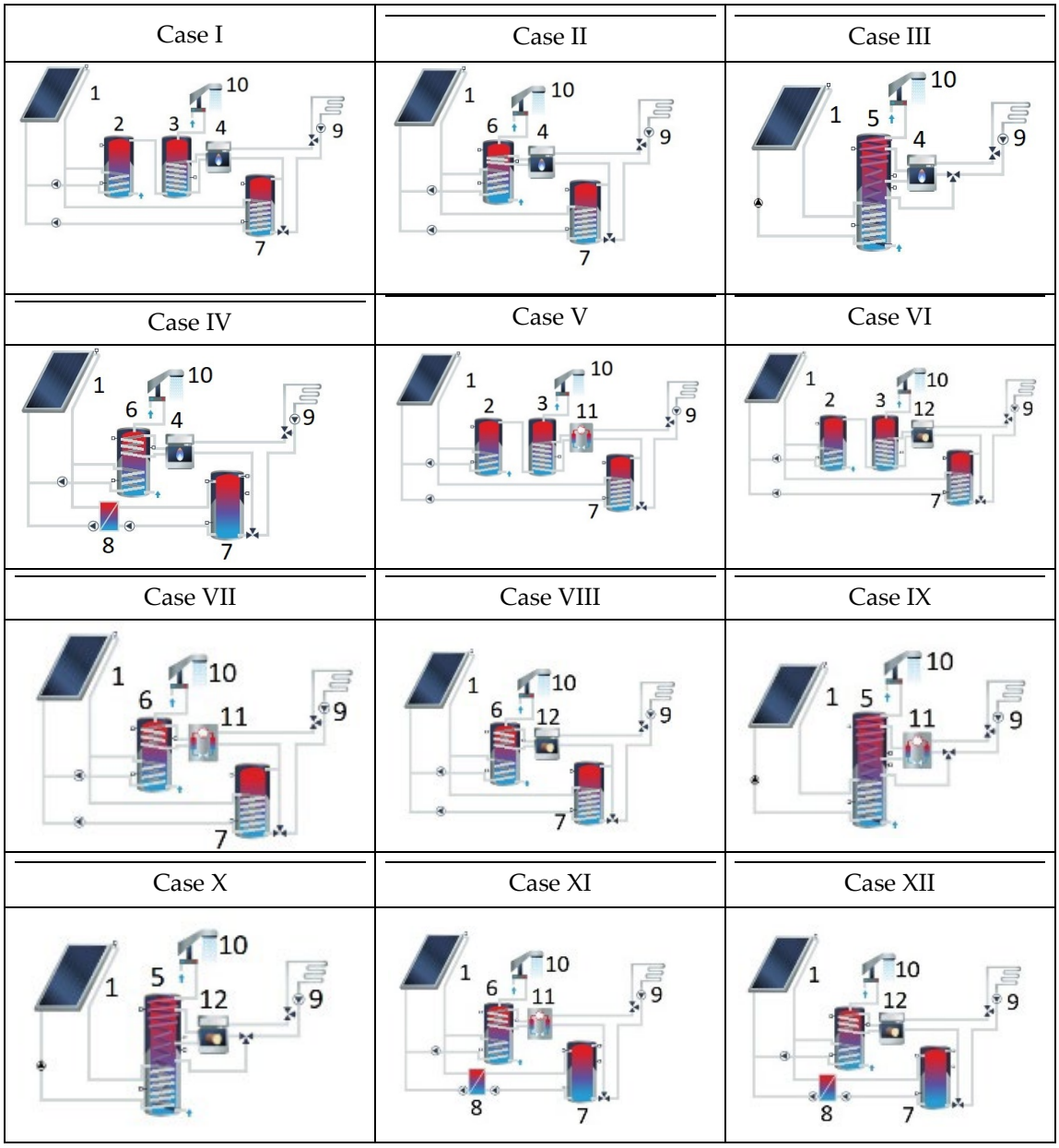

Figure 1 solar thermal schemes

3.1 Financial analysis

Economic analysis of total solar thermal equipment and their lifespan are described in table 1. The lowest starting price has case VI (4664.2 Euro) and the most expensive is case IX (20828.89 Euro). Energy results of simulation in software, which we needed are from additional heating, gas boiler performance with 15 kilowatts and their cost is between 7253 and 4981 euro. In additional heat source heat-pump with performance of 15 kilowatts are prices 20828.89 and 18556.2 euro. In cases where is wood fired boiler as additional source the prices are among 6936.89 and 4664.2 euro.

Table 1 Prices of equipment and lifespan

Equipment	**Case I**	**Case II**	**Case III**	**Case IV**	**Lifespan**
Solar collector TS 300 5x	2128.8	2128.8	2128.8	2128.8	30
Solar Preheating tank 200 l	401.4	-	-	-	20
DHW standby tank 120 l	376.0	-	-		15
Gas Boiler 15 kW	1169.0	1169.0	1169.0	1169.0	15
Combination tank	-	-	3956.1	-	15
Dual coil indirect water tank 300 l	-	1944.8	-	1944.8	25
Space-heating buffer tank 500 l	906.0	906.0	-	906.0	15
Collector loop heat exchanger	-		-	100.0	30
Total Investment	4981.2	6148.6	7253.9	6248.6	
Equipment	**Case V**	**Case VI**	**Case VII**	**Case VIII**	**Lifespan**
Solar collector TS 300 5x	2128.8	2128.8	2128.8	2128.8	30
Solar Preheating tank 200 l	401.4	401.4	-	-	20
DHW standby tank 120 l	376.0	376.0	-	-	15
Heat pump - 14 kW	14744.0	-	14744.0	-	15
Wood fire boiler - 14 kW	-	852.0	-	852.0	15
Combination tank	-	-	-	-	25
Dual coil indirect water tank 120 l	-	-	1944.8	1944.8	15
Space-heating buffer tank 500 l	906.0	906.0	-	906.0	30
Collector loop heat exchanger	-	-	-	-	30
Total Investment	18556.2	4664.2	18817,6	5831.6	
Equipment	**Case IX**	**Case X**	**Case XI**	**Case XII**	**Lifespan**
Solar collector TS 300 5x	2128.8	2128.8	2128.8	2128.8	30
DHW standby tank 120 l	-	-	-	-	20
Heat pump - 14 kW	14744.0	-	14744.0	-	15
Wood fire boiler - 14 kW	-	852.0	-	852.0	15
Combination tank	3956.09	3956.09	-	-	15
Dual coil indirect water tank 120 l	-	-	1944.8	1944.8	25
Space-heating buffer tank 500 l	-	-	906.0	906.0	15
Collector loop heat exchanger	-	-	100.0	100.0	30
Total Investment	20828.89	6936.89	19823.6	5931.6	30

3.2 Energy analysis

Additional source in every case produces relatively the same amount of energy (8900 kWh) a

year, which is showed in table 2. This house has 5 solar thermal panels by brand Thermosolar Žiar TS 300 in each case as a result of domestic hot water consumption 120 liters a day. Table 3 represents difference between simulated energy values and energy values in real-time. Real-time value for example heat-pump we calculated with house area (53m^2) multiplied by his performance 21.34 kWh/ (m^2 a year) which resulted in 3467.79 kWh a year.

Table 2 Energy required from additional heating

Gas Boiler		**Heat pump**		**Wood pellet boiler**	
Case I	8970.7	**Case V**	8969.9	**Case VI**	8970.8
Case II	8911.9	**Case VII**	8970.8	**Case VIII**	8910.2
Case III	8934.1	**Case IX**	8931.5	**Case X**	8930.2
Case IV	8947.5	**Case XI**	8942.2	**Case XII**	8943.7

Table 3 Energy comparison between cases and real time

	Heating		**Domestic hot water**	
Cases	Software	Real-time	Software	Real-time
ST heat pump	8969.90	1131.02	2040.65	768.50
ST wood-fired boiler	8943.70	4547.40	2040.65	725.57
ST gas boiler	8970.70	3467.79	2040.65	792.35

3.3 Economic and lifespan analysis

Table 4 Financial savings for each case (euro/month)

Case I	**Case II**	**Case III**	**Case IV**
159.14	159.81	159.56	159.41
Case V	**Case VI**	**Case VII**	**Case VIII**
247.47	230.73	247.56	230.94
Case IX	**Case X**	**Case XI**	**Case XII**
247.53	230.87	230.87	247.51

In this study we found that for example for case IV monthly savings are 159.4 euro. Following calculations for yearly savings give us 1909.71 euro/year. According to these, there was calculated the net present value which shows equation 2. Total investment for each case we calculated with equation 1.

$$I_0 = 4981.2 + (376.0 + 1169 + 376)e^{-15r} + (401.4)e^{-20r} \quad (1)$$

$$NPV = -\sum I_0 e^{-rt} + \int_0^{T^*} S_i e^{-rt}\, dt = -4981.2 - (376.0 + 1169 + 376)e^{-15*0.02} - \\ -(401.4)e^{-20*0.02} + \int_0^{30} 1909.71 e^{-0.02t}\, dt \quad =37496{,}36 \text{ EUR} \tag{2}$$

Table 5 net present value for every case

Case I	**Case II**	**Case III**	**Case IV**
37496.36	35884.69	33628.54	35671.05
Case V	**Case VI**	**Case VII**	**Case VIII**
49519.68	58207.72	49063.36	56205.22
Case IX	**Case X**	**Case XI**	**Case XII**
45551.76	54261.96	47371.21	61262.56

Calculation results shows that the best choice would be Case VI, instead of Case XII because the payback period is not so relevant priority in this study. Nevertheless, Case VI has the lowest payback period, but from the lifespan criteria is the best case XII.

4 Conclusion

This study demonstrates that applying gas boiler into solar thermal systems may help to meaningful savings. We introduce an approach, how to calculate which option is more suitable considering different additional heat sources. Concerning with future financial investments and savings for the lifespan establishments, we found the best alternative among all the alternatives in a family house in Kosice, Slovakia. The biggest annual working yields are related to heating and DHW preparation. There is no way to decide which is the optimal heating system without calculations and their corresponding results, that's why specialists should have approach to each building separately. In Slovakia, professionals take most of the time only financial site into detail research during the design stage of a house and technical systems. Another important thing to consideration is the maintenance cost, total system establishment and operation. Results of the systems lifespan and their cycle costs may allow us to see the most favorable plan, in cost-effective heating criterion and DHW system criterion.

Acknowledgements

This study was financially supported by Grant Agency of Slovak Republic to support project No. 1/0512/20. This paper is also the result of the Project implementation: University Science Park TECHNICOM for Innovation Applications Supported by Knowledge Technology, ITMS: 26220220182, supported by the Research & Development Operational Programme funded by the ERDFI.

References

[1] Giovannetti F.; Kirchner, M.; Sass R.; Rockdendorf G., (2016). Enameled glass panels for solar thermal building envelopes. *Energy Procedia*. *Volume 91*, 49-55.

[2] Teodorescu D.; Vartires A.; (2016). A study of the influence of solar panels coupled with thermal systems for a residential building, by applying methods of evaluation as EN 15316-4-3:2014 and TRANSOL. *Energy Procedia. Volume 85*, 530-538

[3] Mosallat F.; ELMekkawy T.; Friesen D.; Molinski T.; Loney, S.; Bibeau, E., (2013) Modeling, simulation and control of flat panel solar collectors with thermal storage for heating and cooling applications. *Procedia Computer Science. Volume* 19, 686-693

[4] Yang X.; Cai Z.; Luo T., (2016) A special type of tube receiver unit for solar thermal power generation towers. *Energy Reports 6*, 2841-2850

[5] Mehrali M.; Elshof J.E.; Shani M.; Mahmoudi A., (2021) Simultaneous solar-thermal energy harvesting and storage via shape stabilized salt hydrate phase change material. *Chemical Engineerring Journal 405*.

[6] Tschopp D.; Tian Z.; Berberich M.; Fan J.; Perers B.; Furbo S., (2020) Large-scale solar thermal systems in leading coiuntries: A review and comparative study of Denmark, China, Germany and Austria. *Applied Energy 270*.

[7] Valentin Software, (2018). *T*SOL.* Berlin

[8] Kleiner Y.; Adams B.J.; Rogersm J.S. (2001) Water distribution network renewal planning. J. *Comput. Civ. Eng.*, 15, 15–26.

[9] Burman, E.; Mumovic D.; Kimpian J. (2014) Towards measurement and verification of energy performance under the framework of the European directive for energy performance of buildings. *Energy 77*, 153–163.

[10] Ganiç N.; Yılmaz A.Z., (2014) Adaptation of the cost optimal level calculation method of Directive 2010/31/EU considering the influence of Turkish national factors. *Appl. Energy 123*, 94–107.

[11] Paksoy H.O.; Andersson O.; Abaci S.; Evliya H.; Turgut B. (2000) Heating and cooling of a hospital using solar energy coupled with seasonal thermal energy storage in an aquifer. *Renew. energy 19*, 117–122.

[12] Henning H.-M.; Döll, J. (2012) Solar systems for heating and cooling of buildings. *Energy Procedia 30*, 633–653.

[13] Bouhal T.; Fertahi S. ed-D.; Agrouaz Y.; El Rhafiki T.; Kousksou T.; Zeraouli Y.; Jamil A. (2018) Technical assessment, economic viability and investment risk analysis of solar heating/cooling systems in residential buildings in Morocco. *Sol. Energy* ,*170*, 1043–1062.

[14] Asdrubali F.; Buratti C.; Cotana F.; Baldinelli G.; Goretti M.; Moretti E.; Baldassarri C.; Belloni E.; Bianchi F.; Rotili A.; et al. (2013) Evaluation of green buildings' overall performance through in situ monitoring and simulations. *Energies 6*, 6525–6547.

[15] Cucchiella F.; D'Adamo I.; Gastaldi M.; Stornelli V. (2018) Solar photovoltaic panels combined with energy storage in a residential building: An economic analysis. *Sustain*.

DOI: 10.1515/sspjce-2020-0023

The impact of interior construction on the indoor environmental quality

Katarína Harčárová, Silvia Vilčeková

Technical University of Košice, Slovakia
Civil Engineering Faculty, Institute of Environmental Engineering
e-mail: katarina.harcarova@tuke.sk, silvia.vilcekova@tuke.sk

Abstract

The presented paper deals with the evaluation of the indoor environmental quality (IEQ) in two apartment units in different phases of interior construction. The first apartment is in the initial phase of an unfurnished apartment and the second in the final phase of a fully furnished apartment. The results of IEQ monitoring indicate that in terms of thermal-humidity microclimate, the required legislative limits were met and the differences between the unfurnished and the fully furnished apartment were minimal. Only the operative temperature values were not in the legislative range. The average particulate matter (PM) concentrations of the two representative fractions ($PM_{2.5}$ and PM_{10}) were 21.10 µg/m^3 and 564.72 µg/m^3 for the unfurnished apartment and 4.67 µg/m^3 and 68.15 µg/m^3 for the furnished apartment. The legislative limit of 50 µg/m^3 for PM_{10} was therefore significantly exceeded, especially in the case of an unfurnished apartment in the initial phase. The average TVOC concentration expressed in toluene equivalents was 1955 µg/m^3 in a furnished apartment and 910 µg/m^3 in an unfurnished apartment. Both of these values exceeded Mølhave's recommended limit of 200 µg/m^3. The presence of xylenes (51.19 µg/m^3) and ethylbenzene (17.27 µg/m^3) was detected in an unfurnished apartment. In addition to xylenes (171.63 µg/m^3) and ethylbenzene (79.25 µg/m^3), toluene (78.34 µg/m^3) was also present in the furnished apartment. The concentrations of these compounds were below the legislative limits, except for ethylbenzene for which no legislative limits are set. The above results show that further surface treatment and furnishing of the apartment contribute to the increase of the VOC levels in the indoor environment. In the case of unfurnished apartment, workers are exposed not only to elevated concentrations of TVOC but also to elevated concentrations of PM_{10} and should therefore pay attention to the protection and safety of health during the work.

Key words: indoor environmental quality, residential building, sick building syndrome, interior construction

1 Introduction

People spend almost more than 90% of their time in the indoor environment, where they are exposed to harmful pollutants of various origins [1, 2]. Volatile organic compounds (VOCs) are among the most serious pollutants occurring in the indoor environment. These compounds are monitored due to their negative effect on the human health. Some of them enter the indoor environment of buildings from outdoors, but most originate from internal sources. Increased

presence of volatile organic compounds can be observed especially in newly built or renovated buildings [3, 4].The main sources of VOC in the interiors of newly built or renovated buildings are considered to be the building materials. Particularly during completion, the interior goes through various stages of construction, but it is seldom known in which of these stages the greatest release of VOCs occurs and, in particular, what substances not only building users but also the workers themselves can be exposed to. Up to now, only a few studies have been published dealing with the contamination of the indoor environment at various stages of interior construction. Almost all of these studies are focused on the evaluation of IEQ in terms of the presence of volatile organic compounds. In a study by Park et al. performed several measurements in a newly built apartment complex in Korea. Within these measurements, they found that furniture was the main source of toluene and formaldehyde emissions [5]. Ochs et al. state that door painting is responsible for high emissions of acetone and other carbonyl compounds [6]. Gallon et al. measured VOC concentrations during the six phases of construction on two sites. The results show that the IAQ depends not only on emissions from building materials, but is also closely related to the overall implementation process [7]. Liang et al. measured VOC concentrations during the five stages of construction of a new apartment and found that the concentrations of toluene, α-pinene and ethylbenzene increased significantly after the installation of doors and doorframes. The concentrations of propylene glycol also increased after applying the paint to the walls and benzene after furnishing the apartment [8]. In his next study, Liang monitored VOCs during eight phases of construction in a residential block in Nanjing, China. In this case, the results showed that VOC concentrations were higher for the so-called phases of "dry" material (completed by a carpenter) as for phases of "wet" material (completed by a painter). Alkanes were abundant in every stage of construction [9].
Another group of pollutants present in the indoor environment is particulate matter. During construction, a large amount of particulate matter is produced, which can still persist in a new building for several weeks after its use. Nevertheless, little information is available on the contamination of indoor air with particulate matter during the interior construction phases. For this reason, the objective of this paper is to point out the extent to which selected phases of interior design affect the quality of the indoor environment. At the same time, it focuses on determining the exact PM and VOCs concentrations to which not only apartment users are exposed before moving in, but also the workers themselves during the implementation of interior construction. In addition to these two chemical parameters, this paper evaluates basic physical parameters such as temperature, relative humidity and air velocity.

2 Description of the monitored object

Monitoring of the indoor environmental quality was carried out in a newly built residential building, which is situated in eastern Slovakia in the recreational area of Štrba (High Tatras). The building consists of a reinforced concrete structure. Measurements and air sampling were performed in two residential units at different phases of interior construction. The first apartment unit, located on the third floor, was in the initial unfurnished phase, in which the wall surfaces and ceiling were plastered by applying gypsum plaster. In the case of the second apartment unit, it was a furnished one-room apartment located on the second floor. A laminate floor was installed in this apartment and at the same time the wall surfaces and ceiling were

treated with gypsum plaster and interior wall paint. The interior was equipped with basic furniture (bed, bedside table, closet, living room wall) and kitchen unit made of chipboard, whereas the living room was directly connected to the kitchen. Both monitored apartments are shown in Figure 1. The individual apartments are separated from each other by reinforced concrete load-bearing partitions as well as non-load-bearing acoustic plasterboard partitions. The apartments are equipped with aluminum balcony doors consisting of insulating safety triple glazing and fire and security entrance doors with a laminate surface.

Apartment in initial stage

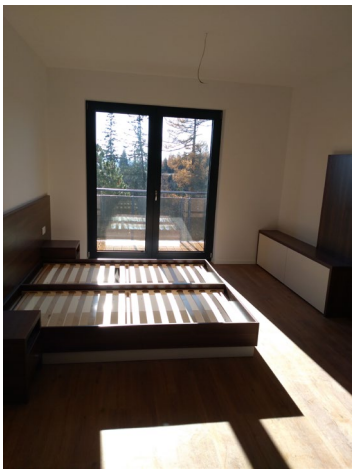

Apartment in final stage

Figure 1: Selected apartments in which indoor air monitoring was performed

3 Method

The parameters of the thermal-humidity microclimate (air temperature, relative humidity and air velocity) were determined using a TESTO 435-4 multifunction device with appropriate probe (Testo, Inc.; Germany). Particulate matter concentrations in the fraction range 0.5 to 10 μm ($PM_{0.5}$–PM_{10}) were determined using a HANDHELD 3016 IAQ meter (Lighthouse Worldwide Solutions, Inc., USA), which uses a laser-diode light source and collecting optics for particle detection. Total volatile organic compound (TVOC) concentrations were determined with a ppbRAE 3000 UV photoionization detector (RAE Systems, Inc.; USA). A two-point calibration, zero and standard reference gas (isobutylene), was performed before the measurement itself. All measured concentrations were recalculated and are expressed in toluene equivalents (correction factor stated by the manufacturer is 0.5). The probes and measuring instruments were placed approximately in the middle of the room at a height of approximately 1.1 m from the floor. The parameters of the thermal-humidity microclimate, particulate matter and total volatile organic compounds were recorded at one minute intervals. The mean radiant temperature at three heights was determined using a Vernon-Jokl spherical thermometer (sphere diameter d = 0.1 m) in accordance with the standard STN EN 7726, according to which the operative temperature was also calculated. Active sampling of the target volatile organic compounds was performed for six hours. The air samples were collected onto an Anasorb CSC sorption tube using an Airlite sampling pump. After

sampling, the samples were further analyzed in an external laboratory by gas chromatography. Monitoring was performed in mid-September in the unheating period. Air exchange was not provided in the apartments during the entire monitoring. Measurements in the furnished apartment were performed approximately one month after the application of surface coatings and two weeks after the equipment of the apartment. In an unfurnished apartment, measurements were taken approximately one and a half months after the ceiling and walls were plastered.

4 Results and Discussion

The statistical evaluation of the measured data for both apartments is summarized in Table 1. The above results were compared with the requirements for the thermal-humidity microclimate and the limit values of harmful factors in indoor air specified in the Decree of the Ministry of Health of the Slovak Republic No. 259/2008 and 210/2016 [10, 11].

Table 1: Statistical evaluation of measured data in apartments in two different phases of interior construction

	Statistics	Temperature [°C]	Relative humidity [%]	Air velocity [m/s]	$PM_{2.5}$ [$\mu g/m^3$]	PM_{10} [$\mu g/m^3$]	TVOC [$\mu g/m^3$]
Initial stage	Average	19.76	61.09	0.00	21.10	564.72	910
	Min	19.37	59.95	0.00	17.50	244.02	509
	Max	20.14	61.69	0.23	24.32	907.42	1134
	SD [1]	0.18	0.37	0.02	1.62	171.63	178.49
Final stage	Average	19.40	56.22	0.00	4.67	68.15	1955
	Min	18.97	52.13	0.00	3.88	43.85	1206
	Max	19.68	58.02	0.07	5.57	104.31	2407
	SD [1]	0.16	1.73	0.01	0.28	13.82	320.27

[1] Standard deviation

4.1 Thermal-humidity microclimate

The average values of temperature and relative humidity measured in both apartment units did not differ significantly from each other. The difference between the average relative humidity in the apartment in the initial stage and in the apartment in the final stage was 5%. The values of relative humidity in both apartments were within the required legislative range of 30-70%. Figure 2 shows the temperature and relative humidity in the selected apartment units throughout the measurement period. In a furnished apartment, the values of relative humidity tended to increase continuously, while in the apartment in the initial stage they mostly fluctuated around one value. The measured values of the air velocity did not exceed the permissible legislative limit of $0 \leq 0.2$ m/s in any of the monitored apartments. The operating

temperature in the unfurnished apartment was set at 19.4 °C and in the furnished apartment at 19 °C. Both values were outside the legislatively optimal (25–28 °C) and permissible (20–29 °C) range.

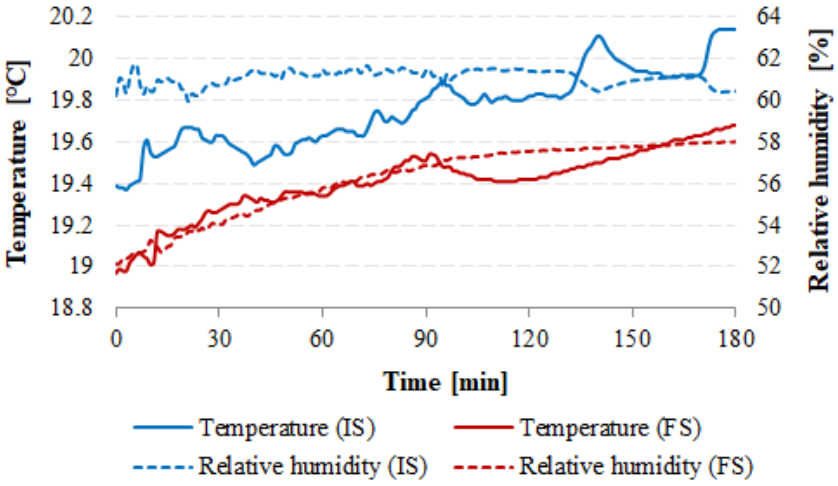

Figure 2: Recording of temperature and relative humidity measurements in the apartment in the initial stage (IS) and in the apartment in the final stage (FS) of interior construction

4.2 PM concentrations

The course of PM concentrations of all monitored fractions in the apartment in the initial stage and in the apartment in the final stage is shown in Figure 3. The difference between the maximum and minimum measured concentration was not higher than 1 µg/m^3 in the case of fractions 0.5 and 1.0 µm in none of the apartments. Particulate matter concentrations in the range $PM_{2.5}$–PM_{10} already had a more fluctuating course. Apparently, fluctuations in $PM_{5.0}$ and PM_{10} concentrations in the first half of the measurement were caused by the presence of two people in the room. In the second half of the measurement, a slow decrease in these concentrations was recorded, as monitoring was performed in the absence of people. The average concentrations of two representative fractions $PM_{2.5}$ and PM_{10} in the furnished apartment reached the values of 4.67 µg/m^3 and 68.15 µg/m^3. Concentrations of $PM_{2.5}$ ranged from 3.88 µg/m^3 to 5.57 µg/m^3 and PM_{10} concentrations from 43.85 µg/m^3 to 104.31 µg/m^3. The highest permissible value of PM_{10} concentrations is according to the Decree of the Ministry of Health of the Slovak Republic 50 µg/m^3. In the case of this apartment unit, the limit value was exceeded by 27%, as the measurement performed in a new building, in which interior construction works were still in progress. Conversely, in an unfurnished apartment, $PM_{2.5}$ concentrations ranged from 17.50 µg/m^3 to 24.32 µg/m^3 and PM_{10} concentrations from 244.02 µg/m^3 to 907.42 µg/m^3. The average particulate matter concentration for the $PM_{2.5}$ fraction was 21.10 µg/m^3 and for PM_{10} 564.72 µg/m^3. In this case, the limit value for PM_{10} was exceeded by up to 91%. Although the apartment is not yet habitable at this stage of construction, it is important from a health point of view to know what concentrations of PM_{10} people can only be exposed to if they work in such an environment. During the presence of

people in the room, the average concentration of PM_{10} in the unfurnished apartment was exceeded by 93% and in the furnished apartment by 37%.

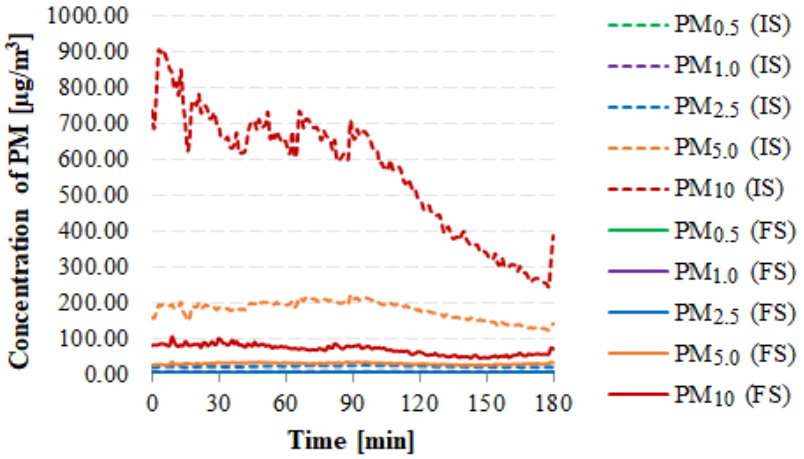

Figure 3: The course of $PM_{0.5}$–PM_{10} concentrations in the apartment in the initial and final stage of interior construction

4.3 VOC concentrations

The figure 4 shows that TVOC concentrations had an increasing trend in both monitored units, as the windows and doors were closed throughout the measurement. The average TVOC concentration in a furnished apartment was 1955 µg/m^3, which represents a 54% increase compared to the unfurnished apartment, in which the average TVOC concentration reached 910 µg/m^3. The recommended concentration of TVOC (200 µg/m^3) according to Mølhave [12], which does not yet cause discomfort or adverse health effects, was exceeded by 78% in the case of an unfurnished apartment and by 90% in the case of a furnished apartment.

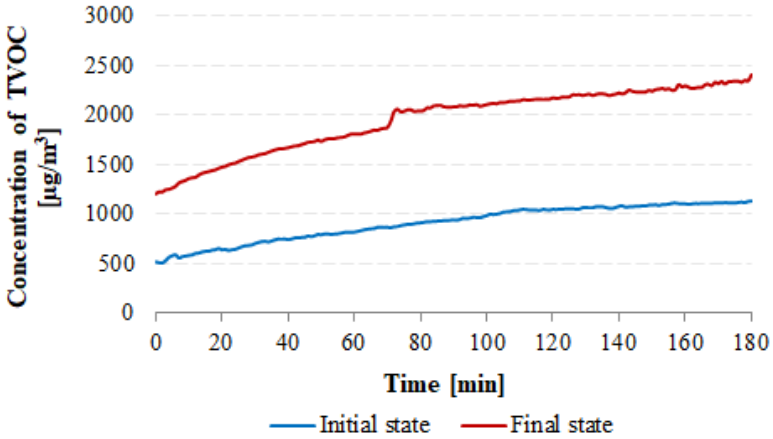

Figure 4: The course of TVOC concentrations in the apartment in the initial (IS) and final state (FS) of interior construction

In addition to the determination of total volatile organic compounds, the identification and determination of target organic compounds listed in the Decree of the Ministry of Health of the Slovak Republic No. 259/2008 and 210/2016 was also performed. Exposure to elevated concentrations of these four priority organic compounds in the indoor environment of buildings, namely toluene, three xylenes, styrene and tetrachlorethylene, may have adverse effects on human health. The results of the analysis of selected VOCs for both phases of interior construction are stated in Table 2. Of these four compounds, only xylenes were present in the unfurnished apartment (initial stage of construction), the concentrations of which were below the legislative limit of 4800 μg/m^3. In the furnished apartment (final stage of construction) the sum of three xylenes was 70.2% higher than in the unfurnished apartment, but it was still below the legislative limit. In addition, the presence of toluene was demonstrated in the furnished apartment. However, this concentration was also below the limit value of 8000 μg/m^3. The presence of styrene and tetrachlorethylene was not confirmed in either of the monitored apartments, as the concentrations of these two substances were below the detection limits. In the case of an unfurnished apartment, these compounds may come from emissions from the plasterboard and the putty paste used in the installation of the plasterboard. It is also possible that these VOCs come from mounted doors. On the contrary, in a furnished apartment it is a bit more complicated to define specific sources of VOCs, because in this case VOCs can come not only from building materials, but also from furnishing.

In addition to the target VOCs, the presence of ethylbenzene was detected in both apartments. For ethylbenzene, the legislation does not specify its limiting concentration in the indoor environment of buildings, but long-term exposure to its increased concentrations may have irritating effects on the human body. Compared to the unfurnished apartment, its concentration in the furnished apartment was 78.2% higher. The most common sources of ethylbenzene in the indoor environment of buildings are wall materials [13].

Table 2: Determined concentrations of target VOCs

	Initial stage	Final stage
Toluene [μg/m^3]	< LOD [2]	78.34
Xylenes [μg/m^3]	51.19	171.63
Styrene [μg/m^3]	< LOD	< LOD
Tetrachloroethylene [μg/m^3]	< LOD	< LOD
Ethylbenzene [μg/m^3]	17.27	79.25

[2] Limit of detection

4.4 I/O ratios for $PM_{2.5}$, PM_{10} and TVOC

As the monitoring of priority pollutants was carried out in a new residential building, in which interior modifications were underway, it is clear that indoor sources will predominate in this building. To confirm this statement, measurements of outdoor air quality were also performed. The ratio of indoor and outdoor air pollutants (I/O) is an important indicator for identifying the origin of different pollutants. Many methods for evaluating I/O ratios have

been described [13, 14]. In this study, I/O ratios were generated in a conventional way, where the outdoor air near the building is monitored simultaneously with the indoor air. A higher I/O ratio value means a larger contribution from indoor sources. If I/O < 1, the selected pollutants come from outdoor sources, if I/O > 1 comes from indoor sources. Figure 5 shows that all monitored pollutants come from indoor sources, whether it is an unfurnished or a furnished apartment. However, a higher increase in TVOC and $PM_{2.5}$ levels can be observed in the case of a furnished apartment. On the contrary, in the unfurnished apartment a significantly higher increase can be observed in terms of PM_{10} levels.

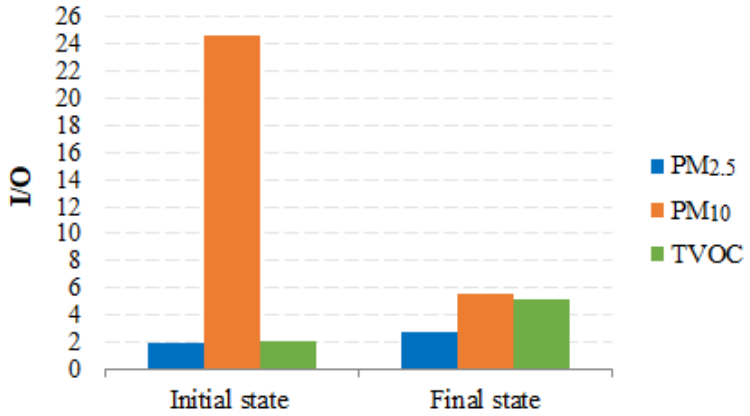

Figure 5: I/O ratios of selected pollutants

5 Conclusion

After evaluating the results, it can be stated that the resulting values of the thermal-humidity microclimate parameters were comparable for both apartments. At the same time, these values were within the required legislative limits, except for the operative temperature values. The average particulate matter concentrations of the two representative fractions ($PM_{2.5}$ and PM_{10}) were significantly different for both apartments. In the case of an apartment in the initial stage, the permissible legislative limit of PM_{10} concentrations was exceeded several times, and therefore workers should pay attention to the protection and safety of health during further work in this apartment. Concentrations of TVOC exceeded Mølhave's recommended limit of 200 $\mu g/m^3$ in both apartments. In a furnished apartment, the average TVOC concentration was up to half as high as in an unfurnished apartment. As part of VOC monitoring, a more detailed analysis of indoor air was performed, focused on the identification and determination of the four target VOCs (xylenes, toluene, tetrachlorethylene and styrene) listed in the Decree of the Ministry of Health of the Slovak Republic. Of these compounds, only xylenes were present in the unfurnished apartment. In addition to xylenes, toluene was also identified in the furnished apartment. The concentrations of all detected VOCs listed in the Decree of the Ministry of Health of the Slovak Republic were below the legislative limits. Simultaneously, the presence of ethylbenzene was detected in both flats, which is not subject to any legislative requirements. The presence of tetrachlorethylene and styrene was not confirmed in any of the apartments. Unambiguous identification of potential sources of detected VOCs is difficult in this case and requires an even more detailed

examination of the individual interphases that the apartment goes through during construction. The fact that the pollution of the indoor environment in both units comes mainly from internal sources was also confirmed by the results of the evaluation of I/O ratios. Monitoring of selected physico-chemical parameters of IEQ turned out for both stages of interior construction according to the assumptions with the possibility to quantify the exact concentrations of individual pollutants to which not only their new users but also the workers themselves may be exposed. It is assumed that even if the individual phases were evaluated within the same apartment, the results would probably not differ significantly from those mentioned in this paper.

Acknowledgements

This research was funded by VEGA grant agency with grant number 1/0512/20.

References

[1] Cakmak, S., Dales, R. E., Liu, L., Kauri, L. M., Lemieux, C. L., Hebbern, C., & Zhu, J. (2014). Residential exposure to volatile organic compounds and lung function: results from a population-based cross-sectional survey. *Environmental pollution*, *194*, 145-151.

[2] Yin, H., Liu, C., Zhang, L., Li, A., & Ma, Z. (2019). Measurement and evaluation of indoor air quality in naturally ventilated residential buildings. *Indoor and Built Environment*, *28*(10), 1307-1323.

[3] Földváry, V., Bekö, G., Langer, S., Arrhenius, K., & Petráš, D. (2017). Effect of energy renovation on indoor air quality in multifamily residential buildings in Slovakia. *Building and Environment*, *122*, 363-372.

[4] Du, L., Leivo, V., Prasauskas, T., Täubel, M., Martuzevicius, D., & Haverinen-Shaughnessy, U. (2019). Effects of energy retrofits on Indoor Air Quality in multifamily buildings. *Indoor air*, *29*(4), 686-697.

[5] Park, J. C., Kwon, Y. C., & Jun, H. D. (2011). A study on the improvement of indoor air quality of newly-built apartment houses using low emission building materials. *Journal of Asian Architecture and Building Engineering*, *10*(1), 235-240.

[6] de Mendonça Ochs, S., de Almeida Furtado, L., Cerqueira, W. V., & Netto, A. D. P. (2016). Characterization of the variation of carbonyl compounds concentrations before, during, and after the renovation of an apartment at Niterói, Brazil. *Environmental Science and Pollution Research*, *23*(15), 15605-15615.

[7] Gallon, V., Le Cann, P., Sanchez, M., Dematteo, C., & Le Bot, B. (2020). Emissions of VOCs, SVOCs, and mold during the construction process: Contribution to indoor air quality and future occupants' exposure. *Indoor air*.

[8] Liang, W., Wang, C., Yang, C., & Yang, X. (2014). Volatile organic compounds in different interior construction stages of an apartment. *Building and environment*, *81*, 380-387.

[9] Liang, W. (2020). Volatile organic compounds, odor, and inhalation health risks during interior construction of a fully furnished residential unit in Nanjing, China. *Building and Environment*, *186*, 107366.

[10] Ministry of Health, Slovak Republic, Governmental Regulation Number 259/2008 Coll. 2008. Detailed Requirements for the internal environment of buildings and on minimum requirements

for apartments of lower standard and accommodation facilities.

[11] Ministry of Health, Slovak Republic, Governmental Regulation Number 210/2016 Coll. 2016. Detailed Requirements for Indoor Environment of Buildings and minimum Requirements for Low-standard Flats and Accommodation Facilities.

[12] Mølhave, L. (1991). Volatile organic compounds, indoor air quality and health. *Indoor Air*, *1*(4), 357-376.

[13] Kozielska, B., Mainka, A., Żak, M., Kaleta, D., & Mucha, W. (2020). Indoor air quality in residential buildings in Upper Silesia, Poland. *Building and Environment*, 106914.

[14] Xu, J., Szyszkowicz, M., Jovic, B., Cakmak, S., Austin, C. C., & Zhu, J. (2016). Estimation of indoor and outdoor ratios of selected volatile organic compounds in Canada. *Atmospheric Environment*, *141*, 523-531.

DOI: 10.1515/sspjce-2020-0024

Experimental diagnostics on potential degradation of a selected building construction

Adriana Eštoková, Miriama Hološová, Eva Terpáková

Technical University of Košice, Slovakia
Faculty of Civil Engineering, Institute of Environmental Engineering
e-mail: miriama.holosova@tuke.sk, adriana.estokova@tuke.sk

Abstract

The aim of the study was to evaluate the historical building of the Old Town Hall of Košice city in terms of degradation processes of building materials. Regular maintenance, especially of historic buildings, is essential in terms of preserving the historic architectural heritage. Research was focused on selected parts of the basement of the historical construction with a special regard to the effect of humidity, salinity and carbonation of masonry structures. Samples were collected in the building basement and subsequently analysed in the laboratory. Chemical analysis of materials was performed by X–ray fluorescence analysis and the soluble salts were investigated by colorimetry. In addition, the content of sulphates was confirmed by infrared spectroscopy. Humidity of individual samples ranged from very low to very high, the highest values were measured around the perimeter of the room (positioning to the outside terrain). The carbonation ranged from grade III to IV, sulphates were detected in practically all samples. The results of study can help to design corrective measures.

Key words: diagnostics, humidity, salinity, analytical methods, assessment of technical conditions

1 Introduction

The diagnostic assessments for all types of constructions is very important. Each building is subject to degradation of individual elements of the structure due to the impact of physical, chemical, biological, but also mechanical factors over the time. At a certain age of the building, defects may appear, so it is necessary to preventively evaluate their condition [1]. Diagnosis of parts of building structures consists of sampling from selected defects locations after visual inspection. With regard to the preservation of the architectural heritage, it is necessary to avoid destructive techniques in solving the problem of determining the condition and design of the protection of historic buildings and to give priority to the contactless method of structural assessment. The non-destructive method in the evaluation of the historic building are widely used by experts, e.g. those dealing with preventive diagnostics in the case of the Italian church of Santa Maria ad Cryptas (from the 13th century) in the area of L'Aquila. Their method consisted of using IR (InfraRed) thermography to evaluate the

agreement between earthquake damage and previous thermography results. They also wanted to confirm the effectiveness of thermography for long-term research [2]. Researchers from the National Technical University of Athens focused in detail on non-destructive technical methods of cultural heritage protection. Among the methods of non-destructive assessment of buildings, they proposed Digital Image Processing (DIP). It is a software that converts an image (photograph) into a digital image, which allows you to classify but also extract properties or recognize patterns on the architectural surface, both at the macro and micro level. Ground Penetrating Radar (GPR) is a non-destructive technique that uses radar pulses to image the subsurface structure under investigation. It uses electromagnetic radiation (100 MHz to 2.6 GHz, which is usually preferred in the case of a historic building). The GPR transmitter transmits electromagnetic energy to the ground. When energy encounters a subsurface object or a boundary between materials with different properties, the radiation may be reflected, refracted or to disperse back to the surface. Ultrasound testing is also an example of a non-destructive method. This detects surface or subsurface defects or discontinuities in materials. High-frequency sound waves are introduced into the surface to be examined. These pass through the material, with a certain loss of energy (attenuation). The waves are then reflected at any interface they encounter as they pass through the material. The reflected beam, which is captured on the surface, is then analyzed to accurately determine the presence and location of the faults or discontinuities sought in the material. It is most often used to detect cracks in structures [3]. A 3D scanner is also used to assess the condition of buildings, which can be used to the actual condition of the assessed building. The result is technical drawings and the overall model of the building, which can be used as a basis in other - design procedures of reconstruction.

If needed, the samples are collected from the detected damaged places. After taking adequate samples (either by destructive or non-destructive method according to the needs and severity of the defects), the next procedure is performed in the laboratory. Based on basic evidence reactions, information about degradation processes are obtained from the extracts of the taken samples. Classical methods are used to evaluate the parameters such as e.g. gravimetric determination of humidity or modern analytical methods, mostly spectral methods for qualitative identification of elements or functional groups, or quantitative determination of selected pollutants.

Modern optical analytical methods of spectrometry such as X-ray diffraction (XRD) or X-ray flouorescence spectrometry (XRF) or colorimetry are used to obtain a more accurate concept of the chemical content in the sample. Fourier-transform infrared spectroscopy is a technique used to obtain the infrared spectrum of a solid, liquid or gas. At the same time, the FTIR spectrometer collects data with high spectral resolution over a wide spectral range. This provides a significant advantage opposite a dispersive spectrometer that measures intensity in a narrow range of wavelengths at once. The output of the FTIR method is the infrared spectrum, which is a graphical representation of the functional energy dependence. The energy dependence on wavelength is logarithmic, therefore the wave number is used which is defined as the inverse value of the wavelength, and thus the energy dependence on wavelength will be a linear function [4].

After determining the factual state of the examined material, the measured parameters are evaluated according to the relevant standards and guidelines. If it is confirmed that the condition does not comply with the required regulations, it is necessary to modify the damaged structure in the form of remediation.

In the past, the buildings were founded and protected against the ingress of water, based on the material and technical possibilities during construction at the time. Humidity problems are one of the most common defects, especially in older buildings [1]. The main causes of wet masonry can include: detrition or absence of masonry waterproofing; damage to sanitary-technical installation pipes; neglect of indoor ventilation; the building surroundings are insufficiently drained; unexpected changes around the building (effects of vegetation, shading, etc.); harmful interventions on the building (asphalt paint is applied to the masonry, which causes capillary water to rise into the zone above the paint); change of vapor-permeable floors to no vapor-permeable floors (from wooden, stone to concrete with asphalt / cardboard insulation); large vapor-tight areas around the building (asphalt carpet on the road, on the sidewalk, in the yard, around the building) etc.
Defects in building elements are related not only to the amount of water present, but also to its quality, i.e. its purity. Water as a transport medium migrates into the pores of the materials, thus allowing the transport or concentration of salts in these elements. The accumulation of salts subsequently leads to the destruction of building structures. Salt sources can be divided into several groups: salts that are primarily contained in one of the materials used in the construction (poor quality sand, lime, bricks, etc.); salts transported by the rise of moisture from the surrounding terrain or the penetration of moisture from other parts of the building; salts formed by chemical corrosion of materials used on the construction site by the influence of the atmosphere (e.g. formation of sulphates by the reaction of carbonates with sulphur oxide - the main component of acid rain); salts formed from biological sources (e.g. by conversion of urea to nitrates); salts formed as a result of remediation measures (e.g. sodium water glass is formed to a sodium as a by-product) [5]; salts as part of building materials or salts formed during the hardening of these materials; salts formed by contact with the environment, especially with the atmosphere or flowing water; salts contained in the material or salts contained in the material as a result of processing [4]. It should be noted that some materials may contain salts before it was built into the structure. E.g. cement may show traces of gypsum and alkalis. Bricks may contain salts depending on the quality of the clay used in their production [5]. The impact of salts in masonry also depends on the solubility of the salts in water. The higher the solubility is, the more harmful are the salt effects in the masonry. These are in particular the effects of calcium, magnesium and sodium salts in the form of chlorides, sulphates and nitrates [6].
This paper is aimed at the investigation of the deterioration state of historical building of the Old Town Hall in Košice city by applying modern analytical methods. Special attention was paid to investigation of humidity, salinity and carbonation of materials used.

2 Material and Methods

2.1 Studied building

The experimental research was devoted to a selected building of the Košice city Old Town Hall, in particular to the basement of the buildings. Firstly, the screening of the deterioration state in whole basement was performed by visual inspection and collecting and analysing the representative samples (Figure 1). Consequently, the more attention was paid to the room,

where the archive was (Figure 2).

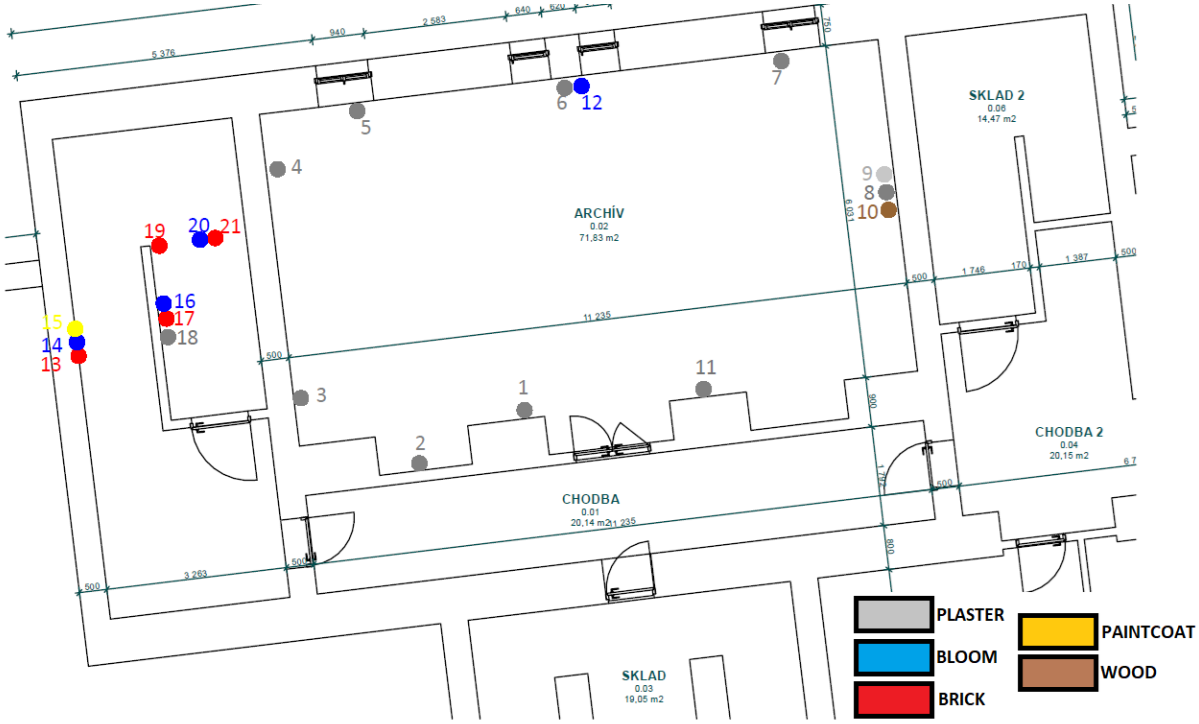

Figure 1: Ground plan of the examined part of the basement with marked screening points

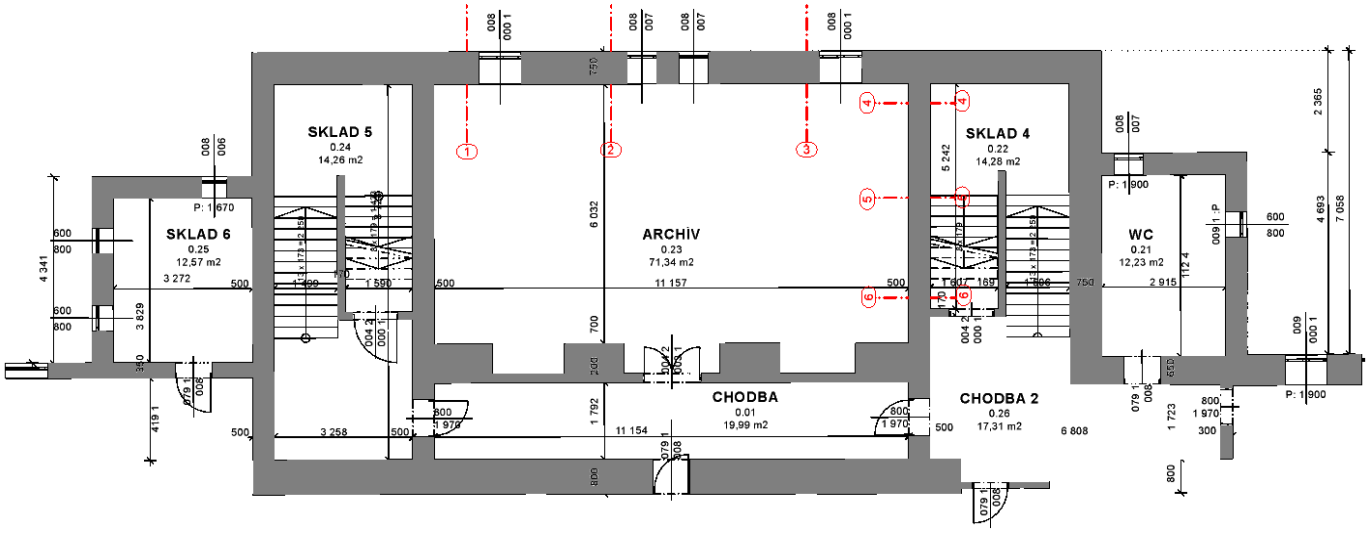

Figure 2: Ground plan of a part of the basement with marked sampling points

2.2 Methodology

Surveys of buildings in general, not only of historical buildings, do not have a precisely defined sequence of steps according to guidelines and standards. Every historical work is unique, it is not possible to create a universal methodology, and therefore it is necessary to approach each object within the survey individually. However, these main common steps were carried out in our study:

- Visual inspection
- Preliminary investigation and identification of major defects
- Selection of sampling points
- Detailed survey, in situ measurements, including sampling
- Processing of samples in the laboratory
- Evaluation of results
- Additional survey and, if necessary, additional samples
- Conclusion of the assessment and possible proposal for remediation measures [7].

After visual inspection, the sampling process was performed in two stages. In both cases, sampling was focused on the basement of the building. In the first phase, the entire basement was screened by sampling various types of materials such as brick, plaster, wood, and masonry and paint coat. The screening of the basement was indicated in the ground plan (Figure 1). 21 samples were obtained, taken by drilling from a depth of up to 10 - 30 mm or by scraping at the same height level - 0.5 m. The drilling method was performed at low speed to not to lose moisture. The samples were closed in PE bags with accurate marking and processed in the laboratory within about 2 hours after sampling.
Based on the results of the screening, in the second phase, the sampling was focused on the archive room. Archive room was used for archiving important documents; therefore, it was a priority to diagnose, analyse and propose corrective measures. Based on the sampling points shown in the ground plan (Figure 2), samples of eleven plasters and mortars were analysed.
The attention was paid to the humidity, salinity and carbonation state of the samples.

2.2.1 Humidity analysis

The most common failures of buildings are closely related to humidity. Humidity assessment is therefore part of every construction survey. Standard ČSN P 73 0610: 2000 Waterproofing of buildings, Rehabilitation of wet masonry, The basic provision [8] characterizes the moisture values in structures (Table 1), which are decisive for the design of remediation measures. Mass moisture was determined gravimetrically according to Equation 1:

$$W_{hm} = \frac{m_v - m_s}{m_s} * 100 \text{ [\%]} \quad (1)$$

where:

- m_v - weight of wet material [g]
- m_s - weight of dry weight [g]
- w_{hm} - mass moisture [%]

Table 2: Evaluation of masonry moisture according to ČSN P 73 0610 [8]

Humidity content w_{hm} [%]	Degree of humidity
$w \leq 3$	humidity very low
$3 \leq w < 5$	humidity low
$5 \leq w < 7.5$	humidity increased
$7.5 \leq w < 10$	humidity high
$10 \leq w$	humidity very high

2.2.2 Salinity analysis

As a representative of salinity, sulfates have been under examination. Sulfate is an anorganic anion that contains sulfur, general formula is (SO_4^{2-}). Sulfate salt solutions are corrosive. Sulphate corrosion can be considered as one of the most common form of deterioration in a masonry structure. This is linked with the process of voluminous sulfate products, such as gypsum, ettringite or thaumasite formation. Example of the gypsum formation in the concretes is given in Eq. 3 and 4.

$$Ca(OH)_2 + Na_2SO_4 + 2H_2O \rightarrow CaSO_4.2H_2O + 2NaOH \quad (2)$$
$$CaCO_3 + H_2SO_4 + H_2O \rightarrow CaSO_4.2H_2O + CO_2 \quad (3)$$

Gypsum ($CaSO_4.2H_2O$) is involved in the volume changes of structures and at a certain stage of moistening it is partially leached [7]. Under certain conditions, recrystallization can occur only to the formation of etringite ($3CaO.Al_2O_3.CaSO_4.32H_2O$) [5].

Table 3: The most important water-soluble sulphate salts occurring in building materials [5]

Sulphates	Solubility [g/l]
$CaSO_4.2H_2O$	2.4
$MgSO_4.7H_2O$	1172
$Na_2SO_4.10H_2O$	583
Na_2SO_4	481
K_2SO_4	111
$3CaO.Al_2O_3.CaSO_4.32H_2O$	-

Table 4: Main reactions of sulphate formation in building elements [5]

Reactions	Increasing the volume %	Multiple increase in solubility
$CaCO_3 + H_2SO_4 + 2H_2O \rightarrow CaSO_4.H_2O + CO_2 + H_2O$	about 100	160
$MgCO_3 + H_2SO_4 + 7\ H_2O \rightarrow MgSO_4.7H_2O + CO_2 + H_2O$	about 430	7 500

$FeCO_3 + H_2SO_4 + 7H_2O \rightarrow FeSO_4.7H_2O + CO_2 + H_2O$	about 480	16 000
$Al_2O_3 + 3H_2SO_4 + 15H_2O \rightarrow Al_2(SO_4)_3.18H_2O$	about 1400	27 000

The concentrations of sulphates in the samples were analysed in two ways: by leaching the samples and consequently determination of the solved ions by colorimetry as well by calculation based on the results from the X-ray fluorescence analysis, which provided the total sulphur content. Subsequently the determined concentrations of sulphates were converted to the percentage of sulphates in the original dry sample. Salinity caused by sulphates was assessed applying the WTA guidelines´ criteria (Tables 5 and 6), [10]. Although, these WTA criteria are primarily considered for masonry materials, for purpose of the study, the criteria were used to evaluate the sulphate content also for all brick materials.

Table 7: Criteria for salinity assessment according to WTA Guidelines 4-5-99: Assessment of masonry, diagnostics of masonry [9]

Salt type	Concentration expressed as % of the weight of the dry sample			
Sulphates	<0.5	0.5 – 2.0	2.0 – 5.0	>5.0
Salinity level	Low	Increased	High	Very high

Table 8: Criteria for evaluating the impact of salt ions according to WTA 2-9-04 / D Remedial plaster systems [10]

Salt type	Concentration expressed as % of the weight of the dry sample		
Sulphates	<0.5	0.5 – 1.5	>1.5
Salinity level	Low impact	Middle impact	High impact

2.2.3 Alkaline reaction and carbonation analysis

The carbonation analysis in the samples was determined based on the alkaline reaction and determination of pH. The samples were crushed, the aggregate grains from the analysed sample were separated and each particular sample was homogenized. To determine the pH, approximately 1 gram of sample was poured into flasks and leached in 100 ml of deionized water. After at least 24 hours, a part of the leachate from the flasks was measured for pH determination. Based on the obtained pH values, the degree of carbonation was estimated (Table 6).

Table 9: Evaluation of carbonation based on the determined pH value [7]

Carbonation	Degree I.	Degree II.	Degree III.	Degree IV.
pH	>10.8	>9.6	8.3-9.6	<8.3

Carbonation takes place not only in conventional concretes but also in other silicate materials such as plasters, masonry mortars or prefabricated samples. The impact of carbonation in silicate materials can reduce the durability of the material and the reliability of the structure [7].

2.2.4 Analytical methods

X-ray fluorescence analysis (XRF) was performed to find the elemental chemical composition of the samples and to obtain the overall content of sulphur. The measurements were carried out on powdered samples by using AMETEC equipment with silicon detector.
Fourier-transform infrared equipment (FTIR) Brucker was used to confirm a presence of the sulphate functional groups in the samples. The measurement was performed in range 400 – 4000 cm^{-1} using ATR unit.
Colorimeter DR2800 Hach Lange was used to analyse the soluble salts – sulphates in the leachates.

3 Results and discussion

3.1 Visual inspection

Figure 3 and Figure 4 illustrate the results of visual inspection in the basement of the historical building of the Old Town City Hall. As it can be seen in the pictures, serious deterioration of materials was observed, represented by mainly biodegradation of walls, floors and ceilings, which were covered by significant mould on the surface (Figure 4) or by leaked walls and places with large patches of dissolved salts (Figure 3).

Figure 3: Results of visual inspection in archive (walls and ceilings)

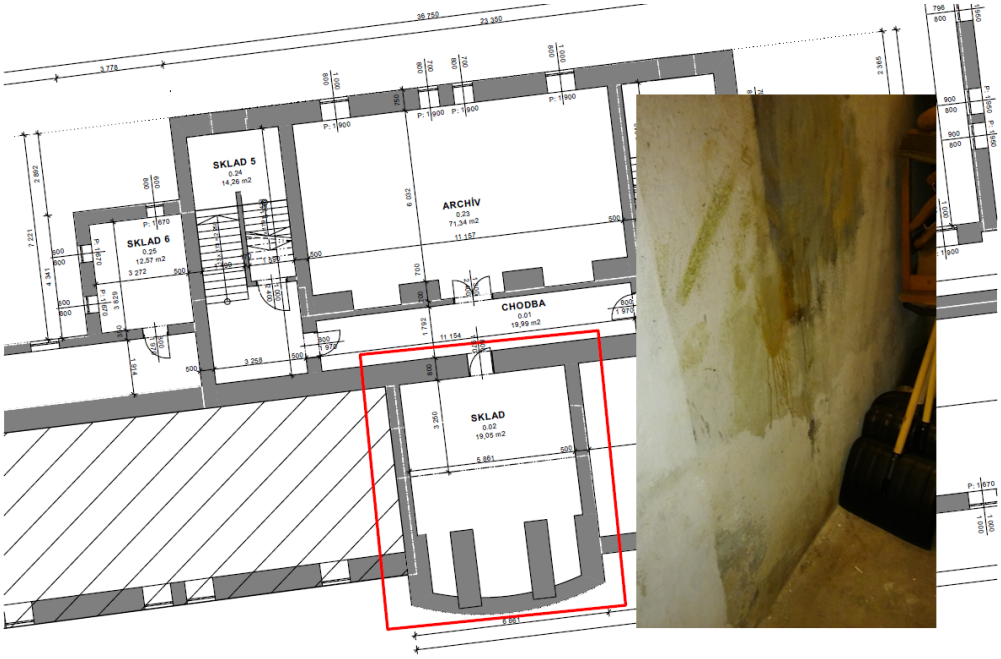

Figure 4: Results of visual inspection in storage (walls and ceilings)

3.2 Screening of the basement

Results of the screening are summarised in the Table 7, where the values of mass, pH, carbonation, salinity and humidity of the samples were determined.

Table 10: Results of the screening samples according to Figure 1

Sample	Material	Mass of sample [g]	pH	Carbonation degree	Salinity degree	Humidity w_{hm} [%]	Humidity degree
1.	Plaster	0.814	8.2	IV	very high	2.34	very low
2.	Plaster	0.702	8.9	III	very high	6.51	increased
3.	Plaster	0.480	8.7	III	very high	7.26	increased
4.	Plaster	0.879	7.9	IV	very high	1.14	very low
5.	Plaster	0.802	7.7	IV	very high	6.73	increased
6.	Plaster	0.820	8.4	III	very high	9.98	high
7.	Plaster	0.597	8.3	III	very high	5.19	increased
8.	Plaster	0.579	8.2	IV	very high	2.98	very low
9.	Plaster	0.823	8.0	IV	very high	5.92	increased
11	Plaster	0.296	8.5	III	very high	27.01	very high
12.	Mortar	0.687	8.4	III	very high	3.19	low
13.	Brick	0.812	8.5	III	very high	2.88	very low
14.	Mortar	0.619	9.2	III	very high	22.29	very high
15.	Paintcoat	0.642	8.2	IV	very high	5.62	increased
16	Mortar	0.451	9.1	III	very high	17.33	very high

17.	Brick	0.748	9.1	III	very high	10.43	very high
18.	Plaster	0.881	9.7	II	very high	6.14	increased
19.	Brick	0.901	8.5	III	very high	1.07	very low
20.	Mortar	0.421	7.9	IV	very high	29.60	very high
21.	Brick	0.875	8.8	III	very high	6.82	increased

According to ČSN P 73 0610, the humidity of individual samples ranged from very low to very high, the highest values were measured around the perimeter of the room (positioning to the outside terrain). Regarding moisture, 16 of the samples evaluated showed increased humidity, high to very high humidity in 10 cases. The degree of carbonation ranged from grade III to IV, salts were detected in practically all samples (Table 7). The presence of sulphates was observed in each sample. The increased content of sulphates in the plasters can be justified mainly by the fact that gypsum could have been used for their realization.
Samples obtained the very high humidity degree were also subjected to investigation by IR spectrometry, the examples of the IR spectra are shown in Figure 5 and Figure 6. Based on the position of the main peaks, very similar spectra can be observed for all analysed samples.

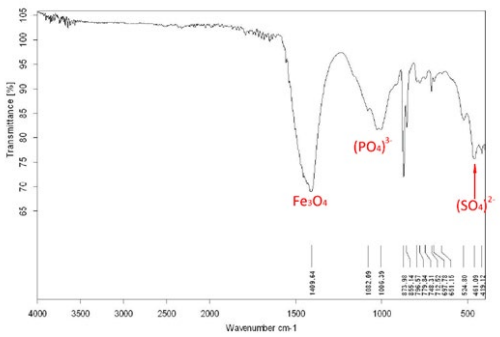

Figure 5: IR spectra of plaster sample

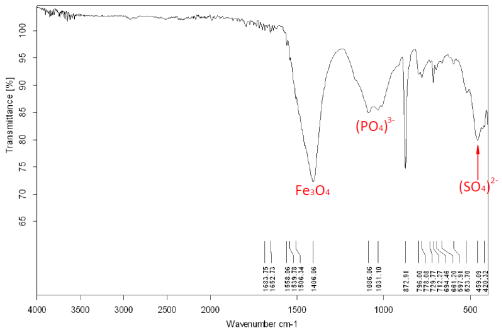

Figure 6: IR spectra of mortar sample

Besides the obvious functional groups present in mortars spectra such as silicate and carbonate, the FTIR measurements confirmed the sulphate and phosphate contents in the samples.

3.3 Results from the archive room

In the archive room, the investigation was exceptionally focused on the places which were visually identified to be damaged. In total, eleven samples from 6 sampling points in the room according to Figure 2 have been collected. The sampling points were located on both internal and external walls at various height levels (0.3 m, 0.5 m, and 1.8 m from the floor). After a semi-quantitative test, where a white precipitate of $BaSO_4$ formed after reacting the salt samples with barium chloride, selected samples were subsequently subjected to XRF spectrometry to determine the exact concentration of the elements. Summarisation of all results from the analysis of the materials in the archive room is given in Table 8.

Table 11: Results of wall materials from the archive room

Sample	Material	m [g]	Alkaline reaction		Sulphates		Humidity		Sampling point location
			pH	Carbonatation	SO_4^{2-} [%]	Salinity degree	w_{hm} [%]	Humidity degree	Height/wall type
22.	Brick	1.0659	8.49	III.	0.09	Low	0.21	Very low	0.3 m interior wall
23.	Plaster	1.0592	8.13	IV.	3.78	High	1.2	Very low	0.3 m interior wall
24.	Plaster	1.0752	8.17	IV.	1.21	Increased	0.75	Very low	0.3 m interior wall
25.	Plaster	1.0426	8.2	IV.	0.29	Low	0.48	Very low	0.3 m interior wall
26.	Brick	1.0693	8.27	IV.	3.74	Very high	0.68	Very low	0.3 m interior wall
27.	Brick	1.312	8.32	III.	0.38	Very high	0.33	Very low	0.3 m interior wall
28.	Plaster	1.0195	8.24	IV.	0	Low	0.65	Very low	0.5 m exterior wall
29.	Plaster	1.0447	8.8	IV.	5.74	High	1.54	Very low	0.5 m exterior wall
30.	Plaster	0.5175	8.11	IV.	0.10	Low	0.35	Very low	0.5 m exterior wall
31.	Plaster (bloom)	0.5032	7.82	IV.	59.14	Very high	39.08	Very high	1.8 m exterior wall
32.	Plaster (bloom)	0.2586	7.83	IV.	55.3	Very high	35.10	Very high	1.8 m exterior wall
33.	Plaster (bloom)	0.1732	7.86	IV.	72.1	Very high	26.72	Very high	1.8 m exterior wall

As seen in Table 8, significant carbonation degree was observed in all analysed samples (degree III and IV). All samples (except the No. 28 sample) contained sulphates in a wide range from low to very high degrees of salinity. Surprisingly, low humidity was detected for almost all samples even for the samples collected at the lower height (30 cm from the floor). Samples No. 31-33, representing crystal flakes from the gypsum plaster (Figure 3, Figure 7) exhibited sulphates in high percentage 59.14% for sample 31, 55.3% for sample 31 and 72.1% for sample 33. The results of the salt analysis are illustrated in Figure 7.

No significant differences were found regarding the measured parameters and the materials analysed. The results in Table 8 did not prove the influence of humidity, type of material, carbonation or height of sampling on the salinity results. However, the salinity results seem to be higher for the exterior walls when compared to the interiors ones. From the obtained results, it is not possible to state any relationship between the damage of the material and the

height of where it was located.
Anyway, the research was carried out during the reconstruction of the Old Town city Hall building and its results were helpful in replacing materials with new ones and proposing corrective measures.

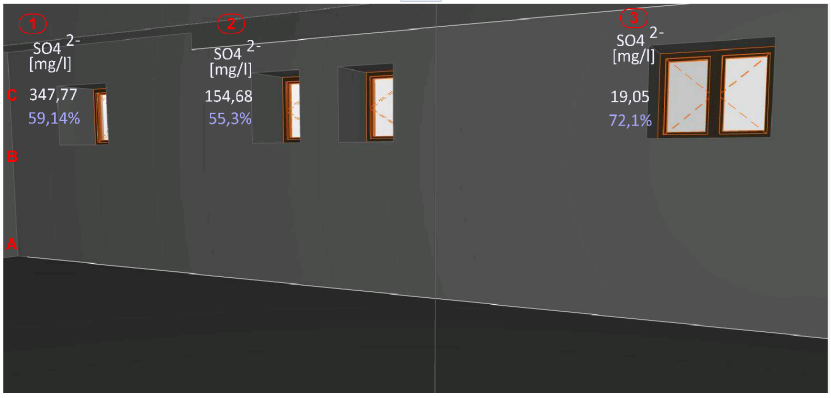

Figure 7: Determined sulphate concentrations for sampling points at 1.8 m

4 Conclusion

The presented work focused on the diagnostic evaluation of the historic building in terms of humidity, carbonation, and salinity with a deeper focus on selected parts of the basement. The visual inspection created a picture of the condition of the building of the Old Town Hall of Košice. The diagnostic of the building showed a significant degradation of the material and structures due to the action of moisture and salinity. The measured values confirmed the need for corrective measures and application novel materials and technologies in reconstruction process.

Acknowledgements

This work has been supported by VEGA 1/0648/17 and 2/0142/19.

References

[1] Balík, M., Starý, J. 2003. *Sklepy opravy a rekonstrukce*. Praha: GRADA Publishing, a.s. ISBN 80-247-0221-5

[2] Moropoulou, A., Labropoulos, K.C., Delegou, E.T. 2013. Non-destructive techniques as a tool for the protection of built cultural heritage. *Consruction and Building Materials, 48*, 1222-1239. DOI 10.1016/j.conbuildmat.2013.03.044

[3] Paoletti., D., Ambrosini., D., Sfarra., S. 2013. Preventive thermographic diagnosis of historical buildings for consolidation. *Journal of Cultural Heritage*, *14*, 116–121. DOI 10.1016/j.culher.2012.05.005

[4] Bálintová, M. *Environmentálna analýza materiálov – Úvod do moderných analytických metód*.

[5] Balík, M. a kol. 2005. *Odvlhčování staveb*. Praha: GRADA Publishing, a.s. ISBN 80-247-

0765-9

[6] Ďurica, P. 2012. *Poruchy budov diagnostika a sanácia*. Žilina: Edis. ISBN 978-80-554-0561-2

[7] Terpáková, E. 2017. *Diagnostika stavebných konštrukcií*. Košice: SvF TUKE.

[8] ČSN P 73 0610: 2000. Hydroizolace staveb - Sanace vlhkého zdiva - Základní ustanovení

[9] WTA Smernice 4-5-99. 2009. Posudzovanie muriva. diagnostika muriva

[10] WTA 2-9-04/D: 2009. Sanační omítkové system

DOI: 10.1515/sspjce-2020-0025

Numerical Modelling of Oedometer Test

Hana Agraine[1], Meriem Fakhreddine Bouali[2*]

[1]Department of Civil Engineering, Faculty of Sciences & Technology, Research Laboratory Civil Engineering, University of Mohamed Khider, Biskra, Algeria
e-mail: hana.agraine@univ-biskra.dz

[2*]Department of Civil Engineering, Faculty of Sciences & Technology, Research Laboratory Civil Engineering, University of Mohammed Cherif Messaadia, Souk Ahras, Algeria
e-mail: m.bouali@univ-soukahras.dz b.meriemfakhreddine@gmail.com

Abstract

The oedometric test is a test widely used in civil engineering. The main objective of this article has been to investigate the primary consolidation behaviour of the intact soil samples by comparing the results obtained from finite element analysis computations in PlAXIS[2D] with the experimental result of the soil samples obtained from the site of the Al-Ahdab oil field in the east of Iraq. Three different material models were utilized during the finite element analysis, comparing the performance of the more advanced constitutive Soft Soil material model against the modified Cam Clay and Mohr-Coulomb material models. Numerical results of Oedomter test show that the Soft Soil model behaviour is the most appropriate model to describe the observed behaviour.

Key words: consolidation, PLAXIS, behaviour, numerical, soil samples

1 Introduction

Fine saturated soils such as clays and silts are characterized by low permeability so that under the effect of an overload transmitted by the foundations to the soil, the pore water slowly infiltrates and the volume of the skeleton granular decreases. The reduction in volume results in a compaction of the soil which changes as the flow of water occurs. This is called a settlement of the soil by consolidation. [1]. Terzaghi (1923) [2] has proposed the one-dimensional consolidation for saturated soils firstly. Several researchers and practitioners such as [3-12] dealt with the limits of Terzaghi's theory in the case of soils compressible clay. L Arabet [13], A. Hana et al. [14] and M Klai et al. [15], discussed the one-dimensional consolidation of fine saturated soils, in the form presented by Terzaghi in 1925, and described the oedometric test, which provides the parameters of this theory. They showed how the theory of one-dimensional consolidation served as a basis for modern models of soil

behaviour.

The progress of the computer code and the provision of various software to researchers save a lot of time and presents an economical solution. Indiscriminate use can sometimes cause bad consequences. To shed light on the effectiveness of the constitutive laws able to better describe the target behaviour of fine saturated soils, a numerical analysis of the oedometer test was carried out using the PLAXIS^{2D} code V8.6 [16]. Four types of Clays (S0, S1, S2 and S3) tested and published by M O. Karkush et al. (2020) [17] were modelled. The compressibility curve will be compared with the experimental ones using different constitutive models: Mohr-Coulomb model "MC", Soft Soil Model "SSM" and Modified Cam Clay "MCC". The effectiveness of the studied constitutive models is discussed based on the comparison made between experimental and numerical results.

2 Simulation of observed behaviour of the soil samples

2.1 Presentation of the soil samples

As indicated in the work of M O. Karkush et al. (2020) [17], the intact soil samples were brought from the site of Al-Ahadab oil field that located in Al-Ahrar city located in the north-west of Wasit province at the east of Iraq.

The saturated soil sample was obtained by drilling to a depth of 3 m below the existing ground level (EGL). The groundwater table was 2.65 m from EGL [17]. Figure 1 shows the shapes of some soil samples. The mechanical properties of the soils tested by samples of clay soils tested by M O. Karkush et al. (2020) [17] are summarized in Table 1.

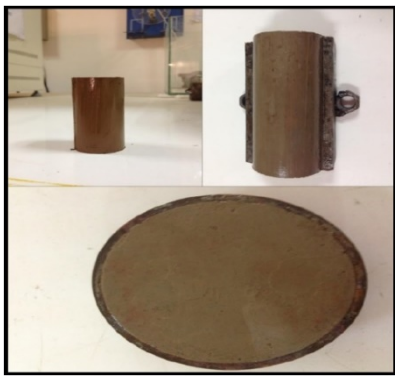

Figure 1: Soil samples [17]

Where:

S0: Undisturbed intact soil sample.

S1: Sample of soil contaminated with 100 g of Pb $(NO_3)_2$

S2: Soil sample contaminated with 200 g of Pb $(NO_3)_2$

S3: Sample of soil contaminated with 300 g of Pb $(NO_3)_2$

Table 1: Parameters of the soils simulated in this study and tested by M. O Karkush et al. (2020) [17]

Parameter	S0	S1	S2	S3	Unit
γ_{sat}	18.35	17.39	17.14	17.99	KN/m^3
γ_{nsat}	15.09	14.68	14.59	15.38	KN/m^3
$K_x = K_y$	3.22e-10	2.6e-10	1.98e-10	1.86e-10	m/s
ν	0.43	0.47	0.47	0.47	/
C	108	59	26	18	KN/m^3
φ	13.4	6.0	5.7	6.0	(°)
λ^*	0.024	0.057	0.066	0.044	/
k^*	7.7e-3	9.5e-3	8.8e-3	0.011	/
K_0^{nc}	0.768	0.895	0.90	0.895	/

2.2 Numerical simulation of Oedometer test

The numerical simulation of oedometer test is used by the two dimensional PLAXIS^{2D} software version 8.6 [16]. Figure 2 showed the mesh adopted in this present study. As shown in Fig. 2, the numerical adopted model has 50mm width and 19mm height. To make the mesh in the plane, we used the axis of symmetry since the specimen has an axis of revolution, and triangular elements with 15 nodes by element, each node can move in two directions.
To find more precise results it was assumed, only vertical displacement allowed to ensure the same principle of the oedometer test.

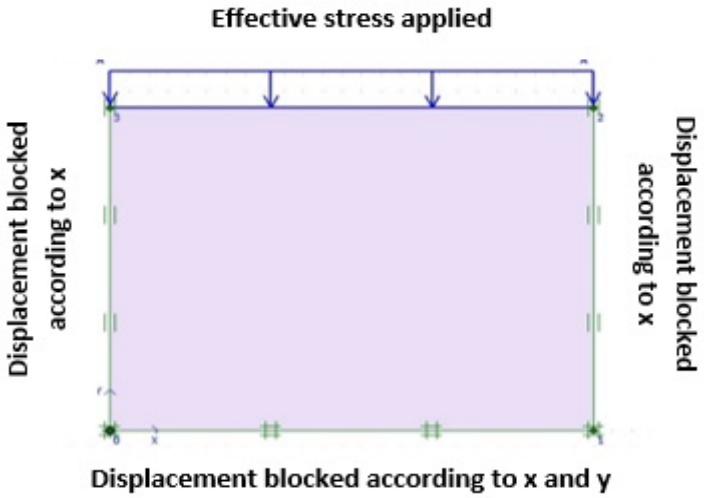

Figure 2: Numerical model of sample geometry

In order to properly simulate the one-dimensional consolidation of the modeled soil, a

uniformly distributed effective stress is applied to the surface of the sample.

3 Results and Discussions

3.1 Results

Numerical results are run by PLAXIS^{2D} software using Soft Soil Model ‘’SSM’’, the Modified Cam Clay model ‘’MCC’’ and Mohr Coulomb model ‘’MC’’ input parameters. Figure 3 compares compressibility curve obtained experimentally by [17] and numerically results predicted by the SSM, MCC and MC models for sample soils (S0, S1, S2 and S3).

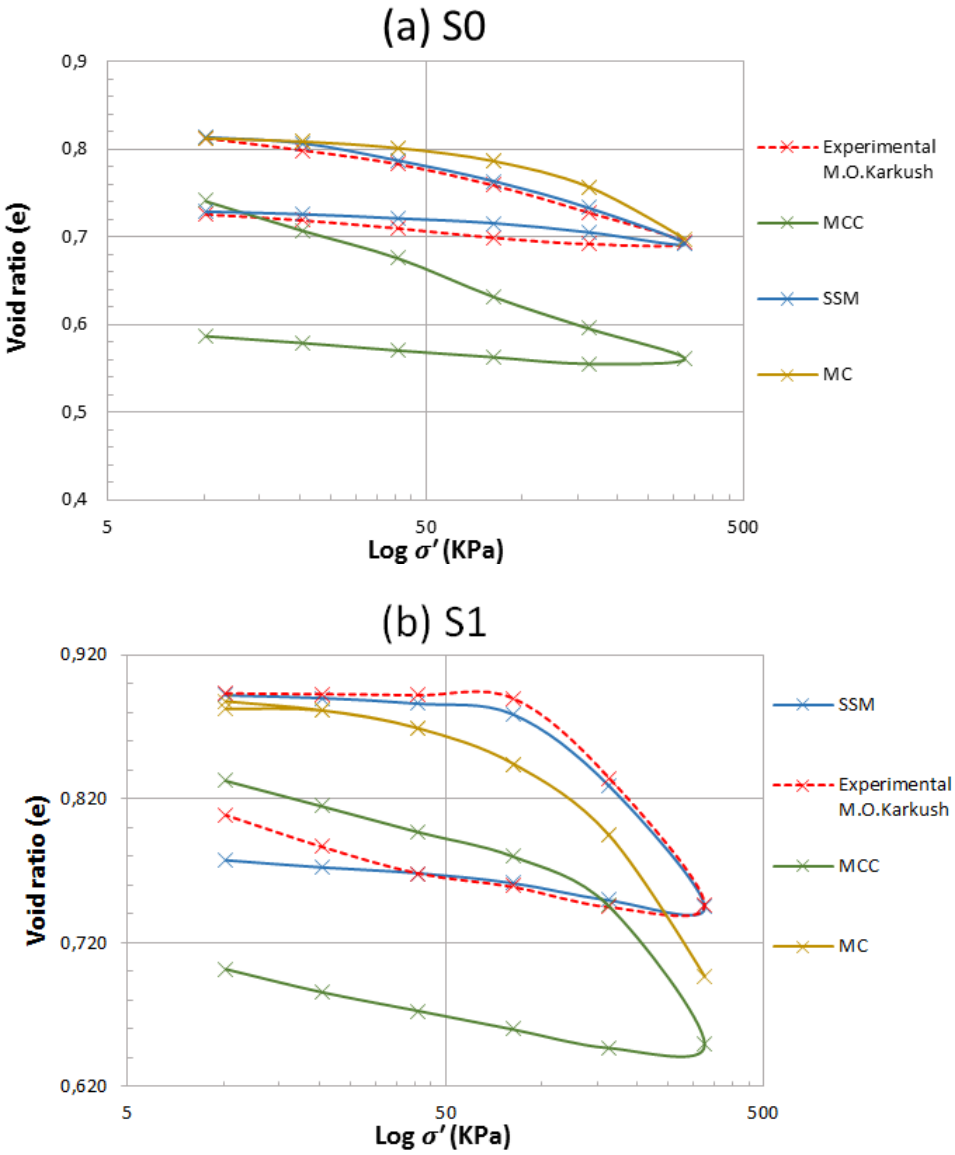

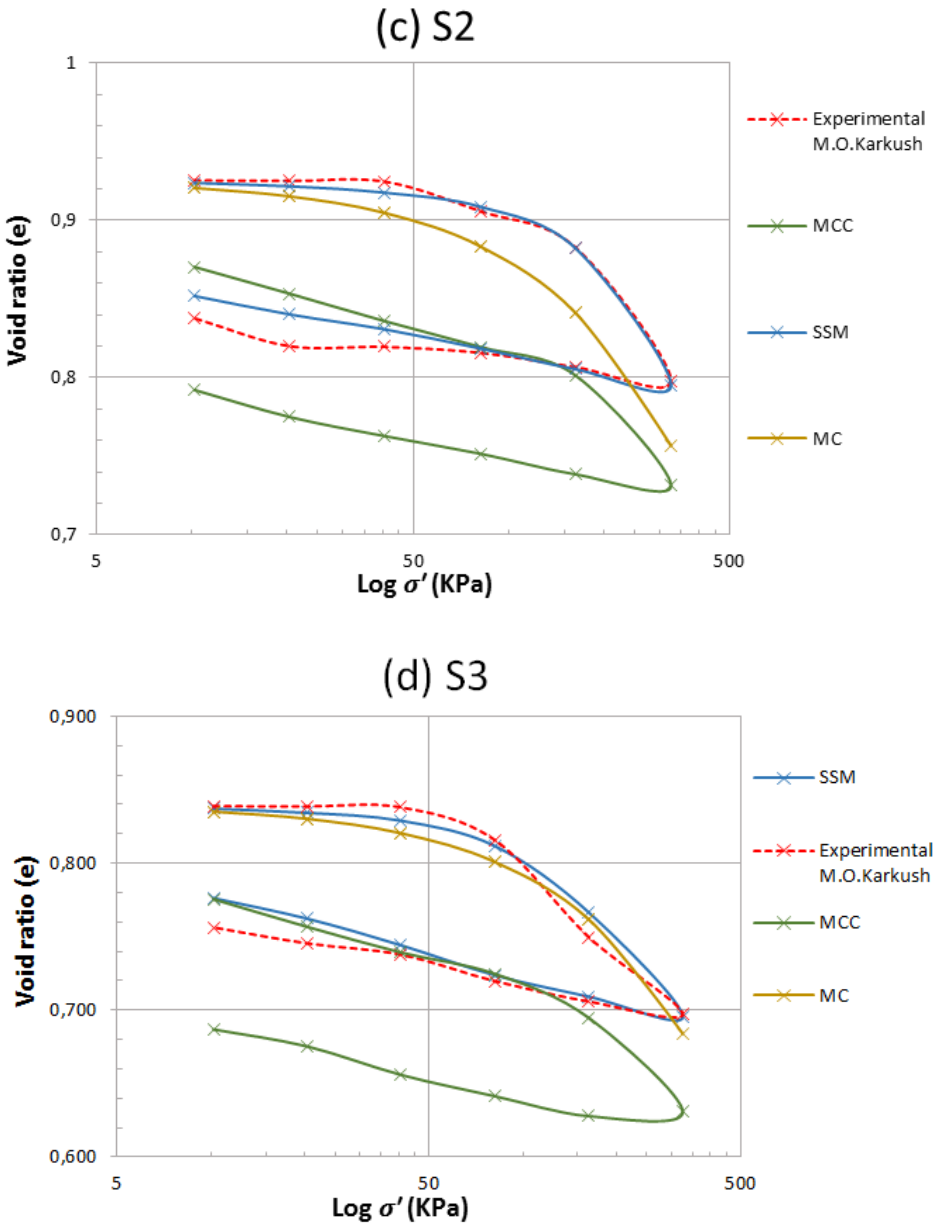

Figure 3: Comparison between predicted behaviours of sample soils modelled by the SSM, MC and MCC model and experimental measurements [17] from oedometer tests

3.2 Discussions

The results obtained in Figures 3 show clearly that the numerical prediction using ‘’MC’’ law of the primary consolidation phase (straight line with slope Cc) is generally in good agreement with the observed behaviour.
In the loading-unloading phase the numerical prediction underestimates the swelling of the

soil, the void index value for each unloading value returns to the same loading value.
We observe that the same values of the void index for loading and unloading; for example, for the studied soil sample S0 the value of the index of loading voids for the effective applied stress σp'= 162.97kPa is equal to e = 0.757 and also equal to e = 0.757 for unloading. So we can say that loading and unloading have the same effects.
The compressibility curves obtained by the "SSM" model are in excellent correlation with the experimental results [17].
The curves plotted in Figures 3 show a remarkable divergence between the experimental compressibility curves [17] and the numerical predictions obtained by the Modified Cam Clay Model "MCC" for all the types of the modelled soils.
According to the samples of soils S0, S1, S2 and S3, the results of the "MCC" model show that a decrease in the void index compared to the experimental curve (Fig 3).
The pre-consolidation stress value, the compressibility index and the swelling index obtained by the numerical simulation are summarized in Tables 2.

Table 2: Values of the compressibility characteristics for sample soils [17]

Parameter	S0	S1	S2	S3
Pre-consolidation pressure σ'_p	69	118	150	70
Compression index C_C	0.10	0.252	0.295	0.189
Swelling index C_S	0.033	0.042	0.039	0.046
The initial void ratio e_0	0.816	0.894	0.926	0.840

In order to compare the pre-consolidation stress, the compressibility index and the experimental swelling index with those obtained numerically by the SSM and MCC models; the relative error percentage is calculated using the following expression:

$$\left|\Delta E\right| = \left(\frac{Value_{num} - Value_{\exp}}{Value_{\exp}} \right) \times 100 \quad (1)$$

Figure 4 presents the relative errors calculated for the different modelled soils (clayey soils S0, S1, S2 and S3) estimated by the models MC, SSM and MCC.

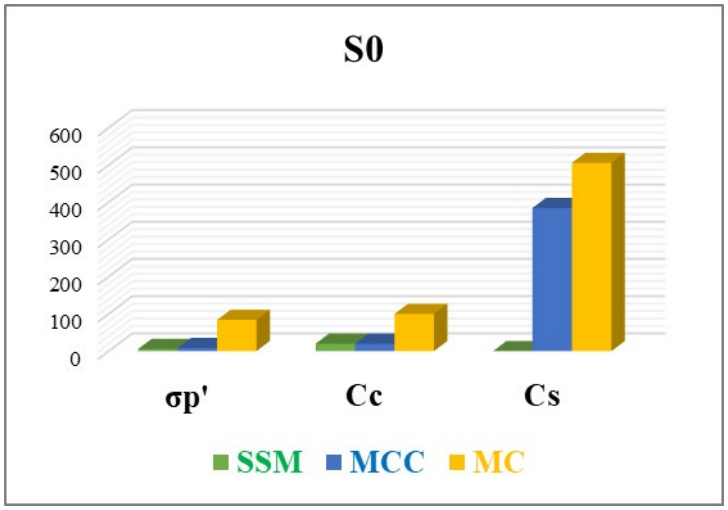
S0
600
500
400
300
200
100
0
σp'
Cc
Cs
SSM
MCC
MC

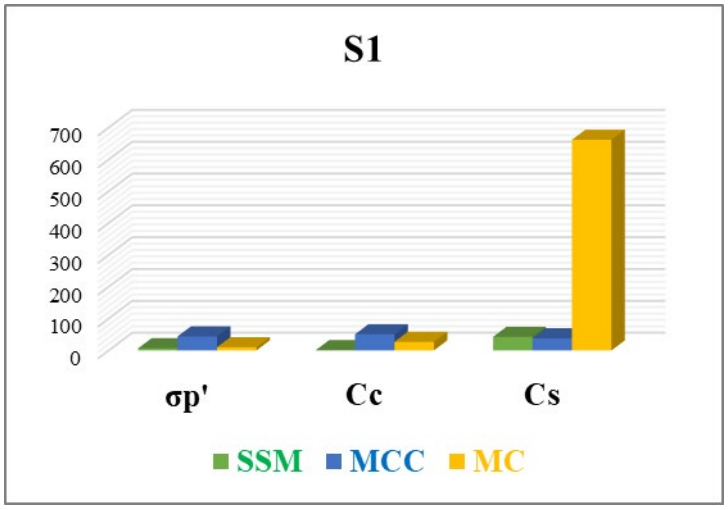
S1
700
600
500
400
300
200
100
0
σp'
Cc
Cs
SSM
MCC
MC

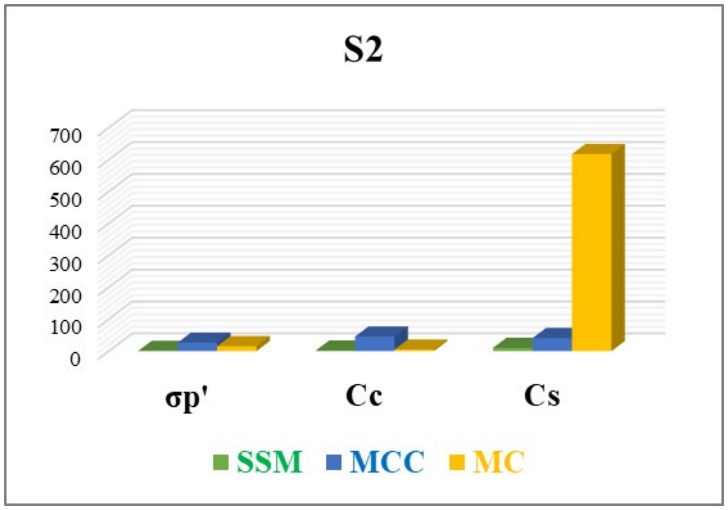
S2
700
600
500
400
300
200
100
0
σp'
Cc
Cs
SSM
MCC
MC

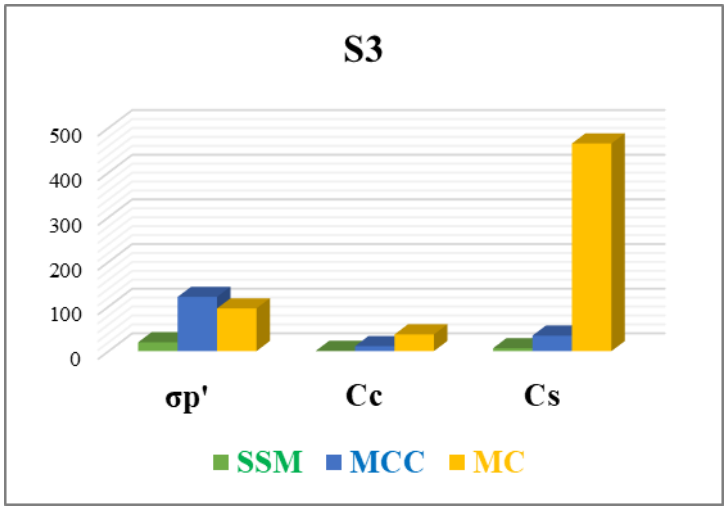

Figure 4: The relative error between numerical predictions obtained by the different 'MC, SSM and MCC' models and those obtained experimentally [17]

The histograms plotted in Figure 4 allow us to see that the Mohr Coulomb model "MC" and the modified Cam Clay model "MCC" have high relative errors by comparing them with those produced with Soft Soil Model "SSM" especially during of the loading-unloading phase.

The numerical calculation of the stress of pre-consolidation σ_p' by the SSM, MCC and MC models of the different modelled soils and its comparison with the experimental ones clearly shows through that the Soft Soil Model "SSM" gives the lowest relative error for the four cases of treated soils (Figure 4). Next is the Mohr Coulomb "MC" for all three soils (except S0) and finally the modified Cam Clay Model "MCC" gives the largest relative error.

So through the numerical computation of the pre-consolidation stress σ_p' we can say that the model of Soft Soil Model "SSM" is the most reliable to describe the observed behaviour.

The numerical estimate of the compressibility index Cc and swelling Cs (Fig. 4) and its comparison with the experimental ones clearly shows that Soft Soil Model "SSM" gives the lowest error, the Modified Cam Clay Model "MCC" comes next and Mohr Coulomb's "MC" presents the greatest relative error.

Through this numerical investigation we can say that the Soft Soil Model "SSM" is in very good agreement with the observed experimental behaviour.

4 Conclusion

The observed behaviour of four types of fine saturated soils was taken as a reference. The compressibility curves were established numerically using different constitutive laws, namely the Mohr Coulomb Model "MC", Soft Soil Model "SSM" and the Modified Cam Clay Model "MCC" by using PLAXIS^{2D} code.

When using computer codes, we are sometimes faced with a choice of the most realistic constitutive model. Our main objective has been to clearly define the most suitable model which can describe the consolidation of fine saturated soils. Through this numerical investigation we can draw the following conclusions:

For compressibility curves, the "SSM" model is recommended; it manages to predict the

compressibility of the soil during the oedometric test in stages. On the other hand, Mohr Coulomb's model "MC" is not recommended because of the unloading module.
Through this work we can say that our numerical model produced by the PLAXIS^{2D} code has proven its reliability and validity in terms of the description of the one-dimensional consolidation under the oedometer.

References

[1] Ali Bouafia, Mouna Mir. (2010). Introduction à la mécanique des sols - Cours et Applications (CD-Rom inclus), 1e édition octobre 2010 (pp.117-144); Publisher: éditions Pages Bleues Internationales, Alger.

[2] Terzaghi K. 1923. Die Berechnung der Durchlässigkeit des Tones aus dem Verlauf der hydrodynamischen Spannungserscheinungen. Akademie der Wissenschaften, Wien, Sitzungsberichte, Math. Naturwiss. KJasse, part. Ii-a, vol. 132 (3/4), pp. 125–138.

[3] Buisman, A. S. (1936). Results of long duration settlement tests. In Proc. 1st ICSMFE (Vol. 1, pp. 103-107). Cambridge.

[4] Biot, M. A. (1941). General theory of three dimensional consolidation. Journal of applied physics, 12 (2), 155-164.

[5] Koppejan, A. W. (1948). A formula combining the Terzaghi load compression relationship and the Buisman secular time effect. Proc. 2nd ICSMFE, Rotterdam, 1948, 3, 32-37.

[6] Gibson, R. E. (1961). A theory consolidation for soils exhibiting secondary compression. Report, 41.

[7] Gibson, R. E., Schiffman, R. L., & Cargill, K. W. (1981). The theory of one-dimensional consolidation of saturated clays. II. Finite nonlinear consolidation of thick homogeneous layers. Canadian geotechnical journal, 18(2), 280-293.

[8] Poskitt, T. J. (1969). The consolidation of saturated clay with variable permeability and compressibility. Geotechnique, 19(2), 234-252.

[9] Magnan, J. P. (1986). Modélisation numérique du comportement des argiles molles naturelles (Doctoral dissertation).

[10] Magnan JP, Baghery S, Brucy M, Tavenas F. (1979). Étude numérique de la consolidation unidimensionnelle en tenant compte des variations de la perméabilité et de la compressibilité du sol, du fluage et de la non- saturation. Bull Liaison Lab Ponts Chaussées 103: 83–94.

[11] Mesri, G. (1973). Coefficient of secondary compression. ASCE J Soil Mech Found Div-v 99, (SM1), 123-137.

[12] Tavenas, F., Brucy, M., Magnan, J. P., La Rochelle, P., & Roy, M. (1979). Analyse critique de la théorie de consolidation unidimensionnelle de Terzaghi. Revue Française de Géotechnique, (7), 29-43.

[13] L. Arabet. (2011). Modélisation numérique du tassement et de la consolidation des sols sous l'oedomètre, Pan-Am CGS Geotechnical Conference.

[14] Agraine, H., Bouali, M. F., & Messameh, A. (2020). Numerical Analysis of One-Dimensional Consolidation in Fine-Grained Soils. In Key Engineering Materials (Vol. 857, pp. 334-340). Trans Tech Publications Ltd.

[15] Klai, M., Bouassida, M., & Tabchouche, S. (2015). Numerical modelling of Tunis soft clay. Geotech Eng J SEAGS AGSSEA, 46(4), 87-95.

[16] R.B.J. Brinkgreve, PLAXIS. (2002). Version 8, Balkema.

[17] Karkush, M. O., & Ali, S. D. (2020). Impacts of lead nitrate contamination of the geotechnical properties of clayey soil. Journal of Engineering Science and Technology, 15(2), 1032-1045.

DOI: 10.1515/sspjce-2020-0026

Structural diagnostics and structural analysis of precast concrete building

Ivo Demjan, Michal Tomko, Róbert Šoltýs

Technical University of Košice, Slovakia
Civil Engineering Faculty, Institute of Structural Engineering
e-mail: ivo.demjan@tuke.sk, michal.tomko@tuke.sk, robert.soltys@tuke.sk

Abstract

The aim of this paper was to estimate further service possibilities of precast concrete structure. It was necessary to remain basic reliability conditions for actual service conditions. To reach this goal a complex experimental diagnostics and structural analysis was applied. On the basis of these methods construction arrangements recommendations were defined.

Key words: structural diagnostics, structural analysis, numerical modelling

1 Introduction

A structural diagnostics was realised to determine the size and development of visible cracks of structural system of a building, i.e. time-dependent monitoring of the development of cracks in the load-bearing reinforced concrete structure and brick masonry, experimental determination of in situ concrete strength of selected reinforced concrete elements, deformation of selected load-bearing concrete structures and determination of floor composition and geological exploration of natural bedrock close to the observed object.

2 Characteristics of the object

The building is composed of three load bearing systems:

1) The middle part, Fig. 1 b):
From a structural point of view, this is a four-storey precast reinforced skeleton revised by Priemstav (MSRP) with a 6 x 4.8 m and 6 x 2.4 m modular system. Ceiling panels are of type PZD 5/475. The reinforcing system consists of four reinforced concrete, or brick walls. The building is fixed to foundation piles with a diameter of 430 mm and a depth of 6.8 meters.

2) The front, Fig. 1 a):
Vertical support structures consist of brick masonry supported by reinforced concrete beams fixed to foundation piles with a depth of 5.5 meters. The horizontal load-bearing structure consists of PPD 918/312 prestressed panels. The cross-section shows a retreating cascade design. The longitudinal panels with a length of 9 m are supported by the peripheral wall between the two floors.

3) Back part, Fig. 1 c):
From a structural point of view, this is a two-storey precast reinforced skeleton revised by Priemstav (MSRP) with a of 6 x 6 m, 6 x 2.4 m and 6 x 12 m modular system. Ceiling panels are of type PZD 5/475, PPD 668/312, and others [1]. Vertical walls are brick masonry based on foundation strips. The building is based on a foundation of precast reinforced concrete footings. Beneath the whole object lies a complicated and dense network of channels for utility services.

a) b) c)

Figure 1: Longitudinal section

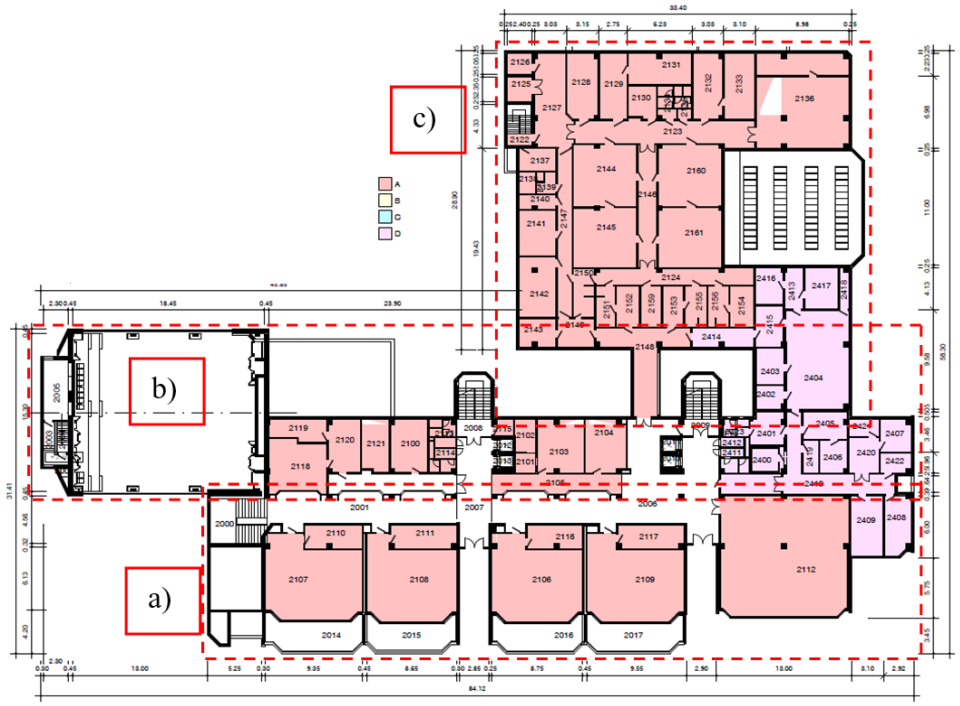

Figure 2: Floorplan of 2nd floor

3 Current condition

The following defects were found in the building structure:
- two rooms (classroom - 1, classroom - 2) precast prestressed concrete ceiling panels (PPD 918/312) show excessive deflections and are supported by steel struts;
- deformed (wavy) floors are observed in several rooms of the building;
- large cracks in the walls, also deformed door frames in one room on the first floor and damaged lining around windows;
- in one room (classroom - 2) a part or the tension reinforcement in part of the precast prestressed concrete ceiling panel is probably damaged;
- rising damp is clearly visible in ceilings and walls due to infiltration from atmospheric precipitation.

a) b) c)

Figure 3: Photo documentation of the current state of the structure;

a) Supports of the deformed panel PPD 918/312
b) Detail of mutual difference in the decline of the two adjacent panels
c) Additionally created downpipes, which damaged the prestressed edge cables in panel PPD 918/312 in room 2109

4 In-situ structural diagnostics of precast concrete building skeletons

Measuring the strength of concrete was carried out on the supporting horizontal panels PPD 918/312 and reinforced peripheral crown using a Schmidt rebound hammer.

4.1 Compressive strength of precast concrete ceiling panels

PPD 918/312 panels in the ceiling structure used for transmitting the vertical load interact mutually through joints made of liquid steel sealants and reinforcement. Malfunctions in the joint of the panel have demonstrated a significant burden of one of the panels and may deform when transferring vertical load.

The experimental findings of in-situ concrete strength of precast prestressed concrete ceiling panels type 918/312 PPD were carried out in room 2109 (classroom - 1), Fig. 4, and room 2106 (classroom - 2), Fig. 5.

Experimental measurements of in-situ strength of the concrete ceiling of unsupported PZD 5/475 reinforced concrete panels were conducted in room 2103, Fig. 6.

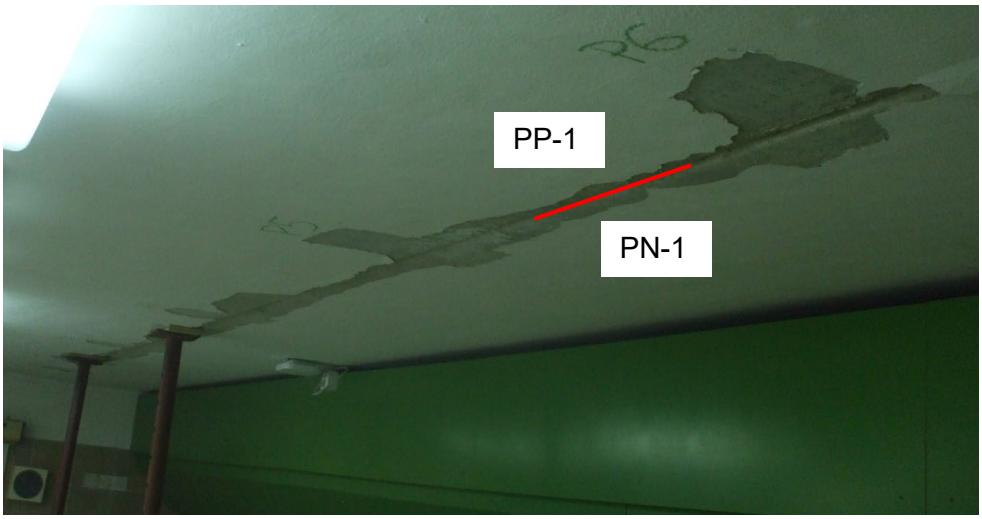

Figure 4: View of the reinforced concrete ceiling panels in room 2109
PP-1 ... ceiling panel (PPD 918/312) supported by steel struts
PN-1 ... ceiling panel (PPD 918/312) not supported by steel struts

Table 1: Measured values of Schmidt recoil hammer N in room 2109
For: PP-1 ... ceiling panel (PPD 918/312) supported by steel struts
PN-1 ... ceiling panel (PPD 918/312) not supported with steel struts

Location	Schmidt rebound	Mean	R_{be}	Schmidt rebound	Mean	R_{be}
Position	PP-1		[MPa]	PN-1		[MPa]
P1 Vertical	57, 58, 58, 58, 57, 58, 58, 56, 56, 56	57.2	64	57, 58, 60, 58, 59	58.4	66
P2 Vertical	58, 58, 58, 59, 58, 57, 56, 58, 59, 57	57.8	65	56, 58, 58, 56, 58	57.2	64
P3 Vertical	56, 58, 56, 58, 58, 56, 58, 58, 56, 58	57.2	64	59, 61, 57, 57, 59	58.6	66
P4 Vertical	58, 56, 56, 58, 56, 56, 55, 58, 58, 56	56.7	63	57, 57, 57, 56, 59	57.2	64
P5 Vertical	56, 58, 54, 58, 56, 55, 59, 58, 57, 58	56.9	63	55, 55, 54, 58, 56	55.6	61
P6 Vertical	57, 57, 58, 58, 58, 54, 56, 58, 54, 53	56.3	62	57, 54, 58, 53, 56	55.6	61

Mean R_{be} = 63.5 MPa
$f_{c,cube}$ = 53.9 MPa

Mean R_{be} = 63.7 MPa
$f_{c,cube}$ = 54.2 MPa

Compressive strength for precast prestressed PPD 918/312 concrete ceiling panel complies with class C 45/55 concrete.

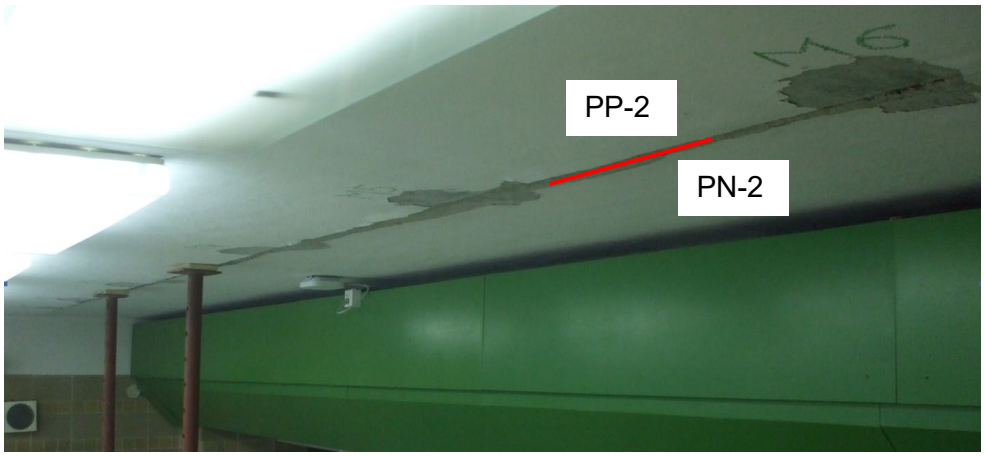

Figure 5: View of the reinforced concrete ceiling panels in room 2106
PP-2 ... ceiling panel (PPD 918/312) supported by steel struts
PN-2 ... ceiling panel (PPD 918/312) not supported by steel struts

Table 2: Measured values of Schmidt recoil hammer N in room 2106
For: PP-2 ... ceiling panel (PPD 918/312) supported by steel struts
PN-2 ... ceiling panel (PPD 918/312) not supported by steel struts

Location Position	Schmidt rebound PP-2	Mean	R_{be} [MPa]	Schmidt rebound PN-2	Mean	R_{be} [MPa]
M1 Vertical	54, 55, 57, 54, 56, 58, 57, 55, 57, 58	56.1	62	53, 54, 55, 54, 53	53.8	59
M2 Vertical	55, 56, 56, 54, 53, 57, 57, 57, 58, 57	56.0	62	60, 57, 53, 54, 58	56.4	62
M3 Vertical	56, 57, 58, 55, 58, 56, 54, 56, 56, 57	56.3	62	54, 56, 55, 52, 52	53.8	59
M4 Vertical	57, 55, 57, 56, 57, 56, 55, 58, 55, 58	56.4	62	55, 55, 56, 55, 57	55.6	61
M5 Vertical	58, 58, 56, 57, 56, 57, 58, 57, 60, 56	57.3	64	56, 55, 56, 54, 51	54.4	60
M6	58, 56, 58, 57,	57.5	64	56, 55, 53, 54, 54	54.4	60

Vertical	58, 57, 58, 58, 57, 58					

Mean R_{be} = 62.7 MPa
$f_{c,cube}$ = 53.3 MPa

Mean R_{be} = 60.2 MPa
$f_{c,cube}$ = 51.2 MPa

Compressive strength for precast prestressed concrete ceiling panel PPD 918/312 complies with class C 45/55 concrete.

Room 2103 is an office and is located on the first floor in the front segment of the building structure.

Figure 6: View of the precast concrete ceiling panel (PZD 5/475) in room 2103

Table 3: Measured values of Schmidt recoil hammer N in room 2103 for panels PZD 5/475

Location Position	Schmidt rebound	Mean	R_{be} [MPa]
S1 Vertical	46, 45, 49, 46, 42, 48, 47, 46, 48, 49	46.6	42

Mean R_{be} = 42.0 MPa
$f_{c,cube}$ = 35.7 MPa

Compressive strength of unsupported precast concrete ceiling panel PZD 5/475 complies with class C 30/37.

4.2 Compressive strength of precast concrete bond beams

The experimental findings of in-situ compressive strength of the peripheral concrete bond beam were carried out in room 2109 (classroom - 1) and in room 2106 (classroom - 2), Fig. 7.

Bond beam (V1) Bond beam (V2)

Figure 7: View of the reinforced concrete bond beam (V1) and (V2)
height of bond beam (V1) is 28.5 cm, plaster thickness 5 to 5.5 cm
height of bond beam (V2) is 29 cm, plaster thickness 2 cm

Table 4: Measured values of Schmidt recoil hammer N in room 2109 (classroom - 1) of precast concrete bond beam V1

Location Position	Schmidt rebound	Mean	R_{be} [MPa]
V1 Horizontal	34, 39, 38, 38, 34, 34, 37, 36, 38, 38	36.6	34
V2 Horizontal	35, 37, 38, 36, 37, 36, 37, 36, 37, 38	36.7	34

Mean R_{be} = 34.0 MPa
$f_{c,cube}$ = 28.9 MPa

Compressive strength of the reinforced concrete ceiling panel complies with class C 25/30.

4.3 Composition and thickness of floors

The thickness and composition of floor on precast prestressed concrete ceiling panel PPD 918/312 and on unsupported precast concrete ceiling panel PZD 5/475 was experimentally determined in-situ via probes.

The thickness of the floor on the ceiling panel consists of levelling concrete and screed with a total thickness of about 8 cm.

Figure 8: Probe to determine the thickness and composition of the floor on the ceiling panels

5 Geological-engineering survey

In terms of the geomorphological structure of Slovakia, the Košice basin, a sub-unit of the Košická plane is an area of geomorphological interest.
According to seismotectonic maps, Slovakia falls in the region affected by seismic shocks with intensity of up to 6 MSK degrees – 64.

According to the climatic areas, the studied area is classified as a warm area (T), which is characterized by the number MEAN 50 and more summer days per year (with a daily maximum air temperature ≥ 25 °C). The area of interest is located in the district T5 (warm, slightly dry ward, with cold winter).

5.1 Geological-engineering extruded cores

Four cores were extruded from a depth of 8.0 m u.t.. During the drilling works extruded cores were documented. Laboratory work was carried out in order to determine the physical-mechanical properties of the soil necessary for the categorizing the soil and to determine soil workability, Tab. 5.

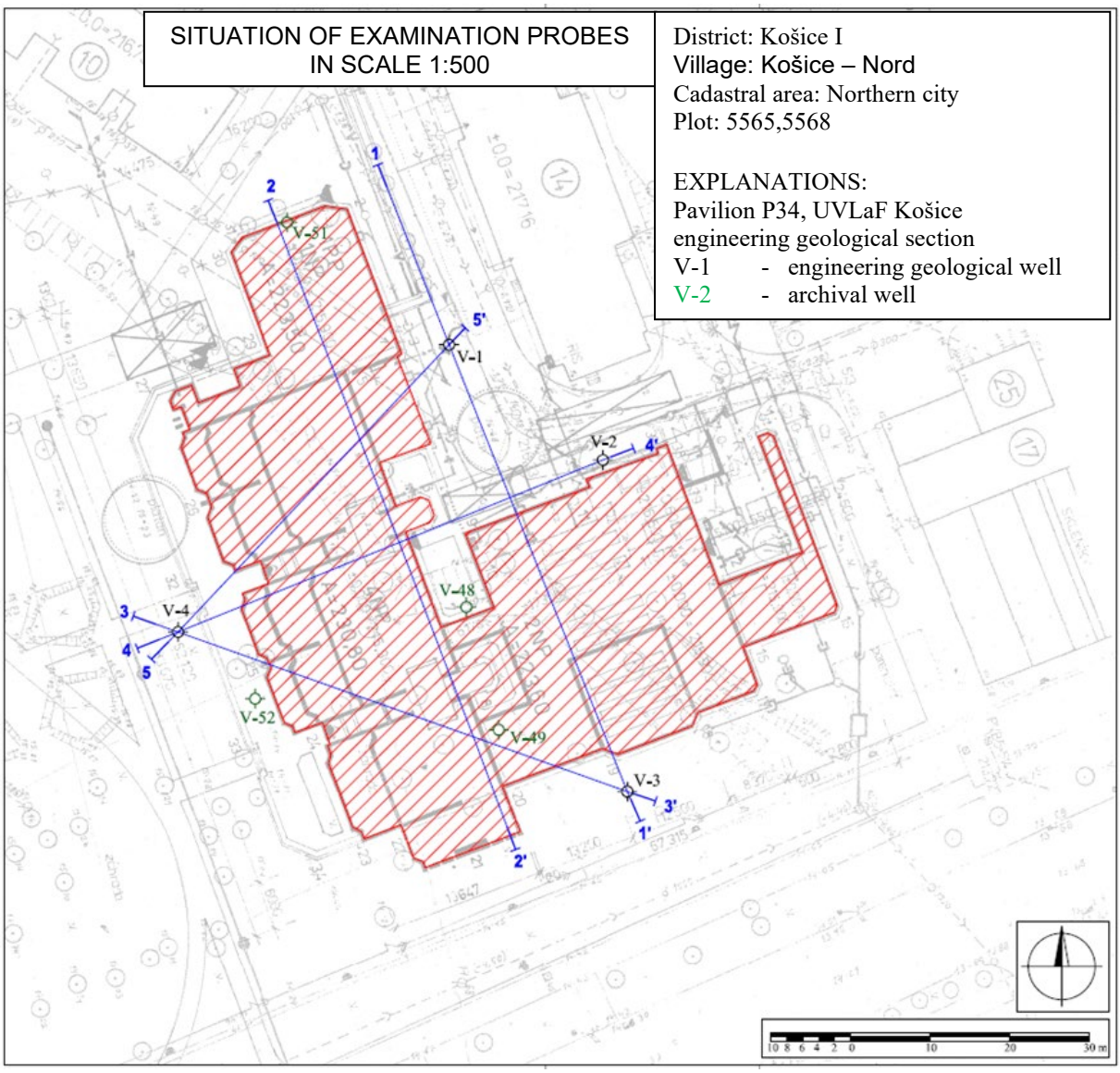

Figure 9: Situation of survey probes

section 1-1´

ENGINEERING GEOLOGICAL SECTION 1-1´ IN SCALE 1:200/100

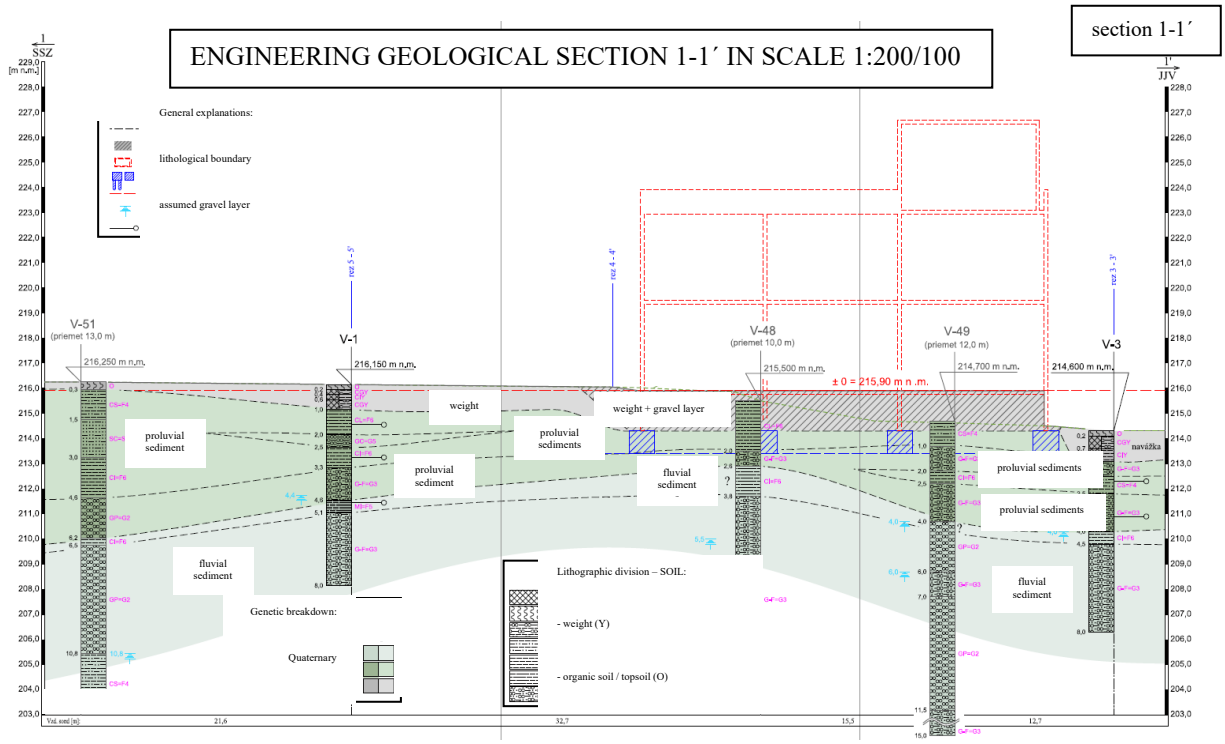

section 2-2´

ENGINEERING GEOLOGICAL SECTION 2-2´
IN SCALE 1:200/100

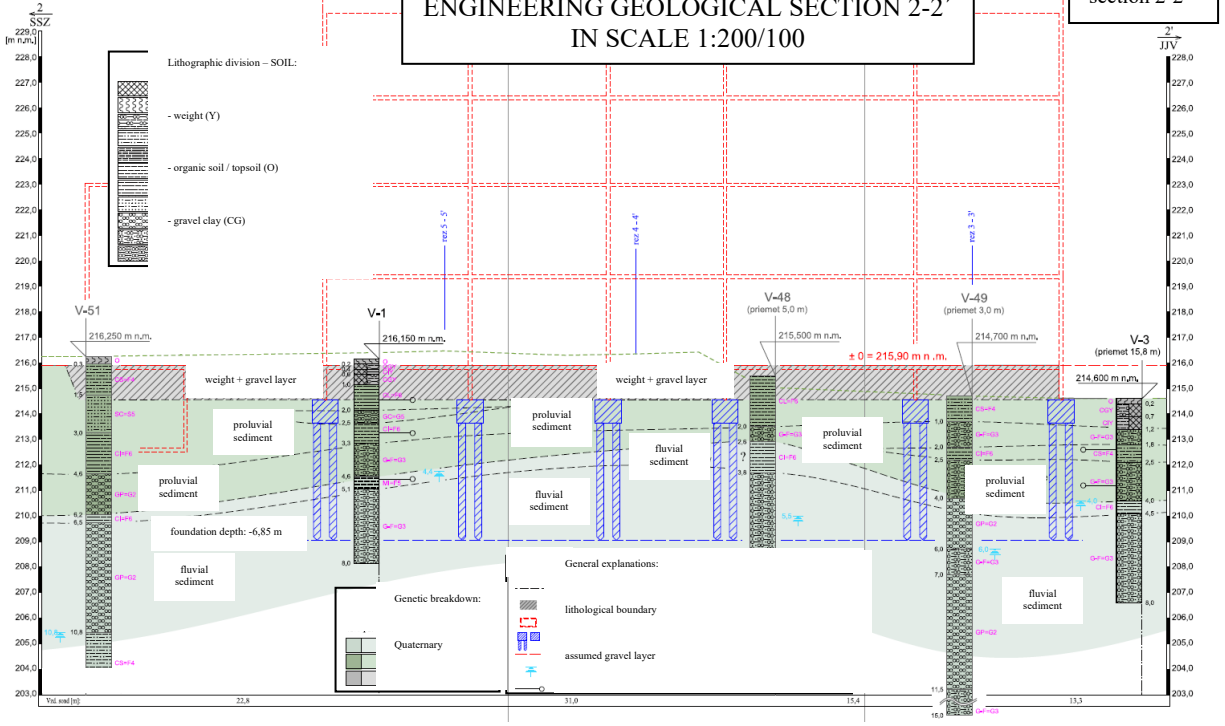

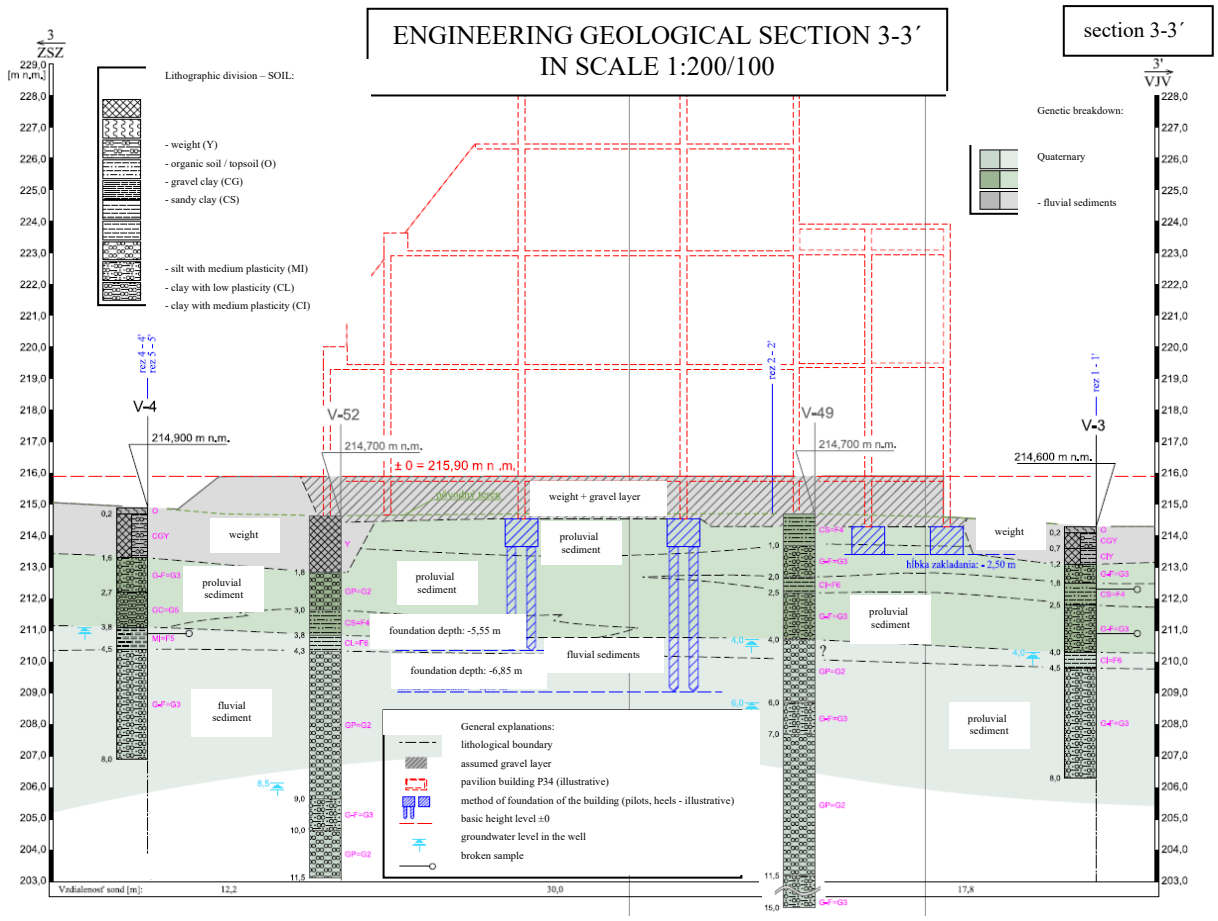

Figure 10: Geological-engineering sections

Table 5: Classification results of analyzed segments of earth samples

Core	Extrusion depth (m)	Liquid limit W_L (%)	Plastic Limit W_P (%)	Plasticity I_P	Moisture Content W_N (%)	Consistency I_C	Grade acc. STN 721001 & 73 1001
V-1	1.6-1.7	34.9	22.7	12.2	28.8	0.50	CL, F6
V-1	2.9-3.0	35.4	23.5	11.9	28.0	0.62	CI, F6
V-1	4.7-4.8	38.7	25.8	12.9	32.8	0.46	MI, F5
V-2	5.4-5.5	26.6	19.6	12.9	24.6	0.29	CS, F4
V-2	6.4-6.5	-	-	-	-	-	G-F, G3
V-3	2.0-2.1	35.0	21.7	13.3	22.2	0.96	CS, F4
V-3	3.4-3.6	-	-	-	-	-	G-F, G3
V-4	4.0-4.1	43.7	26.5	17.2	34.2	0.55	MI, F5

Completed drilling and laboratory test results clearly indicate the presence of cohesive soils at the top and bottom of the verified profile. At the time of the structure's design the soil had a solid and firm consistency. It is likely that over the life of the building changes in consistency

occurred due to infiltration at the foundation base, and also to a change (decrease) of their strength-deformation characteristics.

Damage to structures around the perimeter of the structure indicates a lack of backfill compaction, respectively in areas with rainfall infiltration and the potential leaching of fine grain gravel layer below the building and subsequent settling evidenced by deformation on the surface.

Results of a detailed engineering survey are presented in [6].

6 Ceiling panels check

Structural analysis was realised using finite element based on software ANSYS. The precast ceiling panels were analysed in order to calculate internal forces and stresses:
- prestressed panel PZD 5/475,
- prestressed panel PPD 918/312.

The geometry was modelled in the software with all the structural parts, i.e. concrete, steel reinforcement, prestressing cables with prestressing force 100 kN. Material characteristics of the concrete was applied in accordance with the parameters found by experimental in-situ measurements. Computed response, such as displacements, deformations, stress were checked with technical standards.

6.1 Precast prestressed panel PZD 5/475

Following loadings acting on the panel was considered:
- self weight,
- weight of the floor 2 kN/m^2,
- weight of the wall (height 3 m) with windows 10 kN/m,
- live load 3 kN/m^2.

Max. stress in computed response was 4.35 MPa.

a)

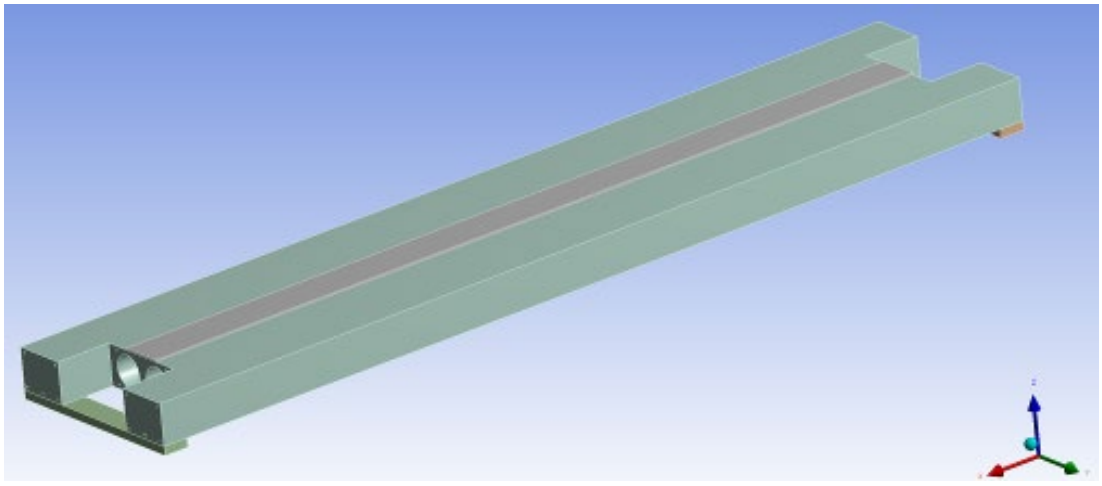

b)

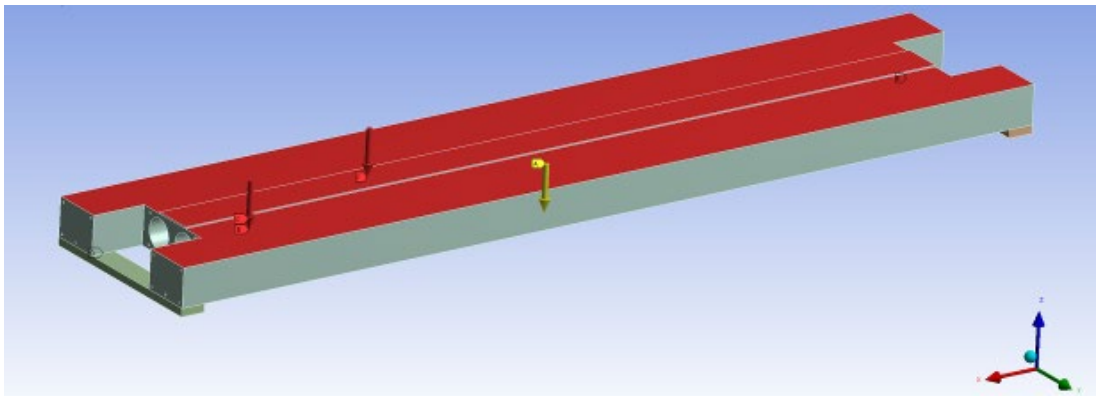

Figure 11: Geometry of the numerical model of panel PZD 5/475;
a) geometry of the panel
b) loadings acting of the panel

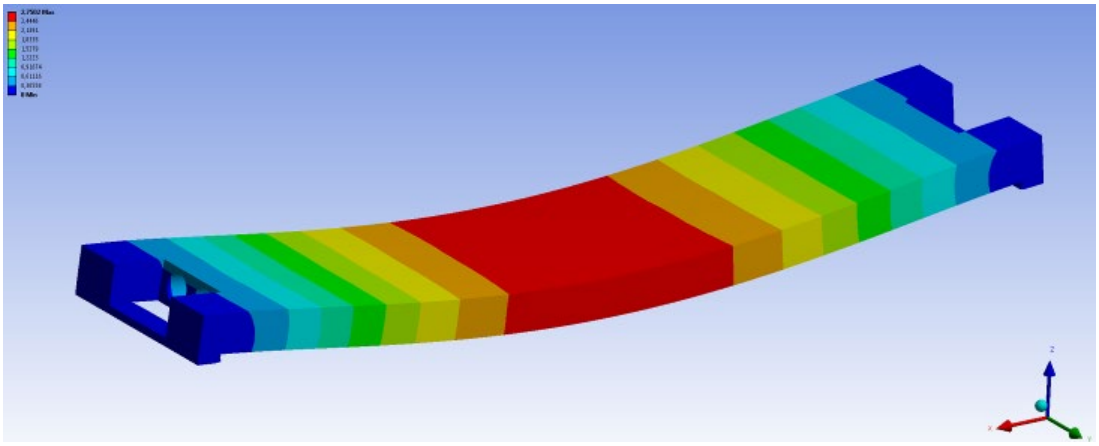

Figure 12: Response – displacements of the panel (max. 2.7 mm)

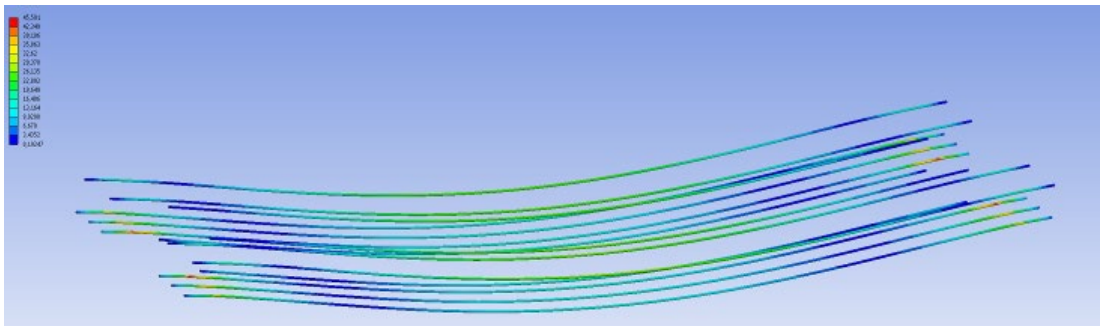

Figure 13: Response – stress in prestressing cables (max. 45.5 MPa)

6.2 Precast prestressed concrete panel PPD 918/312

Following loadings acting on the panel was considered:
- self weight,
- weight of the floor 2 kN/m^2,
- weight of the wall (height 6 m) with windows 20 kN/m,
- live load 3 kN/m^2.

Max. stress in computed response under self weight and permanent loading was 8 MPa.

Max. stress in computed response under self weight and permanent loading and wall was 20 MPa.

Max. stress in computed response under self weight, permanent loading, wall and varying loading was 23 MPa.

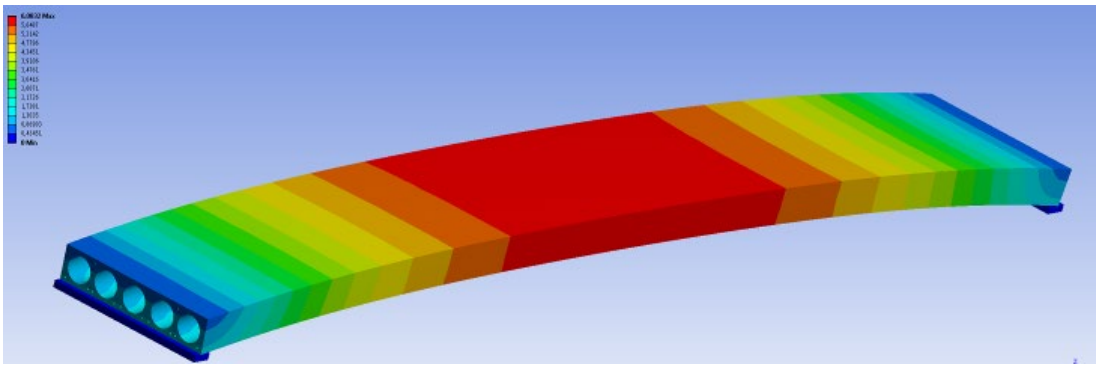

Figure 14: Response under self weight and permanent loading – displacements (max. -6 mm)

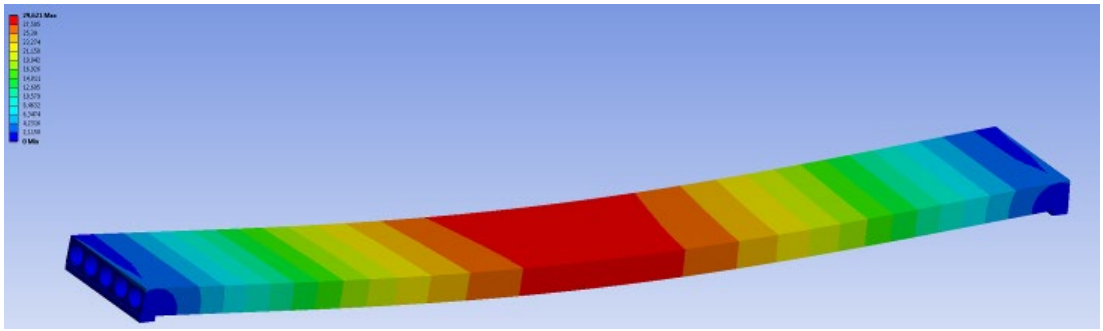

Figure 15: Response under self weight, permanent loading and wall – displacements (max. 29.6 mm)

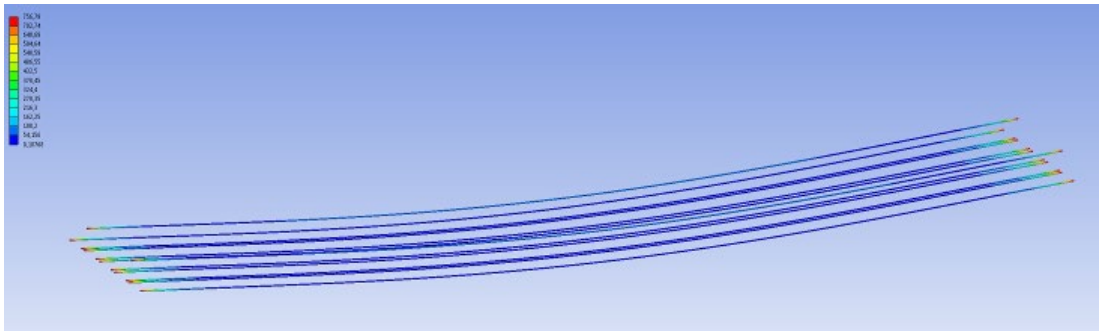

Figure 16: Response – stress in prestressing cables
(max. 756 MPa)

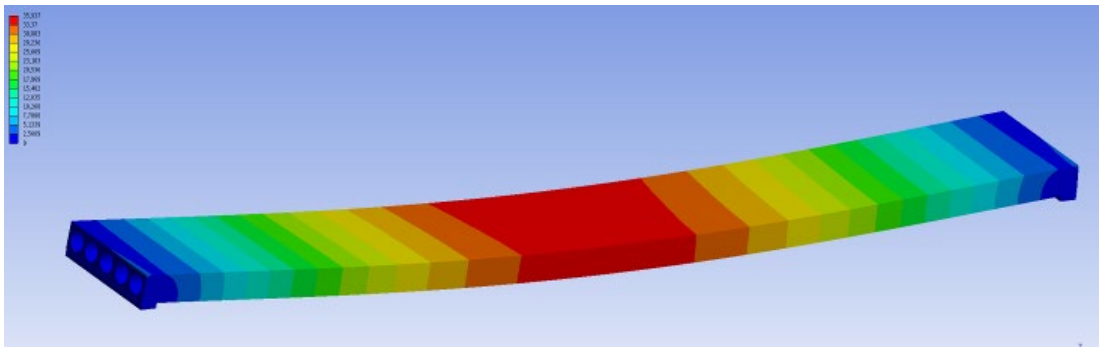

Figure 17: Response under self weight, permanent loading, wall and varying loading – displacements (max. 35.9 mm)

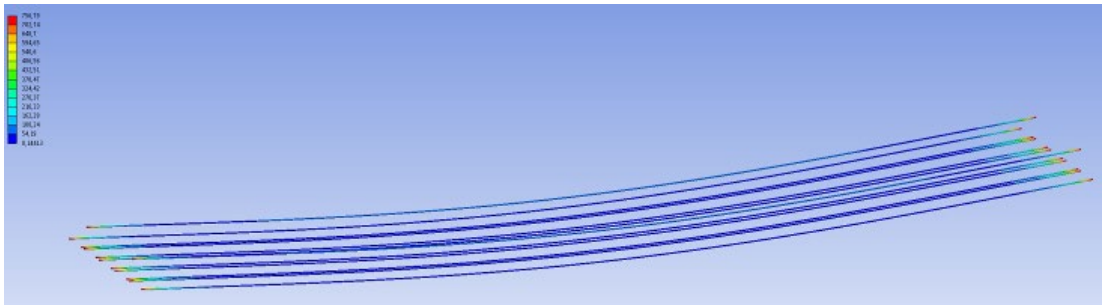

Figure 18: Response – stress in prestressing cables (max. 756 MPa)

Measured difference between displacements of panel loaded with wall and without wall was 35 mm.

7 Structural analysis

Global structural analysis of the precast concrete building was realised using finite element based software SCIA Engineer. Static response of the 2-storey part and 4-storey part of the building was calculated. The model consisted of 1D beam and 2D plate elements. Subsequently, internal forces and stress of structural elements were analysed, as well as the

action on the foundations was calculated. The response of foundations, after taking into consideration in-situ measured geological profiles of the soil, was checked in accordance to normative standards.

Based on the results of the static analysis of the three-dimensional mathematical model, these conclusions were stated:
- for the 4-storey building (located in the middle of the building, the MSRP precast system type), the group of piles consisted of 2 piles (each of 430 mm diameter) with the pile head of dimensions 1600x1600x1100 mm, these piles do not meet the requirements for the vertical resistance. Also the piles separately do not meet the requirements for vertical resistance.
- for the 2-storey building (located in the rear of the building, the MSRP precast system type), the precast footings of dimensions 1700x1700x1100 mm do not meet the requirements for the vertical resistance.

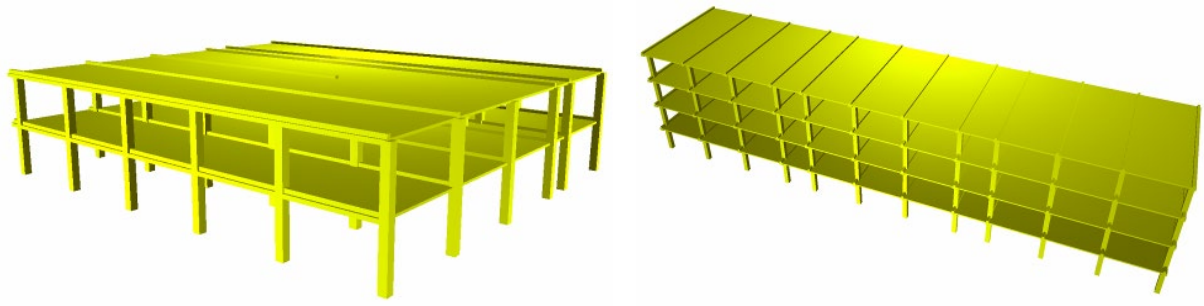

Figure 19: Rendered structural model 2- and 4-storey precast concrete skeleton MSRP type

8 Conclusion

Based on expert analysis, it is possible to evaluate that the diagnosed building structure has been subjected to differential settlement as a result of years of changes in the soil conditions in proximity to the foundations.

Due to differential settlements of foundations under the construction cracking has been observed in the partitions, which are located on first and second floor.

Remediation is required for the foundations (piles) to prevent further subsidence in the foundation and thus jeopardize the support of the reinforced concrete frame building.

Repairs to foundation structures must be implemented via injection after drilling the pile and floor. After implementation of foundation remediation work it is possible to then fill the cracks in the walls with expansive mortar.

In terms of functional and aesthetic requirements it is necessary to carry out remediation of deformed (wavy) floors as well.

It is necessary to carry out a revision of the vertical and horizontal pipes of plumbing beneath the floor structure that are located beneath the base of the building structure.

From the ceilings and walls locally damp areas from rainwater infiltration through the roof construction can clearly be seen, which causes degradation of the concrete bearing part of the

structure. In terms of thermal-technical, operational and aesthetic requirements roof, gutter and downspout repairs are needed.

The vertical bracing of two stiffening walls must be added to increase horizontal stiffness. The precast concrete panel must be supported from the bottom side by adding steel truss substructures.

Acknowledgements

The paper is carried out within the project No. 1/0129/20, partially founded by the Science Grant Agency of the Ministry of Education of Slovak Republic and the Slovak Academy of Sciences. This work was partially supported by the Slovak Research and Development Agency under the contract No. APVV-15-0777.

References

[1] Structural engineering design plan (without civil engineering part and geotechnical part), Stavoprojekt Košice (1984).

[2] Structural expertise of current state of the building,
Technical University of Košice, Faculty of Civil Engineering (2016),

[3] STN EN 1992-1-1: Eurocode 3 (2015): Design of concrete structures - Part 1-1: General rules and rules for buildings, SÚTN.

[4] STN ISO 13 822 (2012): General rules for design of structures. Assesment of existing structures. SÚTN.

[5] STN EN 73 1001 (2010): Geotechnical structures. Foundations of structures. SÚTN.

[6] Geotechnical expertise, UVLF of Košice, Pavilion P-34, TERRA – GEO, s. r. o., Košice (2016).